THE ROLE OF BIOMECHANICS IN LIVER TISSUE ENGINEERING

BY

EMMA CLARE MORAN

A Dissertation Submitted to the Graduate Faculty of
WAKE FOREST UNIVERSITY GRADUATE SCHOOL OF ARTS AND SCIENCES
in Partial Fulfillment of the Requirements
for the Degree of
DOCTOR OF PHILOSOPHY
Biomedical Engineering
May 2015
Winston-Salem, North Carolina

Approved By:

Shay Soker, Ph.D., Advisor

Jessica L. Sparks, Ph.D., Advisor

Rafael Davalos, Ph.D.

Padma Rajagopalan, Ph.D.

Thomas Shupe, Ph.D.

TABLE OF CONTENTS

LIST OF ILLUSTRATIONS AND TABLES

ABBREVIATIONS

LSEC	Liver Sinusoidal Endothelial Cells
NO	Nitric Oxide
ECM	Extracellular Matrix
STM	Septum Transversum Mesenchyme
FGF	Fibroblast Growth Factor
BMP	Bone Morphogenetic Protein
HGF	Hepatocyte growth factor
TGFβ	Transforming growth factor β
OSM	Oncostatin M
ALF	Acute Liver Failure
NAFLD	Nonalcoholic fatty liver disease
BAL	Bioartificial liver
HCC	Hepatocellular carcinoma
CRC	Colorectal cancer
iPSC	Induced pluripotent stem cells
HSC	Hepatic stellate cells
EMT	Epithelial-to-Mesenchymal Transition
PFP	Parenchymal Fluid Pressure
PVE	Poroviscoelastic
PHVE	Porohyperviscoelastic
H&E	Hematoxylin and Eosin
PHE	Porohyperelastic

VHE	Viscohyperelastic
NTI	Nano Tissue Indenter
EC	Endothelial Cell
eNOS	Endothelial nitric oxide synthase
ALB	Albumin
LDH	Lactase dehydrogenase
KLF2	Kruppel-like factor 2
ITGβ1/3	Integrin β1/3
PG	Prostaglandin
COX2	Cyclooxengenase-2
TCP	Tissue culture plastic
EDC	1-Ethyl-3-(3-dimethylaminopropyl)carbodiimide
NHS	N-hydroxysuccinimide
G’	Storage Modulus
G’’	Loss Modulus
MMP	Matrix metalloproteinase
E-cad	E-cadherin
β-cat	β-catenin
hflc	human fetal liver cells
AFP	alpha-Fetoprotein
α-SMA	alpha-smooth muscle actin
CK18/19	Cytokeratin-18/19
HNF4α/1β	Hepatocyte nuclear factor 4 alpha/ 1 beta

G6P	Glucose 6-phosphate
EpCAM	Epithelial cell adhesion molecule
AcTb	Acetylated alpha-tubulin
NCAM	Neural cell adhesion molecule

ABSTRACT

The field of liver bioengineering aims to generate functioning liver tissue in the laboratory in order to study complicated processes such as development, disease, cancer, drug metabolism, or even to engineer organs that can be implanted in patients. One approach in liver tissue engineering is to use the process of decellularization to create acellular liver scaffolds that retain the native tissue's extracellular matrix and architecture. These scaffolds can then be repopulated with a variety of hepatic and non-hepatic cell-types depending on the application, or in the case of human transplantation, the patient's own cells. While there has been some success in transplanting these constructs in animals and applying them towards simplistic models, we are still far away from achieving physiological liver structure and function. In order to achieve this, seeded cells need to be placed within the proper environment and given particular biological cues in order to function as they would physiologically. One important aspect of this process is the mechanical environment and signaling that cells experience within the acellular liver scaffolds. This thesis aims to investigate the role of biomechanics in liver tissue engineering so that we can better understand how to deliver the proper mechanical stimuli to cells in order to optimize their growth and function. To this end, we first characterized changes in liver biomechanics with tissue decellularization, finding that this process increases scaffold permeability and lowers matrix stiffness. Next, we investigated the impact of fluid flow-driven forces on cell seeding, tissue growth and cellular organization in a bioengineered liver with capabilities of modeling liver development and disease. Finally, we developed a bioengineered liver model of colon cancer metastasis in which we analyzed the influence of fluid flow and matrix stiffness on tumor behavior. Overall, the

findings of this thesis demonstrate the importance of the biomechanical environment in creating successful bioengineered liver models.

CHAPTER I

An Introduction to the Human Liver and Liver Tissue Engineering

Emma C. Moran

CONTENTS

1. Liver Anatomy and Physiology

1.1. *Human Liver Structure and Function*

The liver is one of the largest organs in the body and receives 25% of the cardiac output (1). It is the first site of processing for many of the body's nutrients and metabolizes carbohydrates, lipids, and proteins. Another main function of the liver is detoxification, extracting potentially toxic metabolic products and converting them to forms that can be excreted (2). The functions performed by the liver are directly related to its structure. The total blood supply to the liver is 100-130 ml/min per 100g of tissue, two-thirds of which comes from the portal vein and the remaining from the hepatic artery (3). This unique arrangement strategically allows the liver to receive first pass of the blood coming from the intestines, which is important for the metabolism of nutrients as well as detection of toxins. The supply of oxygenated blood from the hepatic artery gives the liver access to systemic circulation. Within the liver itself, blood flows through a vast microvasculature system, known as liver sinusoids. It is through this system that hepatocytes interact with blood and are able to take up amino acids, carbohydrates, lipids, and other compounds in order to maintain metabolic homeostasis. Additionally, the vast blood flow throughout the liver allows it to pick up toxic substances and perform an immunological function through phagocytosis of circulating material (3).

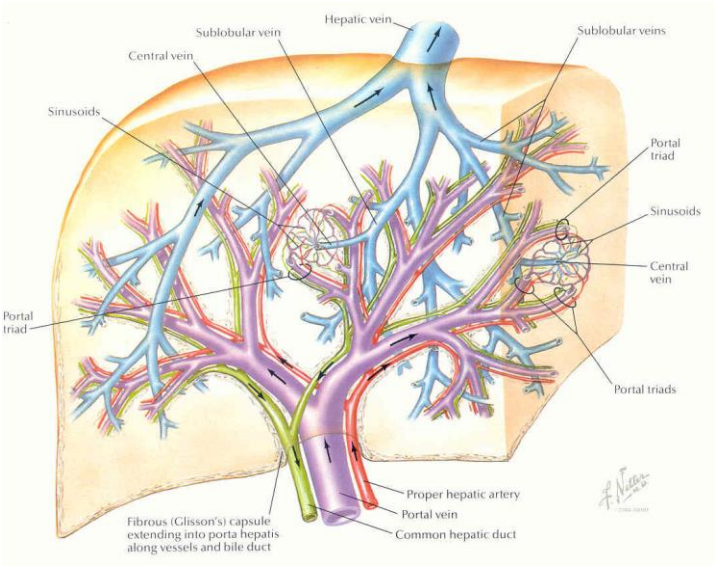

Figure 1: Hepatic Vascular Supply, adapted from Netter *et al* (4)

1.2. *Vascular System*

The liver is functionally organized into eight segments, each of which has its own independent vascular and biliary pedicle and venous drainage. The portal vein, which supplies two thirds of the overall blood flow to the liver, is intra-hepatically divided into two parts. The first division is known as the conducting system and delivers blood to the far reaches of the hepatic parenchyma. The second part of the portal vein is the distributing system, which is connected to the sinusoidal network that perfuses blood throughout the entirety of the organ. Once blood travels through the hepatic sinusoids, it drains into terminal hepatic veins, then to sublobular hepatic veins, and finally one of three main hepatic veins. While the hepatic artery supplies 25% to one third of total hepatic blood flow, necessary for liver oxygen supply, its role in parenchymal perfusion is not completely clear. It is known that the terminations of hepatic arteries are in sinusoids and occur through both arterial and venous channels (3).

1.3. *Liver Lobule*

The functional unit of the liver is usually referred to as a lobule, although the complicated nature of the internal structure of liver has led to other descriptions of functional units, such as the liver acinus (3). In the classical representation of the hepatic lobule, plates of hepatocytes are arranged radially around a central vein (Figure 2). Branches of the portal vein and hepatic artery are located at the periphery of the lobule, and with the central vein form the "portal triad". The hepatocytes within the lobule are perfused by sinusoids, which are low resistance cavities supplied by branches of the portal vein and hepatic artery. Blood from the sinusoids collects in the central vein for eventual drainage from the tissue. Sinusoids differ from the capillaries seen in the rest of the body in that they have the ability to collapse during fasting and swell with blood after meals, when nutrients need to be metabolized. The compliant nature of sinusoids allows large increases in liver blood flow with minimal increases in pressure. Endothelial cells line the walls of the sinusoids and contain specialized openings known as fenestrae. In addition, sinusoidal endothelial cells lack a basement membrane which, along with the fenestrae, allow for easy transport of molecules from the blood to hepatocytes across an area of specialized extracellular matrix (ECM) known as the space of Disse (2). Within the liver sinusoid there exists a gradient of hepatocytes known as metabolic zonation. Metabolic zonation can occur as a result of oxygen gradients due to discrepancies between arterial and venous blood flow, or the gradient of hormones and nutrients. Hepatocytes located in different zones have distinct genes and functionality determined by their position along the gradient (5). Different zones also possess specialized ECM and cell composition in order to perform discrete metabolic functions (6).

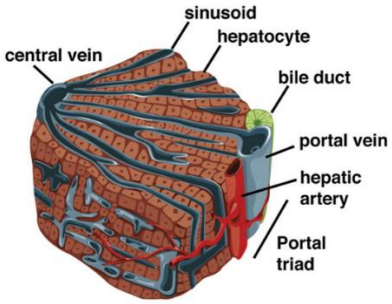

Figure 2: Human Liver Lobule, adapted from Si-Tayeb *et al* (7)

1.4. *Biliary System*

Bile is initially produced in the liver by hepatocytes where it drains into bile canaliculi, which form in between neighboring hepatocytes (8). From there bile drains through the canals of Hering, which contains both hepatocytes and biliary epithelial cells, and recently have been implicated as the location of the hepatic stem cell niche (9). From the Canals of Hering, bile passes though the terminal bile ducts lined by biliary epithelial cells which also secrete bile (Figure 3). Terminal bile ducts drain into the right and left bile ducts which later combine to form the common hepatic duct that leaves the liver. The bile then either goes to the common bile duct, emptying into the duodenum, or the cystic duct leading to the gallbladder (10).

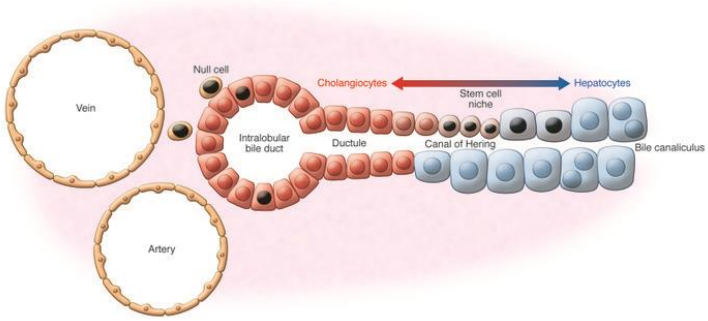

Figure 3: Hepatic Biliary System (11)

1.5. *Liver Cell Types*

There are numerous cell types in the liver in addition to the hepatocyte, which account for an estimated 60% of the liver cell mass (5). Liver sinusoidal endothelial cells (LSEC), the specialized endothelial cells described above, account for roughly 16% of liver cells. The key components of these cells are the large fenestrae that allow free transport of fluids through the space of Disse. Fenestrae are specialized based on their zonal distribution and loss of fenestrae is a key indication of liver fibrosis (5, 12). In addition to filtration and transport, essential functions of the LSEC include production of nitric oxide (NO) to regulate vascular tone, endocytosis, synthesis of ECM and secretion of cytokines (IL6 and IL1) and prostanoids (12). Kupffer cells are the resident macrophages of the liver sinusoid and account for 12% of the liver volume (5). Kupffer cells are generally found in the sinusoidal lumen and sometimes in the space of Disse (12). Their main function is phagocytosis of large particles that enter the liver sinusoid, but they also play an important role in the liver immune response. If activated by pathogenic agents, Kupffer cells secrete a number of cytokines and growth factors, including IL1, IL6 and TGFβ, which are important in the liver inflammatory and regeneration response (5, 12). Hepatic stellate cells are another cell type residing in the space of Disse. While only taking up 8% of total liver cells, stellate cells are the largest reservoir of vitamin A in the body (13). In states of disease or injury, stellate cells transdifferentiate into activated myofibroblasts and secrete cytokines and growth factors that promote the regeneration of hepatic epithelial cells (13). They are also the major secretors of ECM proteins in the liver, including collagens type I, II, III and IV (5). The final liver cell type are biliary epithelial cells, which only make up 3.5% of liver cell mass but are key components in the removal of bile from the liver (5).

The primary function of biliary epithelial cells, also known as cholangiocytes, is the modification of bile through multiple resorption and secretion events (14). Cholangiocytes contain a primary cilia that protrudes into the ductal lumen and acts as chemo-, mechano- and osmo-sensors to regulate bile flow and pH in health and disease (15).

1.6. *Liver Extracellular Matrix*

The liver ECM, as in most organs, is highly specialized and plays an important role in liver function in health and disease. ECM provides structural and biochemical support to cells and is composed of an arrangement of collagens, glycoproteins such as fibronectin and laminin, and proteoglycans. Basement membrane (BM) is a region of specialized ECM that resides between cells and adjacent stroma and mostly contains collagen IV, laminin, entactin and proteoglycans (16). The major constituents of liver ECM are collagens, specifically types I, III, IV and V. Collagen types I, III and V are fibrillar collagens that are mainly confined to the portal and central areas of the liver lobule and provide the main structural support of the liver. Collagen type IV, surrounded by laminin and fibronectin, forms the very low-density BM along the sinusoid wall, also known as the space of Disse (16, 17). Proteoglycans and other glycoproteins, such as fibronectin and nidogen, are also found in the liver ECM (18). The liver ECM is critical in maintaining tissue homeostasis, and changes in ECM composition and arrangement throughout different areas of the liver are critical factors in liver disease (18).

1.7. *Liver Regeneration*

The liver has a remarkable ability to regenerate, safeguarding the body from losing all of the functions that the liver performs. Liver regeneration occurs after partial hepatectomy

or liver injury, where normally quiescent hepatocytes undergo replication to restore the liver mass to its normal size in a hyperplastic response (19-22). This phenomena is a result of the interplay between multiple growth factor and cytokine-mediated and metabolic signaling pathways involving stromal cells and surrounding organs (19, 22). In the model of partial hepatectomy, it is thought that portal hypertension resulting from increased blood flow to the remaining liver mass triggers the liver regeneration cascade (23). There is still much debate in the scientific community about the exact mechanisms and cell types involved in liver regeneration (21, 22, 24). Cirrhosis and chronic liver failure in many cases is the failure of the liver regeneration cascade, highlighting the importance of liver regeneration research in understanding liver disease and developing therapeutic interventions.

2. Liver in Development and Disease

2.1. Liver Development

The liver is derived from the foregut endoderm with hepatic specification occurring as early as embryonic stage 8.5 in the mouse, evidenced by the active transcription of albumin (7, 25, 26). The hepatic endoderm lies adjacent to the cardiac mesoderm and septum transversum mesenchyme (STM) which triggers hepatic specification through the secretion of fibroblast growth factor (FGF) and bone morphogenetic protein (BMP), respectively (25). Studies have also implicated Wnt signaling in the specification of hepatic endoderm (27, 28). After hepatic specification, the committed endodermal cells are liver progenitor cells known as hepatoblasts. At mouse embryonic stage 9.5, hepatoblasts migrate out from their basement membrane and invade into the STM space, forming the liver bud (25). This process is controlled by numerous factors including the GATA6-

HHEX cascade (29) and the transcription factors PROX1 (30), TBX3 (31) and ONECUT1 (32). It is important to note here that this process hinges on the interaction of hepatoblasts with endothelial cells that line hepatoblasts prior to liver bud formation (33).

Following liver bud formation, hepatoblasts undergo intensive proliferation controlled by Wnt, hepatocyte growth factor (HGF), FGF, transforming growth factor β (TGFβ) and mitogen-activated protein kinase K (MAPK) signaling pathways (34-39). The next major process in liver development is the determination of hepatoblast cell fate. Hepatoblasts differentiate into either hepatocytes or cholangiocytes, biliary epithelial cells. There are numerous signals and pathways governing this process, but the main regulators include TGFβ, Notch, Wnt/β-catenin and FGF signaling (40-43). Following differentiation along the hepatocyte or cholangiocyte pathway, there are two simultaneous events; hepatocyte maturation and bile duct formation. Hepatocyte maturation is controlled by several transcription factors, including the six core factors of HNF1A, HNF1B, FOXA2, HNF4A, ONECUT1, and NR5A2 (25, 44) and also extracellular signals. A major function of the fetal liver is to support hematopoiesis and the residing hematopoetic cells secrete Oncostatin M (OSM) which is known to play a role in hepatocyte maturation (45). Sinusoidal endothelial cells can influence the apico-basal polarity of hepatocytes through *heart of glass* and *valentine* proteins (46). Liver zonation also occurs during this time, with the Wnt/β-catenin pathway being integral for the differences in periportal and pericentral hepatocytes (47).

Bile ducts are formed from cholangiocytes that have differentiated from periportal hepatoblasts. Bile duct morphogenesis is a highly coordinated activity resulting from TGFβ, Notch, Wnt and FGF signals (35, 40-43, 48-50). There is also transcriptional control

of cholangiocyte differentiation, specifically HNF6 and HNF1β (49). Biliary tubulogenesis begins with hepatocytes in close proximity with the portal mesenchyme with the formation of single layered ductal plate consisting of cholangiocytes on the portal side and hepatoblasts on the parenchymal side. Then asymmetrical primitive ductal structures are formed followed by a rapid differentiation of hepatoblasts to cholangiocytes. Once all of the ductal cells are cholangiocytes, the duct gradually becomes surrounded by portal mesenchyme (25, 49).

The hepatic vascular network and stromal cells, including LSEC, stellate cells and Kupffer cells, are integral to the proper development of liver tissue (33, 51). The fetal liver is supplied by two major veins, the transient umbilical veins and vitelline veins. Once the umbilical vein collapses at birth it is replaced by the portal vein. The hepatic artery forms alongside the portal vein and is thought to be driven by the ductal plate in humans (51). Finally, sinusoids, the specialized capillaries in the liver, form through angiogenesis from existing vessels within the STM space (52). The coordination of endothelial cells and stellate cells are integral in the proper vascular tube formation. Additionally, stellate cells may play an important role in hepatoblast differentiation and proliferation and bile duct morphogenesis through the secretion of Wnt, FGF, HGF and retinoic acid and possible through the secretion of ECM proteins (13). Due to the importance of Kupffer cells in hepatic regeneration, it is hypothesized that they may also play a critical role in organogenesis although that role is largely unknown (7).

2.2. Liver Disease

Chronic liver disease and cirrhosis is the 12th leading cause of death in the United States and other liver disease complications account for an additional 20,000 deaths per year (53, 54). While there are over 100 different types of liver disease, they can be grouped into three categories: chronic liver disease due to metabolic dysfunction in the absence of scarring, acute liver failure associated with normal architecture but loss of hepatocyte function, and chronic liver failure with cirrhosis (55). Metabolic diseases such as urea cycle disorders, Crigler-Najjar syndrome and familial hypercholesterolaemia are often caused by defects in single enzymes or transport proteins and are seen as good clinical candidates of hepatocyte transplantation therapy as an alternative to orthotopic liver transplantation (56, 57). Acute liver failure (ALF) is the rapid formation (less than 26 weeks) of severe liver injury that can result from a number of causes including various forms of hepatitis, drug induced liver injury, toxin exposure and malignant infiltration, to name a few (58). In most cases, ALF effects liver cell function without large-scale damage to liver architecture and orthotopic liver transplantation is the only treatment. However, the rapid progression of the disease often makes transplantation difficult, with death without transplantation occurring in 30% of ALF patients (58).

Most often, chronic liver failure is accompanied by cirrhosis, the late stages of fibrosis in which there is large distortion of hepatic architecture and the formation of regenerative nodules. The most common causes of cirrhosis include alcohol abuse, chronic hepatitis C and nonalcoholic fatty liver disease (NAFLD) caused by obesity and diabetes (59). Advanced liver fibrosis is characterized by accumulation of fibrillar collagens type I and III in the sinusoidal space resulting in liver failure and portal hypertension (60). This event

is initiated by damage to hepatocytes, which triggers an inflammatory response, including the stimulation of Kupffer cells. Factors released by Kupffer cells trigger activation of hepatic stellate cells which transition into myofibroblasts and deposit fibrillar ECM in the space of Disse. This scar tissue formation leads to loss of hepatocyte microvilli and endothelial fenestrae resulting in hepatocyte impairment (60, 61). As with most liver diseases, orthotopic liver transplantation is the only definitive cure. Extracorporeal bioartifical liver (BAL) devices have been extensively researched to provide a bridge to transplantation to patients on the waiting list to receive a liver. However, BALs suffer from the same limitations that hinder hepatocyte transplantation technology, including the lack of a large-scale and highly functional cell source (62).

2.3. Liver and Cancer

Hepatocellular carcinoma (HCC) is the 3rd leading cause of cancer related deaths worldwide and accounts for 90% of primary liver cancers in the United States (63). HCC usually results from chronic liver disease with cirrhosis, particularly in patients with hepatitis B and C (63). There are numerous mechanisms involved in the pathogenesis of HCC depending on the particular risk factor. Inflammatory responses as a result of viral infections or cirrhosis may lead to activation of a stem cell compartment and genetic alterations to the hepatocyte population leading to cancerous growth, although understanding of the disease pathogenesis is still limited (64). Cholangiocarcinomas account for the other 10% of primary liver cancers in the US and is an epithelial cancer originating from liver bile ducts. Although much is unknown about the disease pathogenesis, it is postulated that cholangiocarcinomas results from malignant transformation of cholangiocytes and possibly hepatic stem and progenitor cells (65).

The liver is the most common site for metastasis from solid tumors, especially in cases of colorectal cancer (CRC). CRC is the third most common cancer and third leading cause of cancer death in both men and women in the United States (66). In almost 30% of cases, the original cancer metastasizes to the liver which is the major cause of death of patients with CRC (67). CRC frequently metastasize to the liver due to colon and upper rectal drainage directly into the hepatic-portal circulatory system (68). Once in the liver, the cancer spreads easily into the parenchyma of the tissue due to the leaky nature of hepatic sinusoids, with large fenestrae in between sinusoidal endothelial cells through which the cancer cells can easily migrate (69). Treatment options include surgical resection, tumor ablation, regional chemotherapy and radiation therapy, although surgery is the only treatment associated with a survival plateau.

3. Liver Tissue Engineering

3.1. Methods of Liver Tissue Engineering

1 in 10 Americans suffer from some sort of liver disease, including hepatitis C, non-alcoholic fatty liver disease, and liver cancer. Complications from these diseases can escalate to a point where the liver can no longer regenerate itself and organ transplantation is the only viable treatment option (3). Currently, there are over 15,000 patients on the waiting list to receive a donor liver in the US. However, based on the Organ Procurement and Transplantation Network (OPTN) data from 2014 there were fewer than 6,000 transplants performed. Liver tissue engineering emerged from the need to find alternative sources to orthotopic liver transplantation. The concept of tissue engineering, in its broadest sense, is to create tissues in the lab that can serve to aid in the repair or regeneration of the failing organ. The tissue engineering process starts with a supporting

scaffold, either a synthetic or biological material, which is then seeded with cells and matured in the lab to create functional tissue.

Early research in liver bioengineering began with studies transplanting hepatocytes, the cells responsible for the majority of liver functions. This technique has been used with varying success in patients with several metabolic diseases (70-74), acute liver disease (75-78) and chronic liver diseases (75, 76, 79). Current limitations of this procedure include lack of standardized and high quality donor hepatocytes, cell loss immediately after transplantation and cell engraftment (80). Reasons for low cell engraftment and survival observed in hepatocyte transplantations include immuno-destruction by the host tissue and the lack of microenvironmental components, including the ECM, to aid in cellular homing and engraftment (81).

The next advancements in liver tissue engineering involved the development of *in vitro* culture systems that improved survival and function of cultured hepatocytes. Researchers identified the importance of ECM components and configuration in improving hepatocyte function in culture, with initial studies performed in a collagen sandwich system (82). Subsequent studies have focused on optimization of substrate morphology and ECM composition in *in vitro* hepatocyte cultures through varying techniques from micro-patterning substrates to using liver-specific ECM (83-86). A parallel, but somewhat opposing approach to optimizing hepatocyte function was the development of cell spheroid systems that forced cell-cell interactions through micro-gravitation or non-adherent substrates to improve cell function (87-89). In all these *in vitro* systems, the importance of co-culturing hepatocytes with other liver cells became apparent (90). Other cell types, including biliary cells and non-epithelial support cells, not only interact directly with

hepatocytes through cell-cell adhesion, but they also secrete ECM and paracrine factors that influence hepatocyte fate (91). Many of these *in vitro* strategies have been used to improve Bioartificial Liver (BAL) technology. Extracorporeal BAL devices are designed to provide temporary support to patients awaiting whole organ transplantation. Hollow fiber devices allow the hepatocytes to attach to a substrate and self-organize (92). Other designs have incorporated hepatocyte spheroids (93) and co-culture systems (94) to improve cell viability and function.

While cell transplantation and BAL may be able to provide temporary support to patients waiting for liver transplantations, researchers began investigating ways to create more permanent structures to reside within the liver. These early tissue engineered constructs demonstrated the functional advantages of culturing hepatocytes in three-dimensional and ECM-rich environments, which improved the functionality and viability of the cells as well as providing structural support and protection from the host immune system (95). The earliest research in liver cell-scaffold constructs used porous biodegradable synthetic polymers such as polyglycolic acid (PGA) or polylactic acid (PLA) (96-98). Initial studies demonstrated the need for vascularization of the scaffold in order to provide oxygen and nutrient transport to the implanted cells. Multiple approaches have been taken to address this need, including pre-vascularization of the scaffold by implantation into the mesenteric space (99), and growth factor release driven neovascularization (100, 101). While some studies have resulted in increased survival in animals with acute and chronic liver failure (102, 103), the issues of cell survival and engraftment remain. Additionally, these tissue engineered constructs do not efficiently

integrate with the host tissue, lack the ideal microenvironment for liver cells and are not properly vascularized (104).

3.2. Engineering Livers for Transplantation

Driven by the limitations in the approaches described above, our lab and others have applied the technique of tissue decellularization initially developed in the whole heart (105) to the liver (104, 106-109). This technique removes all of the cellular components of the organ, while retaining the intact vascular network, extracellular matrix components and tissue micro-architecture. These key components can provide specific hepatic cues for cell survival, proliferation, differentiation and function. The retained vascular network allows the scaffold to be connected to native portal and biliary circulations upon implantation and thus providing oxygen and nutrient transport to the cells. Following decellularization, native liver cells have been introduced into the scaffold and implanted in animals (104, 106, 108, 110-112). While the decellularization approach has shown promising results with definite advantages over earlier approaches, there are still many challenges to address. These include graft survival upon transplantation, improved tissue organization necessary for physiological functionality and scalability and manufacturability of the technology.

3.3. Sources of Cells in Liver Tissue Engineering

Perhaps the most obvious cell choice for engineering liver tissue is to repopulate a scaffold with cell types that are found in the adult human liver. Primary hepatocytes can have functional advantages over less mature liver cells including metabolism and transport functions which are particularly important when studying drug metabolism and toxicity (113). A number of groups have used freshly isolated primary hepatocytes from animal

tissue to repopulate decellularized liver, including rat (104), mouse (108) and pig (112). However, there is limited availability of high quality human hepatocytes, even as methods in cryopreservation have improved and commercial sources have become available (114). This has led to another approach in liver bioengineering using fetal liver progenitor cells, known as hepatoblasts (106, 111). Hepatoblasts have the capability to differentiate into both hepatocytes and cholangiocytes and therefore allows the construction of a tissue with a biliary component. More recently, the use of induced pluripotent stem cells (iPSC) have been intensely researched because the source could be potentially limitless and also patient specific (115-118). The use of stem and progenitor cell sources in liver bioengineering also allows studies into liver development and developmental diseases; applications that are not possible with adult cell sources. A third option for liver bioengineering epithelial cell sources are cell lines. HepG2 cells are the most commonly used liver cell line. Derived from well differentiated hepatocellular carcinoma, HepG2 cells secrete plasma proteins such as albumin and express most phase 1 and 2 enzymes. However, their genetic profile differs from primary hepatocytes and they can underestimate metabolic-dependent toxicity (119). Due to these limitations, HepG2 cells must be used with caution, especially in predictive studies, although their unlimited availability and ease of use makes them a great model for proof-of-concept studies.

When engineering liver tissue, it is also crucial to consider the non-parenchymal liver cells that are vital to tissue homeostasis in health and disease. Endothelial cells are crucial in establishing patent vasculature for any transplantation applications, but are also important in the secretion of paracrine factors that drive tissue development and organization (33). Thus far, studies have used vascular endothelial cells for repopulation

(104, 106) although future work might require the use of sinusoidal endothelial cells that possess specialized structures for liver-specific functions. Another important cell type are the hepatic stellate cells which secrete paracrine factors as well as deposit ECM proteins (111). Although there are commercial sources for stellate cells, they can be difficult to culture long-term due to their de-differentiation into myofibroblasts. Finally, it may be important to include Kupffer cells into the bioengineered liver, as they place a crucial role in the immune response within the liver (120).

3.4. Liver Model Systems

While the evolution and perhaps primary objective of liver tissue engineering has been focused on generating organs for transplantation, bioengineered livers can be valuable tools in studying liver development, diseases and drug metabolism and toxicity. The distinct advantage bioengineered livers have over other models across all of these applications is the ability to re-create the native liver microenvironment. This includes culturing multiple cell types in liver-specific ECM, allowing physiological cell-cell and cell-matrix interactions that are crucial to organ function. Since for these model purposes transplantation is a non-factor, many approaches have used microfabrication, microfluidics, and other high-throughput, high-precision techniques to build artificial livers from the bottom up (121). An alternative approach is to allow liver tissue to self-assemble through the use of stem cells (115). The next sections will detail current models to study liver development, disease, and drug toxicity and describe the advantages and progress of bioengineered livers in each application.

3.4.1. Models of Liver Development

Research in human development is driven not only by a quest to fully comprehend human life but also to study numerous diseases that are caused by developmental defects. Compared to other areas of science, however, human embryonic development is very difficult to study and as a result, there is still very much to learn. Liver organogenesis is a highly coordinated cascade of multiple signaling events that drives stem cell differentiation, tissue organization and organ function. Replicating this complexity *in vitro* has remained elusive; therefore much of what we have studied concerning liver development has taken place in model organisms. While animal models in mice, chicks, xenopus and zebrafish have led to much progress in understanding liver organogenesis (25, 122), there are limitations in using these models to understand human development and diseases (123). For example, roughly 1% of human genes do not have a mouse homolog (124) and there can be important differences in gestational stages and spatial and temporal regulation of organ development between species (123). As a result, animal models may not serve as the best system for studying human disease (123).

Other important constraints in the use of animal models to study liver development and developmental diseases include high-cost as well as a lack of "real-time" results because animal studies often only result in end point snapshots. For these reasons, many researchers have used various stem cell systems to study human development (123, 125). However, cell-only systems lack the surrounding microenvironment that provides important signals driving tissue development. In particular, decellularized liver consists of organ specific ECM which plays a significant role in liver development and developmental diseases (17, 126, 127) and can direct differentiation and organization of human liver

progenitor cells (106, 128). A liver tissue engineering approach may also include multiple cell types, including both epithelial and non-epithelial support cells. In liver development, non-epithelial cells including sinusoidal and vascular endothelial cells, stellate cells, Kupffer cells, angioblasts and fibroblasts all play roles in a highly coordinated effort driving organogenesis (33, 44, 129-131). Seeding acellular liver scaffolds with liver progenitor cells in addition to this supporting cell population can recapitulate important events in liver organogenesis include hepatocyte maturation and bile duct formation (128).

A bioengineered liver using liver progenitor cells can not only allow us to better understand human liver development, but it can provide a valuable platform to study developmental diseases. For example, there are a myriad of diseases associated with improper biliary development (132). A bioengineered liver construct could be designed to study bile duct morphogenesis in health and disease and subsequently be used as a drug screening tool to identify compounds that target these deficiencies. Overall, a tissue engineered model of liver development will address many limitations of animal studies and cell-only systems and has potential to be a valuable resource for the scientific community.

3.4.2. Models of Liver Disease

It is estimated that over 30 million Americans are living with some form of liver disease, of which there are over 100 different types (54). Diseases affecting the liver include infectious diseases, such as hepatitis or malaria, metabolic disorders, non-alcoholic fatty-liver disease (NAFLD) and liver cancers. The development of highly functional and accurate models of liver disease could drive further understanding of disease progression, identify methods for diagnosis and detection and lead to new therapies and treatments.

While animal models can recapitulate many disease manifestations, the underlying mechanisms driving disease progression may differ greatly from humans (133). For this reason, many researchers are moving towards the use of human cells to study disease. However, hepatocytes, often the target for disease studies, lose phenotype and functionality in two dimensional conditions (84, 134) and these models lack the interaction with other cell types and the underlying ECM, which are critical factors in many liver diseases.

One technique of modeling liver disease researches infectious diseases that target hepatocytes, such as hepatitis C virus (HCV) and malaria. Only recently has it been possible to examine HCV infection in hepatocytes, which was accomplished by the development of a micro-scale system that cultures hepatocytes on collagen substrates and subsequently seeds them with stromal support cells (135, 136). This microsystem is capable of generating the infectious virus, which has not been achieved in standard hepatocyte cultures and highlights the importance of physiological microenvironments. This same platform was also used to examine the infection of hepatocytes with the malaria parasites *Plasmodium falciparum and vivax* (137). Another large class of liver diseases are metabolic disorders, which result from genetic mutations affecting key proteins in hepatocytes. One approach to studying these diseases has been using induced pluripotent stem cells (iPSC) from patients with metabolic disorders to develop mature liver cells with patient specific mutations (138, 139). Integrating these techniques with other tissue engineering components including 3D ECM and multiple cell types could lead to patient-specific metabolic disease models. A similar approach could be used to look at the effects of genetically engineered iPSC derived hepatocytes on complicated liver diseases such as NAFLD (140). Liver cancer is another class of liver disease that would greatly benefit from

accurate *in vivo* models. Hepatocellular carcinoma has been shown to display increased growth, chemotherapy resistance and functionality when cultured in ECM scaffolds under dynamic perfusion compared to traditional culture methods (141, 142). Finally, liver fibrosis, a disease state in which the ECM surrounding liver cells gets inherently stiffer, has been researched using tunable polyacrylamide gels in order to understand the role of substrate stiffness on stellate cell activation (143). Decellularized liver, which consists of not only liver-specific ECM proteins but also the physiological micro-architecture that cells experience *in vivo*, could greatly enhance tissue engineered liver disease models by providing the necessary environment for cells to behave as they would in the human body.

3.4.3. Models of Cancer Metastasis

Cancer metastasis is the major cause of cancer-related deaths, yet many of the mechanisms governing this process are not well understood. Animal models often fall short in properly mimicking the complex process of human metastasis and are limited by time, quantity, and confinement to endpoint snapshots (144). Tissue engineered constructs can provide an ideal platform to study cancer metastasis due to the ability to replicate the tumor microenvironment. Multiple studies have demonstrated the benefit of tissue engineering techniques, including three dimensionality, co-cultures, ECM components and dynamic culture in metastatic research (145-148). Decellularized liver shows large potential in modeling liver metastasis due to the organ-specific ECM and the potential for microenvironmental perturbations, such as studying the effects of stiffness on metastatic behavior (149). This system could also study cell-cell interactions between the invading tumor and the host tissue, providing insight into the mechanisms driving metastatic growth.

3.4.4. Models of Drug Development

The most recent figures for the cost of bringing a drug to market is $2.6 billion with estimates that 90% of drug candidates that enter clinical trials will fail (150). Of the chemical compounds that reach preclinical safety studies in animals, 40% of them fail due to toxicity (150). There is still a great risk of hepatotoxicity in clinically approved drugs, with estimates that 13-50% of all cases of acute liver failure in the U.S. are resulting from drug-induced liver injury (151). As highlighted with these figures, there is a tremendous need for successful models to predict liver toxicity in drug development. In 50% of compounds, animal models fail to capture drugs that cause human liver toxicity and often animal models do not represent the diversity of human patients that may receive a certain drug (152). Human hepatocytes in 2D culture quickly lose liver-specific function and phenotype and are a poor model of the complex liver environment. Tissue engineered constructs are a promising alternative to traditional drug development models due to their ability to replicate human liver functionality to a much higher degree.

Recent research has elucidated the specific requirements needed to engineer a liver with high functionality capable of better predicting human liver drug toxicity. Cells cultured in a 3D environment experience physiological mechanical cues and interaction with ECM components which improves cell phenotype, organization and function (83, 84, 134). Co-culturing hepatocytes with non-parenchymal cells helps improve hepatocyte function, likely due to the release of soluble factors, cell-cell interactions and deposition of ECM (90, 91). Additionally, the immune-mediated response to disease and drug reactions requires the interaction of hepatocytes with other liver cell types, including biliary cells, stellate cells, sinusoidal endothelial cells and Kupffer cells (120, 153). Pluripotent stem

cell technology is particularly promising in the generation of liver organoids for drug development because they provide a theoretically limitless cell source with high levels of functionality. Recently, Takebe *et al* engineered human liver organoids using iPSC derived liver cells alongside mesenchymal and endothelial cells (115).

The applications of *in vitro* liver models in drug discovery are numerous. Besides the ADMET (absorption, distribution, metabolism, excretion, toxicity) analysis needed for a compound to enter human clinical trials, liver models could allow the study of transporter interactions, drug-drug interactions and drug-induced liver injury, to name a few (Khetani, 2015). Key requirements for translating these technologies to the pharmaceutical industry are the development of high-throughput, cost-effective, replicable and highly functional constructs. Recent microfabrication techniques have led to the development of numerous *in vitro* liver models that have demonstrated increased functionality over hepatocyte cultures, the former industry gold-standard alternative to animal models (154-159). As a result, there are several companies specializing in engineered liver models for drug discovery applications, including InSphero, Organovo, Regenemed and Bio Innovations (LiverChip). Decellularized liver technology has high potential in this field due to its benefits on cell organization and functionality, both integral components for drug discovery research. Further advancements in liver tissue engineering will lead to more models that can better predict hepatotoxicity, reduce costs of drug development and ultimately reduce harm to human patients.

References

1. Lautt WW. Hepatic Circulation: Physiology and Pathophysiology. Granger DN, Granger J, editors: Morgan & Claypool Life Sciences; 2010.
2. Koeppen BM, Stanton BA. Berne & Levy Physiology. 6 ed. Philadelphia, Pennsylvania: Mosby Elsevier; 2010.
3. Zakim D, Boyer TD. Hepatology: A Textbook of Liver Disease. 4 ed. Philadelphia, Pennsylvania: Saunders; 2003.
4. Frank H. Netter M. The Netter Collection of Medical Illustrations- Digestive System. 1st ed: Elsevier; 1964.
5. Ishibashi H, Nakamura M, Komori A, Migita K, Shimoda S. Liver architecture, cell function, and disease. Seminars in Immunopathology. 2009 Sep;31(3):399-409. PubMed PMID: WOS:000270326500010.
6. Damania A, Jain E, Kumar A. Advancements in in vitro hepatic models: application for drug screening and therapeutics. Hepatology International. 2014 Jan;8(1):23-38. PubMed PMID: WOS:000330808600006. English.
7. Si-Tayeb K, Lemaigre FP, Duncan SA. Organogenesis and Development of the Liver. Developmental Cell. 2010 Feb;18(2):175-89. PubMed PMID: WOS:000275100400005.
8. Guyton A, Hall J. Human Physiology and Mechanisms of Disease. 6th ed. Philadelphia, Pa: Saunders; 1997.
9. Saxena R, Theise N. Canals of Hering: Recent insights and current knowledge. Seminars in Liver Disease. 2004 Feb;24(1):43-8. PubMed PMID: WOS:000220926900004.
10. Martini FH, Timmons MJ, Tallitsch RB. Human Anatomy. 6 ed. San Francisco, CA: Pearson Benjamin Cummings; 2009.
11. Kordes C, Haussinger D. Hepatic stem cell niches. Journal of Clinical Investigation. 2013 May;123(5):1874-80. PubMed PMID: WOS:000319025100006.
12. Smedsrod B, Debleser PJ, Braet F, Lovisetti P, Vanderkerken K, Wisse E, et al. CELL BIOLOGY OF LIVER ENDOTHELIAL AND KUPFFER CELLS. Gut. 1994 Nov;35(11):1509-16. PubMed PMID: WOS:A1994PN99000002.
13. Yin CY, Evason KJ, Asahina K, Stainier DYR. Hepatic stellate cells in liver development, regeneration, and cancer. Journal of Clinical Investigation. 2013 May;123(5):1902-10. PubMed PMID: WOS:000319025100009. English.
14. Marzioni M, Glaser SS, Francis H, Phinizy JL, LeSage G, Alpini G. Functional heterogeneity of cholangiocytes. Seminars in Liver Disease. 2002 Aug;22(3):227-40. PubMed PMID: WOS:000178344300003. English.
15. D'Angelo A, Franco B. The primary cilium in different tissues-lessons from patients and animal models. Pediatric Nephrology. 2011 May;26(5):655-62. PubMed PMID: WOS:000288712800002.
16. Martinezhernandez A, Amenta PS. THE HEPATIC EXTRACELLULAR-MATRIX .1. COMPONENTS AND DISTRIBUTION IN NORMAL LIVER. Virchows Archiv a-Pathological Anatomy and Histopathology. 1993 Jul;423(1):1-11. PubMed PMID: WOS:A1993LU94800001.
17. Amenta PS, Harrison D. Expression and potential role of the extracellular matrix in hepatic ontogenesis: A review. Microscopy Research and Technique. 1997 Nov;39(4):372-86. PubMed PMID: WOS:A1997YJ73600007.
18. Bedossa P, Paradis V. Liver extracellular matrix in health and disease. Journal of Pathology. 2003 Jul;200(4):504-15. PubMed PMID: WOS:000183925700010. English.
19. Fausto N, Campbell JS, Riehle KJ. Liver regeneration. Hepatology. 2006 Feb;43(2):S45-S53. PubMed PMID: WOS:000235193700013. English.
20. Michalopoulos GK. Liver regeneration. Journal of Cellular Physiology. 2007 Nov;213(2):286-300. PubMed PMID: WOS:000249938900002. English.

21. Michalopoulos GK. Liver Regeneration after Partial Hepatectomy Critical Analysis of Mechanistic Dilemmas. American Journal of Pathology. 2010 Jan;176(1):2-13. PubMed PMID: WOS:000274111200001.
22. Taub R. Liver regeneration: From myth to mechanism. Nature Reviews Molecular Cell Biology. 2004 Oct;5(10):836-47. PubMed PMID: WOS:000224558200017.
23. Sato Y, Koyama S, Tsukada K, Hatakeyama K. Acute portal hypertension reflecting shear stress as a trigger of liver regeneration following partial hepatectomy. Surgery Today-the Japanese Journal of Surgery. 1997;27(6):518-26. PubMed PMID: WOS:A1997XB00900007.
24. Fausto N. Liver regeneration and repair: Hepatocytes, progenitor cells, and stem cells. Hepatology. 2004 Jun;39(6):1477-87. PubMed PMID: WOS:000221849000002. English.
25. Zong YW, Stanger BZ. Molecular mechanisms of liver and bile duct development. Wiley Interdisciplinary Reviews-Developmental Biology. 2012 Sep-Oct;1(5):643-55. PubMed PMID: WOS:000321263100003.
26. Zaret KS. Regulatory phases of early liver development: Paradigms of organogenesis. Nature Reviews Genetics. 2002 Jul;3(7):499-512. PubMed PMID: WOS:000176563400012.
27. McLin VA, Rankin SA, Zorn AM. Repression of Wnt/beta-catenin signaling in the anterior endoderm is essential for liver and pancreas development. Development. 2007 Jun;134(12):2207-17. PubMed PMID: WOS:000247720000002.
28. Goessling W, North TE, Lord AM, Ceol C, Lee S, Weidinger G, et al. APC mutant zebrafish uncover a changing temporal requirement for wnt signaling in liver development. Developmental Biology. 2008 Aug;320(1):161-74. PubMed PMID: WOS:000258262500017.
29. Zhao RO, Watt AJ, Li JX, Luebke-Wheeler J, Morrisey EE, Duncan SA. GATA6 is essential for embryonic development of the liver but dispensable for early heart formation. Molecular and Cellular Biology. 2005 Apr;25(7):2622-31. PubMed PMID: WOS:000227679000009.
30. Sosa-Pineda B, Wigle JT, Oliver G. Hepatocyte migration during liver development requires Prox1. Nature Genetics. 2000 Jul;25(3):254-5. PubMed PMID: WOS:000087920900007.
31. Ludtke THW, Christoffels VM, Petry M, Kispert A. Tbx3 Promotes Liver Bud Expansion During Mouse Development by Suppression of Cholangiocyte Differentiation. Hepatology. 2009 Mar;49(3):969-78. PubMed PMID: WOS:000263817000030.
32. Margagliotti S, Clotman F, Pierreux CE, Beaudry JB, Jacquemin P, Rousseau GG, et al. The Onecut transcription factors HNF-6/OC-1 and OC-2 regulate early liver expansion by controlling hepatoblast migration. Developmental Biology. 2007 Nov;311(2):579-89. PubMed PMID: WOS:000251123900025.
33. Matsumoto K, Yoshitomi H, Rossant J, Zaret KS. Liver organogenesis promoted by endothelial cells prior to vascular function. Science. 2001 Oct 19;294(5542):559-63. PubMed PMID: WOS:000171695600037.
34. Suksaweang S, Lin CM, Jiang TX, Hughes MW, Widelitz RB, Chuong CM. Morphogenesis of chicken liver: identification of localized growth zones and the role of beta-catenin/Wnt in size regulation. Developmental Biology. 2004 Feb;266(1):109-22. PubMed PMID: WOS:000188931200009.
35. Tan XP, Yuan YZ, Zeng G, Apte U, Thompson MD, Cieply B, et al. beta-catenin deletion in hepatoblasts disrupts hepatic morphogenesis and survival during mouse development. Hepatology. 2008 May;47(5):1667-79. PubMed PMID: WOS:000255507500026.
36. Schmidt C, Bladt F, Goedecke S, Brinkmann V, Zschiesche W, Sharpe M, et al. SCATTER FACTOR/HEPATOCYTE GROWTH-FACTOR IS ESSENTIAL FOR LIVER DEVELOPMENT. Nature. 1995 Feb;373(6516):699-702. PubMed PMID: WOS:A1995QH92800054.
37. Berg T, Rountree CB, Lee LL, Estrada JQ, Sala FG, Choe A, et al. Fibroblast growth factor 10 is critical for liver growth during embryogenesis and controls hepatoblast survival via

beta-catenin activation. Hepatology. 2007 Oct;46(4):1187-97. PubMed PMID: WOS:000249910500029.
38. Einstein M, Monga SPS, Liu Y, Brodie SG, Tang Y, Li CL, et al. Smad proteins and hepatocyte growth factor control parallel regulatory pathways that converge on beta 1-integrin to promote normal liver development. Molecular and Cellular Biology. 2001 Aug;21(15):5122-31. PubMed PMID: WOS:000169829800026.
39. Nishina H, Vaz C, Billia P, Nghiem M, Sasaki T, De la Pompa JL, et al. Defective liver formation and liver cell apoptosis in mice lacking the stress signaling kinase SEK1/MKK4. Development. 1999 Feb;126(3):505-16. PubMed PMID: WOS:000078713700008.
40. Clotman F, Jacquemin P, Plumb-Rudewiez N, Pierreux CE, Van der Smissen P, Dietz HC, et al. Control of liver cell fate decision by a gradient of TGF beta signaling modulated by Onecut transcription factors. Genes & Development. 2005 Aug;19(16):1849-54. PubMed PMID: WOS:000231277600004.
41. Zong YW, Panikkar A, Xu J, Antoniou A, Raynaud P, Lemaigre F, et al. Notch signaling controls liver development by regulating biliary differentiation. Development. 2009 May;136(10):1727-39. PubMed PMID: WOS:000265529200015.
42. Yanai M, Tatsumi N, Hasunuma N, Katsu K, Endo F, Yokouchi Y. FGF signaling segregates biliary cell-lineage from chick hepatoblasts cooperatively with BMP4 and ECM components in vitro. Developmental Dynamics. 2008 May;237(5):1268-83. PubMed PMID: WOS:000255842900006.
43. Decaens T, Godard C, de Reynies A, Rickman DS, Tronche F, Couty JP, et al. Stabilization of beta-catenin affects mouse embryonic liver growth and hepatoblast fate. Hepatology. 2008 Jan;47(1):247-58. PubMed PMID: WOS:000252143200032.
44. Lemaigre FP. Mechanisms of Liver Development: Concepts for Understanding Liver Disorders and Design of Novel Therapies. Gastroenterology. 2009 Jul;137(1):62-79. PubMed PMID: WOS:000267410100016.
45. Kamiya A, Kinoshita T, Ito Y, Matsui T, Morikawa Y, Senba E, et al. Fetal liver development requires a paracrine action of oncostatin M through the gp130 signal transducer. Embo Journal. 1999 Apr;18(8):2127-36. PubMed PMID: WOS:000079959200012.
46. Sakaguchi TF, Sadler KC, Crosnier C, Stainier DYR. Endothelial Signals Modulate Hepatocyte Apicobasal Polarization in Zebrafish. Current Biology. 2008 Oct;18(20):1565-71. PubMed PMID: WOS:000260551400026.
47. Torre C, Perret C, Colnot S. Transcription dynamics in a physiological process: beta-Catenin signaling directs liver metabolic zonation. International Journal of Biochemistry & Cell Biology. 2011 Feb;43(2):271-8. PubMed PMID: WOS:000287115600014.
48. Geisler F, Nagl F, Mazur PK, Lee M, Zimber-Strobl U, Strobl LJ, et al. Liver-specific inactivation of Notch2, but not Notch1, compromises intrahepatic bile duct development in mice. Hepatology. 2008 Aug;48(2):607-16. PubMed PMID: WOS:000258247400027.
49. Raynaud P, Carpentier R, Antoniou A, Lemaigre FP. Biliary differentiation and bile duct morphogenesis in development and disease. International Journal of Biochemistry & Cell Biology. 2011 Feb;43(2). PubMed PMID: WOS:000287115600011.
50. McDaniell R, Warthen DM, Sanchez-Lara PA, Pai A, Krantz ID, Piccoli DA, et al. NOTCH2 mutations cause Alagille syndrome, a heterogeneous disorder of the notch signaling pathway. American Journal of Human Genetics. 2006 Jul;79(1):169-73. PubMed PMID: WOS:000238341200019.
51. Gouysse G, Couvelard A, Frachon S, Bouvier R, Nejjari M, Dauge MC, et al. Relationship between vascular development and vascular differentiation during liver organogenesis in humans. Journal of Hepatology. 2002 Dec;37(6):730-40. PubMed PMID: WOS:000179584700004.

52. Collardeau-Frachon S, Scoazec J-Y. Vascular development and differentiation during human liver organogenesis. Anatomical Record-Advances in Integrative Anatomy and Evolutionary Biology. 2008 Jun;291(6):614-27. PubMed PMID: WOS:000256718800002.
53. Kim R, Brown R, Terrault N, El-Serag H. Burden of liver disease in the United States: Summary of a workshop Atlanta, GA2001.
54. Murphy SL, Xu J, Kochanek KD. Deaths: Final Data for 2010. Hyattsville, MD: National Center for Health Statistics, 2013 Contract No.: 4.
55. Bhatia SN, Underhill GH, Zaret KS, Fox IJ. Cell and tissue engineering for liver disease. Science Translational Medicine. 2014 Jul;6(245). PubMed PMID: WOS:000339661200002.
56. Dhawan A, Mitry RR, Hughes RD. Hepatocyte transplantation for liver-based metabolic disorders. Journal of Inherited Metabolic Disease. 2006 Apr;29(2-3):431-5. PubMed PMID: WOS:000238156500029. English.
57. Jorns C, Ellis EC, Nowak G, Fischler B, Nemeth A, Strom SC, et al. Hepatocyte transplantation for inherited metabolic diseases of the liver. Journal of Internal Medicine. 2012 Sep;272(3):201-23. PubMed PMID: WOS:000307958000001. English.
58. Lee WM, Squires RH, Nyberg SL, Doo E, Hoofnagle JH. Acute liver failure: Summary of a workshop. Hepatology. 2008 Apr;47(4):1401-15. PubMed PMID: WOS:000254637100032.
59. Heidelbaugh JJ, Bruderly M. Cirrhosis and chronic liver failure: Part I. Diagnosis and evaluation. American Family Physician. 2006 Sep;74(5):756-62. PubMed PMID: WOS:000240324000008. English.
60. Iredale JP. Models of liver fibrosis: exploring the dynamic nature of inflammation and repair in a solid organ. Journal of Clinical Investigation. 2007 Mar;117(3):539-48. PubMed PMID: WOS:000244662500009.
61. Friedman SL. Molecular regulation of hepatic fibrosis, an integrated cellular response to tissue injury. Journal of Biological Chemistry. 2000 Jan;275(4):2247-50. PubMed PMID: WOS:000085128000001.
62. Carpentier B, Gautier A, Legallais C. Artificial and bioartificial liver devices: present and future. Gut. 2009 Dec;58(12):1690-702. PubMed PMID: WOS:000271911900024.
63. Altekruse SF, McGlynn KA, Reichman ME. Hepatocellular Carcinoma Incidence, Mortality, and Survival Trends in the United States From 1975 to 2005. Journal of Clinical Oncology. 2009 Mar;27(9):1485-91. PubMed PMID: WOS:000266194000025.
64. Farazi PA, DePinho RA. Hepatocellular carcinoma pathogenesis: from genes to environment. Nature Reviews Cancer. 2006 Sep;6(9):674-87. PubMed PMID: WOS:000240025600014. English.
65. Blechacz B, Gores GJ. Cholangiocarcinoma: Advances in pathogenesis, diagnosis, and treatment. Hepatology. 2008 Jul;48(1):308-21. PubMed PMID: WOS:000257301100035. English.
66. Siegel R, Jemal A. Colorectal Cancer Facts & Figures 2014-2016. Atlanta: American Cancer Society, 2014.
67. Manfredi S, Lepage C, Hatem C, Coatmeur O, Faivre J, Bouvier AM. Epidemiology and management of liver metastases from colorectal cancer. Annals of Surgery. 2006 Aug;244(2):254-9. PubMed PMID: WOS:000239358700012.
68. Chambers AF, Groom AC, MacDonald IC. Dissemination and growth of cancer cells in metastatic sites. Nature Reviews Cancer. 2002 Aug;2(8):563-72. PubMed PMID: WOS:000180447300010. English.
69. Gupta GP, Massague J. Cancer metastasis: Building a framework. Cell. 2006 Nov;127(4):679-95. PubMed PMID: WOS:000242330600016.
70. Fox IJ, Chowdhury JR, Kaufman SS, Goertzen TC, Chowdhury NR, Warkentin PI, et al. Treatment of the Crigler-Najjar syndrome type I with hepatocyte transplantation. New England Journal of Medicine. 1998 May 14;338(20):1422-6. PubMed PMID: WOS:000073563700004.

71. Horslen SP, McCowan TC, Goertzen TC, Warkentin PI, Cai HB, Strom SC, et al. Isolated hepatocyte transplantation in an infant with a severe urea cycle disorder. Pediatrics. 2003 Jun;111(6):1262-7. PubMed PMID: WOS:000183696000018.
72. Ambrosino G, Varotto S, Strom SC, Guariso G, Franchin E, Miotto D, et al. Isolated hepatocyte transplantation for Crigler-Najjar syndrome type 1. Cell Transplantation. 2005 2005;14(2-3):151-7. PubMed PMID: WOS:000228757800009.
73. Muraca M, Gerunda G, Neri D, Vilei MT, Granato A, Feltracco P, et al. Hepatocyte transplantation as a treatment for glycogen storage disease type 1a. Lancet. 2002 Jan 26;359(9303):317-8. PubMed PMID: WOS:000173588100014.
74. Sokal EM, Smets F, Bourgois A, Van Maldergem L, Buts JP, Reding R, et al. Hepatocyte transplantation in a 4-year-old girl with peroxisomal biogenesis disease: Technique, safety, and metabolic follow-up. Transplantation. 2003 Aug 27;76(4):735-8. PubMed PMID: WOS:000185135100024.
75. Strom SC, Fisher RA, Rubinstein WS, Barranger JA, Towbin RB, Charron M, et al. Transplantation of human hepatocytes. Transplantation Proceedings. 1997 Jun;29(4):2103-6. PubMed PMID: WOS:A1997XE83300092.
76. Strom SC, Chowdhury JR, Fox IJ. Hepatocyte transplantation for the treatment of human disease. Seminars in Liver Disease. 1999 1999;19(1):39-48. PubMed PMID: WOS:000080225400005.
77. Strom SC, Fisher RA, Thompson MT, Sanyal AJ, Cole PE, Ham JM, et al. Hepatocyte transplantation as a bridge to orthotopic liver transplantation in terminal liver failure. Transplantation. 1997 Feb 27;63(4):559-69. PubMed PMID: WOS:A1997WL85500014.
78. Soriano HE, Wood RP, Kang DC, Ozaki CF, Finegold MJ, Bischoff FC, et al. Hepatocellular transplantation (HCT) in children with fulminant liver failure (FLF). Hepatology. 1997 Oct;26(4):443-. PubMed PMID: WOS:A1997XY87400442.
79. Mito M, Kusano M, Kawaura Y. HEPATOCYTE TRANSPLANTATION IN MAN. Transplantation Proceedings. 1992 Dec;24(6):3052-3. PubMed PMID: WOS:A1992KC41300315.
80. Hughes RD, Mitry RR, Dhawan A. Current Status of Hepatocyte Transplantation. Transplantation. 2012 Feb;93(4):342-7. PubMed PMID: WOS:000300415800006.
81. Soltys KA, Soto-Gutierrez A, Nagaya M, Baskin KM, Deutsch M, Ito R, et al. Barriers to the successful treatment of liver disease by hepatocyte transplantation. Journal of Hepatology. 2010 Oct;53(4):769-74. PubMed PMID: WOS:000282622800025.
82. Dunn JCY, Tompkins RG, Yarmush ML. HEPATOCYTES IN COLLAGEN SANDWICH - EVIDENCE FOR TRANSCRIPTIONAL AND TRANSLATIONAL REGULATION. Journal of Cell Biology. 1992 Feb;116(4):1043-53. PubMed PMID: WOS:A1992HD55000019.
83. Berthiaume F, Moghe PV, Toner M, Yarmush ML. Effect of extracellular matrix topology on cell structure, function, and physiological responsiveness: Hepatocytes cultured in a sandwich configuration. Faseb Journal. 1996 Nov;10(13):1471-84. PubMed PMID: WOS:A1996VU98200004. English.
84. Gomez-Lechon MJ, Jover R, Donato T, Ponsoda X, Rodriguez C, Stenzel KG, et al. Long-term expression of differentiated functions in hepatocytes cultured in three-dimensional collagen matrix. Journal of Cellular Physiology. 1998 Dec;177(4):553-62. PubMed PMID: WOS:000077299700006.
85. Richert L, Binda D, Hamilton G, Viollon-Abadie C, Alexandre E, Bigot-Lasserre D, et al. Evaluation of the effect of culture configuration on morphology, survival time, antioxidant status and metabolic capacities of cultured rat hepatocytes. Toxicology in Vitro. 2002 Feb;16(1):89-99. PubMed PMID: WOS:000173770100011. English.

86. Sellaro TL, Ranade A, Faulk DM, McCabe GP, Dorko K, Badylak SF, et al. Maintenance of Human Hepatocyte Function In Vitro by Liver-Derived Extracellular Matrix Gels. Tissue Engineering Part A. 2010 Mar;16(3):1075-82. PubMed PMID: WOS:000275041500030.
87. Wu FJ, Friend JR, Remmel RP, Cerra FB, Hu WS. Enhanced cytochrome P450IA1 activity of self-assembled rat hepatocyte spheroids. Cell Transplantation. 1999 May-Jun;8(3):233-46. PubMed PMID: WOS:000081623900002.
88. Koide N, Sakaguchi K, Koide Y, Asano K, Kawaguchi M, Matsushima H, et al. FORMATION OF MULTICELLULAR SPHEROIDS COMPOSED OF ADULT-RAT HEPATOCYTES IN DISHES WITH POSITIVELY CHARGED SURFACES AND UNDER OTHER NONADHERENT ENVIRONMENTS. Experimental Cell Research. 1990 Feb;186(2):227-35. PubMed PMID: WOS:A1990CM87700005.
89. Yuasa C, Tomita Y, Shono M, Ishimura K, Ichihara A. IMPORTANCE OF CELL-AGGREGATION FOR EXPRESSION OF LIVER FUNCTIONS AND REGENERATION DEMONSTRATED WITH PRIMARY CULTURED-HEPATOCYTES. Journal of Cellular Physiology. 1993 Sep;156(3):522-30. PubMed PMID: WOS:A1993LU99400010.
90. Guguenguillouzo C, Clement B, Baffet G, Beaumont C, Morelchany E, Glaise D, et al. MAINTENANCE AND REVERSIBILITY OF ACTIVE ALBUMIN SECRETION BY ADULT-RAT HEPATOCYTES CO-CULTURED WITH ANOTHER LIVER EPITHELIAL-CELL TYPE. Experimental Cell Research. 1983;143(1):47-54. PubMed PMID: WOS:A1983QD40000005.
91. Bhatia SN, Balis UJ, Yarmush ML, Toner M. Effect of cell-cell interactions in preservation of cellular phenotype: cocultivation of hepatocytes and nonparenchymal cells. Faseb Journal. 1999 Nov;13(14):1883-900. PubMed PMID: WOS:000083660700001.
92. Kamlot A, Rozga J, Watanabe FD, Demetriou AA. Review: Artificial liver support systems. Biotechnology and Bioengineering. 1996 May;50(4):382-91. PubMed PMID: WOS:A1996UG32600006. English.
93. Park JK, Yoon HH, Lee DH, Lee SK. Development of bioartificial liver system and future perspective of human hepatocyte source. Journal of Biotechnology. 2010 Nov;150:S94-S. PubMed PMID: WOS:000288873400227.
94. Sauer IM, Neuhaus P, Gerlach JC. Concept for modular extracorporeal liver support for the treatment of acute hepatic failure. Metabolic Brain Disease. 2002 Dec;17(4):477-84. PubMed PMID: WOS:000180326700026. English.
95. Smith MK, Mooney DJ. Biomaterials in Liver Tissue Engineering. e-biomed. 2000;1:65-73. Epub May 17, 2000.
96. Davis MW, Vacanti JP. Toward development of an implantable tissue engineered liver. Biomaterials. 1996 Feb;17(3):365-72. PubMed PMID: WOS:A1996TY45900016.
97. Mikos AG, Sarakinos G, Lyman MD, Ingber DE, Vacanti JP, Langer R. PREVASCULARIZATION OF POROUS BIODEGRADABLE POLYMERS. Biotechnology and Bioengineering. 1993 Sep;42(6):716-23. PubMed PMID: WOS:A1993LT78000005.
98. Kaufmann PM, Heimrath S, Kim BS, Mooney DJ. Highly porous polymer matrices as a three-dimensional culture system for hepatocytes. Cell Transplantation. 1997 Sep-Oct;6(5):463-8. PubMed PMID: WOS:A1997XZ17400003.
99. Uyama S, Kaufmann PM, Takeda T, Vacanti JP. DELIVERY OF WHOLE LIVER EQUIVALENT HEPATOCYTE MASS USING POLYMER DEVICES AND HEPATOTROPHIC STIMULATION. Transplantation. 1993 Apr;55(4):932-5. PubMed PMID: WOS:A1993KY80000045.
100. Sheridan MH, Shea LD, Peters MC, Mooney DJ. Bioadsorbable polymer scaffolds for tissue engineering capable of sustained growth factor delivery. Journal of Controlled Release. 2000 Feb;64(1-3):91-102. PubMed PMID: WOS:000085378900009.
101. Kedem A, Perets A, Gamlieli-Bonshtein I, Dvir-Ginzberg M, Mizrahi S, Cohen S. Vascular endothelial growth factor-releasing scaffolds enhance vascularization and engraftment

of hepatocytes transplanted on liver lobes. Tissue Engineering. 2005 May;11(5-6):715-22. PubMed PMID: WOS:000230320600007.
102. Soto-Gutierrez A, Navarro-Alvarez N, Rivas-Carrillo JD, Tanaka K, Chen Y, Misawa H, et al. Construction and transplantation of an engineered hepatic tissue using a polyaminourethane-coated nonwoven polyteltrafluoroethylene fabric. Transplantation. 2007 Jan;83(2):129-37. PubMed PMID: WOS:000243955000002.
103. Navarro-Alvarez N, Soto-Gutierrez A, Chen Y, Caballero-Corbalan J, Hassan W, Kobayashi S, et al. Intramuscular transplantation of engineered hepatic tissue constructs corrects acute and chronic liver failure in mice. Journal of Hepatology. 2010 Feb;52(2):211-9. PubMed PMID: WOS:000275390500012.
104. Uygun B, Soto-Gutierrez A, Yagi H, Izamis M, Guzzardi M, Shulman C, et al. Organ reengineering through development of a transplantable recellularized liver graft using decellularized liver matrix. Nat Med. 2010 Jul;16(7):814-20. PubMed PMID: 20543851. PMCID: PMC2930603. eng.
105. Ott H, Matthiesen T, Goh S, Black L, Kren S, Netoff T, et al. Perfusion-decellularized matrix: using nature's platform to engineer a bioartificial heart. Nature Medicine. 2008 FEB 2008;14(2):213-21. PubMed PMID: ISI:000252946700032. English.
106. Baptista PM, Siddiqui MM, Lozier G, Rodriguez SR, Atala A, Soker S. The use of whole organ decellularization for the generation of a vascularized liver organoid. Hepatology. 2011 Feb;53(2):604-17. PubMed PMID: 21274881. eng.
107. Baptista PM, Orlando G, Mirmalek-Sani SH, Siddiqui M, Atala A, Soker S. Whole organ decellularization - a tool for bioscaffold fabrication and organ bioengineering. Conf Proc IEEE Eng Med Biol Soc. 2009;2009:6526-9. PubMed PMID: 19964173. eng.
108. Soto-Gutierrez A, Zhang L, Medberry C, Fukumitsu K, Faulk D, Jiang H, et al. A Whole-Organ Regenerative Medicine Approach for Liver Replacement. Tissue Engineering Part C-Methods. 2011 Jun;17(6):677-86. PubMed PMID: WOS:000291202200007.
109. Shupe T, Williams M, Brown A, Willenberg B, Petersen BE. Method for the decellularization of intact rat liver. Organogenesis. 2010 Apr-Jun;6(2):134-6. PubMed PMID: WOS:000290262200009.
110. Bao J, Shi Y, Sun H, Yin X, Yang R, Li L, et al. Construction of a Portal Implantable Functional Tissue-Engineered Liver Using Perfusion-Decellularized Matrix and Hepatocytes in Rats. Cell Transplantation. 2011 2011;20(5):753-66. PubMed PMID: WOS:000292532000013.
111. Barakat O, Abbasi S, Rodriguez G, Rios J, Wood RP, Ozaki C, et al. Use of Decellularized Porcine Liver for Engineering Humanized Liver Organ. Journal of Surgical Research. 2012 Mar;173(1):E11-E25. PubMed PMID: WOS:000300612500002.
112. Yagi H, Fukumitsu K, Fukuda K, Kitago M, Shinoda M, Obara H, et al. Human-Scale Whole-Organ Bioengineering for Liver Transplantation: A Regenerative Medicine Approach. Cell Transplantation. 2013 2013;22(2):231-42. PubMed PMID: WOS:000316158100003.
113. LeCluyse EL, Witek RP, Andersen ME, Powers MJ. Organotypic liver culture models: Meeting current challenges in toxicity testing. Critical Reviews in Toxicology. 2012 Jul;42(6):501-48. PubMed PMID: WOS:000305247900004.
114. Li AP. In Vitro Human Hepatocyte-Based Experimental Systems for the Evaluation of Human Drug Metabolism, Drug-Drug Interactions, and Drug Toxicity in Drug Development. Current Topics in Medicinal Chemistry. 2014;14(11):1325-38. PubMed PMID: WOS:000337169800002.
115. Takebe T, Sekine K, Enomura M, Koike H, Kimura M, Ogaeri T, et al. Vascularized and functional human liver from an iPSC-derived organ bud transplant. Nature. 2013 Jul 25;499(7459):481-+. PubMed PMID: WOS:000322157900041.
116. Takayama K, Nagamoto Y, Mimura N, Tashiro K, Sakurai F, Tachibana M, et al. Long-Term Self-Renewal of Human ES/iPS-Derived Hepatoblast-like Cells on Human Laminin 111-

Coated Dishes. Stem Cell Reports. 2013 Oct;1(4):322-35. PubMed PMID: WOS:000336633000005. English.
117. Si-Tayeb K, Noto FK, Nagaoka M, Li JX, Battle MA, Duris C, et al. Highly Efficient Generation of Human Hepatocyte-Like Cells from Induced Pluripotent Stem Cells (vol 51, pg 297, 2010). Hepatology. 2010 Mar;51(3):1094-. PubMed PMID: WOS:000275472300050.
118. Chen YF, Tseng CY, Wang HW, Kuo HC, Yang VW, Lee OK. Rapid generation of mature hepatocyte-like cells from human induced pluripotent stem cells by an efficient three-step protocol. Hepatology. 2012 Apr;55(4):1193-203. PubMed PMID: WOS:000302069900023.
119. Olsavsky KM, Page JL, Johnson MC, Zarbl H, Strom SC, Omiecinski CJ. Gene expression profiling and differentiation assessment in primary human hepatocyte cultures, established hepatoma cell lines, and human liver tissues. Toxicology and Applied Pharmacology. 2007 Jul;222(1):42-56. PubMed PMID: WOS:000247853900005.
120. Sunman JA, Hawke RL, LeCluyse EL, Kashuba ADM. Kupffer cell-mediated IL-2 suppression of CYP3A activity in human hepatocytes. Drug Metabolism and Disposition. 2004 Mar;32(3):359-63. PubMed PMID: WOS:000189104600011. English.
121. Griffith LG, Wells A, Stolz DB. Engineering Liver. Hepatology. 2014 Oct;60(4):1426-34. PubMed PMID: WOS:000342662100034.
122. Lemaigre F, Zaret KS. Liver development update: new embryo models, cell lineage control, and morphogenesis. Current Opinion in Genetics & Development. 2004 Oct;14(5):582-90. PubMed PMID: WOS:000224337700018.
123. Zhu Z, Huangfu D. Human pluripotent stem cells: an emerging model in developmental biology. Development. 2013 Feb 15;140(4):705-17. PubMed PMID: WOS:000314405000002.
124. Waterston RH, Lindblad-Toh K, Birney E, Rogers J, Abril JF, Agarwal P, et al. Initial sequencing and comparative analysis of the mouse genome. Nature. 2002 Dec;420(6915):520-62. PubMed PMID: WOS:000179611600053.
125. Ben-David U, Kopper O, Benvenisty N. Expanding the Boundaries of Embryonic Stem Cells. Cell Stem Cell. 2012 Jun;10(6):666-77. PubMed PMID: WOS:000305768400012.
126. Reid LM, Fiorino AS, Sigal SH, Brill S, Holst PA. EXTRACELLULAR-MATRIX GRADIENTS IN THE SPACE OF DISSE - RELEVANCE TO LIVER BIOLOGY. Hepatology. 1992 Jun;15(6):1198-203. PubMed PMID: WOS:A1992HX53200034.
127. Martinezhernandez A, Amenta PS. LIVER REGENERATION .1. THE EXTRACELLULAR-MATRIX IN HEPATIC REGENERATION. Faseb Journal. 1995 Nov;9(14):1401-10. PubMed PMID: WOS:A1995TF67800004.
128. Vyas D, Baptista PM, Moran E, Soker S. Recapitulation of Human Hepato-Biliary Organogenesis in Self-Assembled Liver Organoid Culture. Tissue Engineering Part A. 2014 Dec;20:S29-S. PubMed PMID: WOS:000345684300106.
129. Wang YF, Yao HL, Cui CB, Wauthier E, Barbier C, Costello MJ, et al. Paracrine Signals from Mesenchymal Cell Populations Govern the Expansion and Differentiation of Human Hepatic Stem Cells to Adult Liver Fates. Hepatology. 2010 Oct;52(4):1443-54. PubMed PMID: WOS:000282613000031.
130. Boulter L, Govaere O, Bird TG, Radulescu S, Ramachandran P, Pellicoro A, et al. Macrophage-derived Wnt opposes Notch signaling to specify hepatic progenitor cell fate in chronic liver disease. Nature Medicine. 2012 Apr;18(4):572-9. PubMed PMID: WOS:000302617800034.
131. Boulter L, Lu WY, Forbes SJ. Differentiation of progenitors in the liver: a matter of local choice. Journal of Clinical Investigation. 2013 May;123(5):1867-73. PubMed PMID: WOS:000319025100005.
132. Kamath BM, Piccoli DA. Heritable disorders of the bile ducts. Gastroenterology Clinics of North America. 2003 Sep;32(3):857-+. PubMed PMID: WOS:000185617400006.
133. Seok J, Warren HS, Cuenca AG, Mindrinos MN, Baker HV, Xu WH, et al. Genomic responses in mouse models poorly mimic human inflammatory diseases. Proceedings of the

National Academy of Sciences of the United States of America. 2013 Feb;110(9):3507-12. PubMed PMID: WOS:000315841900063.
134. Pampaloni F, Reynaud EG, Stelzer EHK. The third dimension bridges the gap between cell culture and live tissue. Nature Reviews Molecular Cell Biology. 2007 Oct;8(10):839-45. PubMed PMID: WOS:000249642900016. English.
135. Ploss A, Khetani SR, Jones CT, Syder AJ, Trehan K, Gaysinskaya VA, et al. Persistent hepatitis C virus infection in microscale primary human hepatocyte cultures. Proceedings of the National Academy of Sciences of the United States of America. 2010 Feb;107(7):3141-5. PubMed PMID: WOS:000274599500078. English.
136. Khetani SR, Bhatia SN. Microscale culture of human liver cells for drug development. Nature Biotechnology. 2008 Jan;26(1):120-6. PubMed PMID: WOS:000252222500032. English.
137. March S, Ng S, Velmurugan S, Galstian A, Shan J, Logan DJ, et al. A Microscale Human Liver Platform that Supports the Hepatic Stages of Plasmodium falciparum and vivax. Cell Host & Microbe. 2013 Jul;14(1):104-15. PubMed PMID: WOS:000330851300014. English.
138. Rashid ST, Corbineau S, Hannan N, Marciniak SJ, Miranda E, Alexander G, et al. Modeling inherited metabolic disorders of the liver using human induced pluripotent stem cells. Journal of Clinical Investigation. 2010 Sep;120(9):3127-36. PubMed PMID: WOS:000281458800019. English.
139. Ordonez MP, Goldstein LSB. Using Human-Induced Pluripotent Stem Cells to Model Monogenic Metabolic Disorders of the Liver. Seminars in Liver Disease. 2012 Nov;32(4):298-306. PubMed PMID: WOS:000311657000005. English.
140. Handa K, Matsubara K, Fukumitsu K, Guzman-Lepe J, Watson A, Soto-Gutierrez A. Assembly of Human Organs from Stem Cells to Study Liver Disease. American Journal of Pathology. 2014 Feb;184(2):348-57. PubMed PMID: WOS:000330257700005.
141. Leung M, Kievit FM, Florczyk SJ, Veiseh O, Wu J, Park JO, et al. Chitosan-Alginate Scaffold Culture System for Hepatocellular Carcinoma Increases Malignancy and Drug Resistance. Pharmaceutical Research. 2010 Sep;27(9):1939-48. PubMed PMID: WOS:000280650200017.
142. Cheng S, Prot JM, Leclerc E, Bois FY. Zonation related function and ubiquitination regulation in human hepatocellular carcinoma cells in dynamic vs. static culture conditions. Bmc Genomics. 2012 Feb;13. PubMed PMID: WOS:000301440400001.
143. Olsen AL, Bloomer SA, Chan EP, Gaca MDA, Georges PC, Sackey B, et al. Hepatic stellate cells require a stiff environment for myofibroblastic differentiation. American Journal of Physiology-Gastrointestinal and Liver Physiology. 2011 Jul;301(1):G110-G8. PubMed PMID: WOS:000292135000012.
144. Rusciano D, Lorenzoni P, Burger MM. MURINE MODELS OF LIVER METASTASIS. Invasion & Metastasis. 1994 Jan-Dec;14(1-6):349-61. PubMed PMID: WOS:A1994RV53800034.
145. Yates C, Shepard CR, Papworth G, Dash A, Stolz DB, Tannenbaum S, et al. Novel three-dimensional organotypic liver bioreactor to directly visualize early events in metastatic progression. In: VandeWoude GF, Klein G, editors. Advances in Cancer Research, Vol 97. Advances in Cancer Research. 97. San Diego: Elsevier Academic Press Inc; 2007. p. 225-+.
146. David L, Dulong V, Coquerel B, Le Cerf D, Cazin L, Lamacz M, et al. Collagens, stromal cell-derived factor-1 alpha and basic fibroblast growth factor increase cancer cell invasiveness in a hyaluronan hydrogel. Cell Proliferation. 2008 Apr;41(2):348-64. PubMed PMID: WOS:000253978100012.
147. Wang RX, Xu JC, Juliette L, Castilleja A, Love J, Sung SY, et al. Three-dimensional co-culture models to study prostate cancer growth, progression, and metastasis to bone. Seminars in Cancer Biology. 2005 Oct;15(5):353-64. PubMed PMID: WOS:000232018800004.
148. McDaniel SM, Rumer KK, Biroc SL, Metz RP, Singh M, Porter W, et al. Remodeling of the mammary microenvironment after lactation promotes breast tumor cell metastasis. American

Journal of Pathology. 2006 Feb;168(2):608-20. PubMed PMID: WOS:000235122600024. English.
149. Moran EC, Gaston B, Baptista PM, Atala A, Soker S. Acellular Liver Scaffolds as a Model to Study Colon Cancer Metastasis. Tissue Engineering Part A. 2014 Dec;20:S28-S9. PubMed PMID: WOS:000345684300104.
150. McKim JM. Building a Tiered Approach to In Vitro Predictive Toxicity Screening: A Focus on Assays with In Vivo Relevance. Combinatorial Chemistry & High Throughput Screening. 2010 Feb;13(2):188-206. PubMed PMID: WOS:000274432800009. English.
151. van Tonder JJ, Steenkamp V, Gulumian M. Pre-Clinical Assessment of the Potential Intrinsic Hepatotoxicity of Candidate Drugs. In: Gowder DS, editor. New Insights into Toxicity and Drug Testing: InTech; 2013.
152. Olson H, Betton G, Robinson D, Thomas K, Monro A, Kolaja G, et al. Concordance of the toxicity of pharmaceuticals in humans and in animals. Regulatory Toxicology and Pharmacology. 2000 Aug;32(1):56-67. PubMed PMID: WOS:000090145100007.
153. Jaeschke H, McGill MR, Ramachandran A. Oxidant stress, mitochondria, and cell death mechanisms in drug-induced liver injury: Lessons learned from acetaminophen hepatotoxicity. Drug Metabolism Reviews. 2012 Feb;44(1):88-106. PubMed PMID: WOS:000299086000004. English.
154. Goral VN, Hsieh YC, Petzold ON, Clark JS, Yuen PK, Faris RA. Perfusion-based microfluidic device for three-dimensional dynamic primary human hepatocyte cell culture in the absence of biological or synthetic matrices or coagulants. Lab on a Chip. 2010;10(24):3380-6. PubMed PMID: WOS:000284589000010.
155. Gallego-Perez D, Higuita-Castro N, Sharma S, Reen RK, Palmer AF, Gooch KJ, et al. High throughput assembly of spatially controlled 3D cell clusters on a micro/nanoplatform. Lab on a Chip. 2010;10(6):775-82. PubMed PMID: WOS:000275471000014.
156. Toh YC, Ng S, Khong YM, Samper V, Yu H. A configurable three-dimensional microenvironment in a microfluidic channel for primary hepatocyte culture. Assay and Drug Development Technologies. 2005 Apr;3(2):169-76. PubMed PMID: WOS:000229434700005.
157. Toh YC, Lim TC, Tai D, Xiao GF, van Noort D, Yu HR. A microfluidic 3D hepatocyte chip for drug toxicity testing. Lab on a Chip. 2009;9(14):2026-35. PubMed PMID: WOS:000267572000010.
158. Legendre A, Baudoin R, Alberto G, Paullier P, Naudot M, Bricks T, et al. Metabolic Characterization of Primary Rat Hepatocytes Cultivated in Parallel Microfluidic Biochips. Journal of Pharmaceutical Sciences. 2013 Sep;102(9):3264-76. PubMed PMID: WOS:000330240900033.
159. Sung JH, Shuler ML. A micro cell culture analog (mu CCA) with 3-D hydrogel culture of multiple cell lines to assess metabolism-dependent cytotoxicity of anti-cancer drugs. Lab on a Chip. 2009 May;9(10):1385-94. PubMed PMID: WOS:000268227400011.

CHAPTER II

The Role of Biomechanics and Mechanobiology in the Human Liver and Implications in Liver Tissue Engineering

Emma C. Moran

CONTENTS

1. Liver Biomechanics

In addition to responding to biochemical signals, cell behavior is highly influenced by the mechanical environment, including the topography and stiffness of the surrounding tissue, fluid shear stress, and interstitial fluid pressure. The capability of a cell to respond to mechanical cues can lead to an array of cellular processes, including differentiation, injury response, motility and morphological changes (1-3). Mediators of mechanotransduction include cell-cell adhesions (cadherins and gap junctions), cell-ECM adhesions (integrins and focal adhesions), cytoskeletal filaments, nuclear components, membrane components (ion channels and surface receptors), and surface processes (primary cilia) (4). When stimulated, these components trigger transcriptional regulators that alter cell behavior (5).

The material properties of tissue are determined by the chemical structure of the tissue as well as the organization of those components. Collagen, fibronectin, and proteoglycans all contribute to mechanical strength and behavior and modifications to any of these components leads to alterations in the mechanical properties of the tissue (6). In most cases, the stiffness of a tissue or substrate is described in terms of an Elastic or Young's modulus, a constant describing the materials ability to resist deformation, or the ratio of stress to strain. However, soft tissues, including the liver, are inherently more complex than a linear elastic modulus describes, displaying non-linear elasticity (non-linear stress strain relationship) and viscoelasticity (rate dependence in both fluid and solid components) (7). The effects of these more complicated material behaviors on cell mechanosensitivity are largely unknown.

2. Liver Cell Mechanobiology in Health and Disease

Cell-matrix interactions occur at points known as focal adhesion complexes, which consist of integrins that connect the ECM to the actin-myosin cytoskeleton in a cell. Contraction of this actin-myosin cytoskeleton allows the cell to survey its mechanical environment through movement of the integrins, which pull on the ECM and then transmit that force back to the cytoskeleton. For example, if the ECM became stiffer, it would be more difficult for the cytoskeleton to contract, resulting in accumulation of more integrins, enlarged focal adhesions, and further development of the cytoskeleton (2). Integrin movement is related to downstream signaling pathways; the main mediators of this process are Rho guanosine triphosphatases (Rho GTPase) and the contraction of the actin-myosin cytoskeleton (6). While less understood than cell-matrix interactions, cell-cell junctions are equally important in cell mechanosensitivity. Cell-cell interactions are thought to occur via cadherins that form a bridge between the cytoskeleton of two neighboring cells (8).

Variations in the stiffness of the tissue, a process that occurs in certain disease states, may lead to alterations in the normal behavior of a particular cell. In liver cirrhosis and fibrosis, liver tissue can increase by an order of magnitude (9), triggering an array of responses by various liver cells. When cultured on stiff substrates, hepatocytes begin to dedifferentiate and become proliferative which is in stark contrast to their normally quiescent state (10-12). Portal fibroblasts differentiate into myofibroblasts when supplemented with transforming growth factor-beta (TGF-β) and cultured on a stiff substrate, an important process in the early stages of biliary fibrosis (13). Hepatic stellate cells (HSCs), the major ECM producers in the liver, become increasingly transdifferentiated towards fibrogenic myofibroblasts as the stiffness of the underlying

matrix is increased (14, 15). Disruption of HSC integrins, through disruption of $\alpha_5\beta_1$ and $\alpha_v\beta_3$ and by culturing the cells on poly-L-lysine enabling non-integrin dependent cell adhesion, promotes growth cycle arrest and maintains cells in a non-myofibroblastic state (16). Additionally, Rho GTPases, mediators of the integrin-sensing signaling pathways, are necessary for HSC transdifferentiation (17). The transdifferentiation process of HSCs to myofibroblasts is the primary mechanism of liver fibrosis and recent research suggests that the mechanosensitivity of HSCs plays a vital role in this process. Hepatocytes have also been shown to respond to another of mechanical force, parenchymal (interstitial) fluid pressure (18), which is known to increase in certain disease progressions.

Endothelial cells, not only in the liver but in all tissues, display mechanosensitivity as well. When blood flows past endothelial cells lining vascular structures, shear stress is detected by the cell through the above mentioned mechanosensors. This initiates a rapid response by the cell, including the opening of ion channels, release of nitric oxide and prostacyclin, and ATP release and transport (19). These events trigger the activation of transcription factors such as EGR1 (20), NF-κB (21), and KLF2 (22). In situations of abnormal flow, the endothelial cell response to altered shear stress can trigger atherogenesis (19, 23, 24), angiogenesis (25), and particularly relevant for our research, liver regeneration (26-29). After partial hepatectomy, in which the diseased portions of the liver are removed, the overall blood flow to liver mass ratio is increased. This leads to portal hypertension, resulting in elevated shear stresses which induce nitric oxide and prostacyclin production and triggers the liver regeneration cascade (28-30). This phenomenon is the result of HGF and EGF mediated control of eNOS signaling cascades, resulting in hepatocyte proliferation and therefore, regeneration (23, 27).

Mechanosensitivity is also an important characteristic of cholangiocytes in detecting bile flow. Cholangiocytes contain primary cilia, a non-motile organelle that projects out from the plasma membrane of most differentiated or quiescent cells in the body. The primary cilia consists of an axoneme with microtubules arranged in a 9+0 arrangement that extends from the mother centriole contained within the basal body (31-34). In addition to detecting osmolality and chemical composition of bile, cholangiocyte primary cilia act as mechanosensors. The primary cilium bends in response to bile flow and transmits the signal through increases in intracellular calcium, ATP release, and Cl^- transport (35, 36). Defects in these cilia lead to serious ciliopathies, including autosomal dominant polycystic kidney disease (ADPKD) and Meckel-Gruber syndrome (MKS1) (34, 37, 38).

3. Mechanobiology and Stem and Progenitor Cells

A groundbreaking paper by Engler *et al* demonstrated that stem cell differentiation could be directed towards different lineages by altering the mechanical properties of the substrate to mimic specific tissue types (1). Mesenchymal stem cells (MSCs) cultured on soft substrates mimicking brain differentiated towards neurogenic phenotypes, MSCs cultured on matrix mimicking muscle were myogenic, and the stiffest matrix mimicking collagenous bone produced osteogenic cells. These findings are incredibly important for the field of stem cell therapy in directing differentiation of stem cells for clinical therapies. Following this work, Lozoya *et al* (39) researched a similar question pertaining to liver cells: can mimicking the physiological mechanical properties of liver tissue regulate liver stem and progenitor cells populations? The human liver contains a population of liver stem

and progenitors cells that reside in a defined stem cell niche containing a specialized ECM. Due to this altered composition of ECM components, one can infer that the mechanical properties, or stiffness, of that region may also be uniquely different than the rest of the liver. In the work completed by Lozoya *et al*, hHpSCs were cultured in 3D microenvironments constituted by hyaluronic acid (HA) hydrogels that mimicked the Canals of Hering. The major indicator of hHpSC mechanosensitivity came from analysis of the stem cell marker CDH1, also known as E-cadherin. CDH1 is a cell surface protein that establishes cell-cell adhesions, assesses the mechanical stiffness of neighboring cells, and triggers downstream signaling pathways involved in mechanosensitivity (8). The protein expression levels of CDH1 exhibited a dependence on stiffness, with the highest levels of expression occurring when the cells were cultured on the HA hydrogel with a shear modulus of 200 Pa. CDH1 expression on the apical side of the 200 Pa HA hydrogel seeded cells demonstrates that these exposed cells may coordinate mechanical signals to adjacent cells through CDH1. This result demonstrates a stiffness-dependent behavior of the hHpSCs, suggesting that culturing the cells in their preferable mechanical environment allows them to organize themselves in the same manner observed in the stem cell niche. However, there is still a lack of convincing evidence that substrate stiffness can direct differentiation of hHpSCs towards mature liver cells, which would have huge implications for liver regeneration in medicine as well as understanding the involvement of hHpSCs in liver disease. In addition to responding to the mechanical properties of the substrate, liver stem and progenitor cells and human embryonic stem cells have been shown to differentiate into mature liver cells when exposed to shear stress in perfusion bioreactor cultures (40, 41).

4. Role of Mechanobiology in Cancer

In healthy tissue, the extracellular matrix is constantly remodeling in a carefully coordinated effort between the degradation of ECM proteins by matrix metalloproteinases (MMPs) and deposition of new ECM by surrounding cells. In states of disease, including cancer, there are abnormal ECM dynamics that are implicated in disease progression. The tumor microenvironment greatly differs from that of normal tissue, exhibiting increased stiffness as a result of fibrillar collagen deposition, collagen crosslinking and the bundling of individual fibers (42-44). This phenomena is best studied in breast cancer research, where it is known that diseased breast tissue can be up to 10 times stiffer than normal breast tissue (45). Increased stiffness is thought to lead to integrin clustering which transcriptionally activates β-catenin and MYC, initiating a microRNA circuit that leads to tumor cell migration and invasion (46). Increasing matrix stiffness driving cancer progression also occurs in the liver, where increasing stiffness measurements as a result of liver fibrosis is a predictor of hepatocellular carcinoma (HCC) (47). Additionally, increased stiffness is observed in already established tumors within the liver parenchyma (48). Recent research has elucidated the role of basal and hepatocyte growth factor-stimulated mitogenic signaling as well as β1-integrin and focal adhesion kinase (FAK) in modulating HCC cell response to matrix stiffness. These pathways promote HCC proliferation and chemotherapeutic resistance when the cell resides within a stiff environment (49).

Primary tumor metastasis to distant sites is also thought to be regulated by the mechanical environment. The metastatic process consists of vascularization and detachment from the primary tumor, intravasation into nearby blood vessels, circulation throughout the vascular system, extravasation to a distant site, and finally growth of a

secondary tumor (42, 43). The initiation of this process includes a phenomena where the primary tumor cells undergoes epithelial-to-mesenchymal transition (EMT) (50). Matrix stiffness has been hypothesized to play a role in this process, although there is still much more research to be done (43). Matrix stiffening also occurs at the metastatic site, either from production of ECM by the cancer cells or from stromal cells within the invaded tissue (51). An additional biomechanical change that may play a role in tumor metastasis through EMT are changes in the mechanical properties of the cell itself. Cancer cells are softer than normal cells, which may allow them to migrate through dense tissue and allow intravasation into blood vessels (52). The shear stress that circulating tumor cells experience within the vascular system may also be involved in extravasation into distant tissue sites (53).

5. Conclusion

Cells in the human body are constantly exposed to mechanical forces, including tensile and compression forces, hydrostatic pressure and shear stress. These forces play a critical role in a myriad of processes, including tissue development, homeostasis and disease. Within the liver, there is evidence that biomechanics play a role in stem and progenitor cell differentiation, liver fibrosis and disease, cancer growth and metastasis and maintaining normal liver function. In order to elucidate the mechanisms involved in these phenomena, it is crucial to have proper *in vitro* models. Bioengineered livers contain the complex microenvironment that is crucial for replicating and modifying mechanical forces to study the effects of mechanical forces on cell behavior.

References

1. Engler AJ, Sen S, Sweeney HL, Discher DE. Matrix elasticity directs stem cell lineage specification. Cell. 2006 Aug 25;126(4). PubMed PMID: WOS:000240276700017.
2. Janmey PA, Miller RT. Mechanisms of mechanical signaling in development and disease. Journal of Cell Science. 2011 Jan;124(1). PubMed PMID: WOS:000285242200003.
3. Discher DE, Janmey P, Wang YL. Tissue cells feel and respond to the stiffness of their substrate. Science. 2005 Nov 18;310(5751). PubMed PMID: WOS:000233437300033.
4. Ingber DE. Cellular mechanotransduction: putting all the pieces together again. Faseb Journal. 2006 May;20(7):811-27. PubMed PMID: WOS:000240157700003.
5. Mammoto A, Mammoto T, Ingber DE. Mechanosensitive mechanisms in transcriptional regulation. Journal of Cell Science. 2012 Jul;125(13):3061-73. PubMed PMID: WOS:000308417300005.
6. Wells R. The role of matrix stiffness in regulating cell behavior. Hepatology. 2008 APR 2008;47(4):1394-400. PubMed PMID: ISI:000254637100031. English.
7. Suh J, DiSilvestro M. Biphasic poroviscoelastic behavior of hydrated biological soft tissue. Journal of Applied Mechanics-Transactions of the Asme. 1999 JUN 1999;66(2):528-35. PubMed PMID: ISI:000081476100032. English.
8. Smutny M, Yap AS. Neighborly relations: cadherins and mechanotransduction. Journal of Cell Biology. 2010 Jul 28;189(7). PubMed PMID: WOS:000279188400005.
9. Georges PC, Hui J-J, Gombos Z, McCormick ME, Wang AY, Uemura M, et al. Increased stiffness of the rat liver precedes matrix deposition: implications for fibrosis. American Journal of Physiology-Gastrointestinal and Liver Physiology. 2007 Dec;293(6). PubMed PMID: WOS:000251510500006.
10. Hansen LK, Wilhelm J, Fassett JT. Regulation of hepatocyte cell cycle progression and differentiation by type I collagen structure. Current Topics in Developmental Biology, Vol 72. 2006 2006;72. PubMed PMID: WOS:000236800100004.
11. Fassett J, Tobolt D, Hansen LK. Type I collagen structure regulates cell morphology and EGF signaling in primary rat hepatocytes through cAMP-dependent protein kinase A. Molecular Biology of the Cell. 2006 Jan;17(1). PubMed PMID: WOS:000234399300032.
12. Semler EJ, Ranucci CS, Moghe PV. Mechanochemical manipulation of hepatocyte aggregation can selectively induce or repress liver-specific function. Biotechnology and Bioengineering. 2000 Aug 20;69(4). PubMed PMID: WOS:000088421700002.
13. Li Z, Dranoff JA, Chan EP, Uemura M, Sevigny J, Wells RG. Transforming growth factor-beta and substrate stiffness regulate portal fibroblast activation in culture. Hepatology. 2007 Oct;46(4). PubMed PMID: WOS:000249910500035.
14. Wells RG. The role of matrix stiffness in hepatic stellate cell activation and liver fibrosis. Journal of Clinical Gastroenterology. 2005 Apr;39(4). PubMed PMID: WOS:000227989200019.
15. Guvendiren M, Perepelyuk M, Wells RG, Burdick JA. Hydrogels with differential and patterned mechanics to study stiffness-mediated myofibroblastic differentiation of hepatic stellate cells. J Mech Behav Biomed Mater. 2014 Oct;38:198-208. PubMed PMID: 24361340. eng.
16. Iwamoto H, Sakai H, Nawata H. Inhibition of integrin signaling with Arg-Gly-Asp motifs in rat hepatic stellate cells. Journal of Hepatology. 1998 Nov;29(5). PubMed PMID: WOS:000077182400010.
17. Yee HF. Rho directs activation-associated changes in rat hepatic stellate cell morphology via regulation of the actin cytoskeleton. Hepatology. 1998 Sep;28(3). PubMed PMID: WOS:000075606000036.
18. Hsu WM, Carraro A, Kulig KM, Miller ML, Kaazempur-Mofrad M, Weinberg E, et al. Liver-assist device with a microfluidics-based vascular bed in an animal model. Ann Surg. 2010 Aug;252(2):351-7. PubMed PMID: 20647924. eng.

19. Hahn C, Schwartz MA. Mechanotransduction in vascular physiology and atherogenesis. Nature Reviews Molecular Cell Biology. 2009 Jan;10(1):53-62. PubMed PMID: WOS:000261949800016.
20. Schwachtgen JL, Houston P, Campbell C, Sukhatme V, Braddock M. Fluid shear stress activation of egr-1 transcription in cultured human endothelial and epithelial cells is mediated via the extracellular signal-related kinase 1/2 mitogen-activated protein kinase pathway. Journal of Clinical Investigation. 1998 Jun 1;101(11):2540-9. PubMed PMID: WOS:000074165900026.
21. Orr AW, Sanders JM, Bevard M, Coleman E, Sarembock IJ, Schwartz MA. The subendothelial extracellular matrix modulates NF-kappa B activation by flow: a potential role in atherosclerosis. Journal of Cell Biology. 2005 Apr 11;169(1):191-202. PubMed PMID: WOS:000228327500017.
22. Dekker RJ, van Soest S, Fontijn RD, Salamanca S, de Groot PG, VanBavel E, et al. Prolonged fluid shear stress induces a distinct set of endothelial cell genes, most specifically lung Kruppel-like factor (KLF2). Blood. 2002 Sep 1;100(5):1689-98. PubMed PMID: WOS:000177667700028.
23. Tzima E, Irani-Tehrani M, Kiosses WB, Dejana E, Schultz DA, Engelhardt B, et al. A mechanosensory complex that mediates the endothelial cell response to fluid shear stress. Nature. 2005 Sep;437(7057):426-31. PubMed PMID: WOS:000231849100057.
24. Yurdagul A, Chen J, Funk SD, Albert P, Kevil CG, Orr AW. Altered nitric oxide production mediates matrix-specific PAK2 and NF-kappa B activation by flow. Molecular Biology of the Cell. 2013 Feb;24(3):398-408. PubMed PMID: WOS:000321116700020.
25. Mammoto A, Connor KM, Mammoto T, Yung CW, Huh D, Aderman CM, et al. A mechanosensitive transcriptional mechanism that controls angiogenesis. Nature. 2009 Feb;457(7233):1103-U57. PubMed PMID: WOS:000263680100034.
26. Murohara T, Witzenbichler B, Spyridopoulos I, Asahara T, Ding B, Sullivan A, et al. Role of endothelial nitric oxide synthase in endothelial cell migration. Arteriosclerosis Thrombosis and Vascular Biology. 1999 May;19(5):1156-61. PubMed PMID: WOS:000080467900003.
27. Mei Y, Thevananther S. Endothelial Nitric Oxide Synthase Is a Key Mediator of Hepatocyte Proliferation in Response to Partial Hepatectomy in Mice. Hepatology. 2011 Nov;54(5):1777-89. PubMed PMID: WOS:000296443100029.
28. Schoen JM, Wang HH, Minuk GY, Lautt WW. Shear stress-induced nitric oxide release triggers the liver regeneration cascade. Nitric Oxide-Biology and Chemistry. 2001 Oct;5(5):453-64. PubMed PMID: WOS:000171571700004.
29. Smith JMS, Lautt WW. The role of prostaglandins in triggering the liver regeneration cascade. Nitric Oxide-Biology and Chemistry. 2005 Sep;13(2):111-7. PubMed PMID: WOS:000231491300003.
30. Sato Y, Koyama S, Tsukada K, Hatakeyama K. Acute portal hypertension reflecting shear stress as a trigger of liver regeneration following partial hepatectomy. Surgery Today-the Japanese Journal of Surgery. 1997;27(6):518-26. PubMed PMID: WOS:A1997XB00900007.
31. Veland I, Awan A, Pedersen L, Yoder B, Christensen S. Primary Cilia and Signaling Pathways in Mammalian Development, Health and Disease. Nephron Physiology. 2009 2009;111(3):39-53. PubMed PMID: WOS:000264026600003. English.
32. Berbari NF, O'Connor AK, Haycraft CJ, Yoder BK. The Primary Cilium as a Complex Signaling Center. Current Biology. 2009 Jul 14;19(13). PubMed PMID: WOS:000268059200015.
33. Christensen ST, Pedersen LB, Schneider L, Satir P. Sensory cilia and integration of signal transduction in human health and disease. Traffic. 2007 Feb;8(2). PubMed PMID: WOS:000243508100002.

34. D'Angelo A, Franco B. The primary cilium in different tissues-lessons from patients and animal models. Pediatric Nephrology. 2011 May;26(5):655-62. PubMed PMID: WOS:000288712800002.
35. Masyuk AI, Masyuk TV, Splinter PL, Huang BQ, Stroope AJ, LaRusso NF. Cholangiocyte cilia detect changes in luminal fluid flow and transmit them into intracellular Ca2+ and cAMP signaling. Gastroenterology. 2006 Sep;131(3). PubMed PMID: WOS:000240561800028.
36. Woo K, Dutta AK, Patel V, Kresge C, Feranchak AP. Fluid flow induces mechanosensitive ATP release, calcium signalling and Cl(-) transport in biliary epithelial cells through a PKC zeta-dependent pathway. Journal of Physiology-London. 2008 Jun 1;586(11). PubMed PMID: WOS:000256345800015.
37. Clotman F, Libbrecht L, Killingsworth MC, Loo CCK, Roskams T, Lemaigre FP. Lack of cilia and differentiation defects in the liver of human foetuses with the Meckel syndrome. Liver International. 2008 Mar;28(3). PubMed PMID: WOS:000253258100012.
38. Masyuk AI, Masyuk TV, LaRusso NF. Cholangiocyte primary cilia in liver health and disease. Developmental Dynamics. 2008 Aug;237(8). PubMed PMID: WOS:000258482300007.
39. Lozoya O, Wauthier E, Turner R, Barbier C, Prestwich G, Guilak F, et al. Regulation of hepatic stem/progenitor phenotype by microenvironment stiffness in hydrogel models of the human liver stem cell niche. Biomaterials. 2011 OCT 2011;32(30):7389-402. PubMed PMID: ISI:000294829300012. English.
40. Schmelzer E, Triolo F, Turner ME, Thompson RL, Zeilinger K, Reid LM, et al. Three-Dimensional Perfusion Bioreactor Culture Supports Differentiation of Human Fetal Liver Cells. Tissue Engineering Part A. 2010 Jun;16(6). PubMed PMID: WOS:000278164800019.
41. Miki T, Ring A, Gerlach J. Hepatic Differentiation of Human Embryonic Stem Cells Is Promoted by Three-Dimensional Dynamic Perfusion Culture Conditions. Tissue Engineering Part C-Methods. 2011 May;17(5). PubMed PMID: WOS:000289937100006.
42. Lu P, Weaver VM, Werb Z. The extracellular matrix: a dynamic niche in cancer progression. J Cell Biol. 2012 Feb;196(4):395-406. PubMed PMID: 22351925. PMCID: PMC3283993. eng.
43. Wirtz D, Konstantopoulos K, Searson PC. The physics of cancer: the role of physical interactions and mechanical forces in metastasis. Nature Reviews Cancer. 2011 Jul;11(7):512-22. PubMed PMID: WOS:000292028300016.
44. Butcher DT, Alliston T, Weaver VM. A tense situation: forcing tumour progression. Nat Rev Cancer. 2009 Feb;9(2):108-22. PubMed PMID: 19165226. PMCID: PMC2649117. eng.
45. Lopez JI, Kang I, You WK, McDonald DM, Weaver VM. In situ force mapping of mammary gland transformation. Integr Biol (Camb). 2011 Sep;3(9):910-21. PubMed PMID: 21842067. PMCID: PMC3564969. eng.
46. Mouw JK, Yui Y, Damiano L, Bainer RO, Lakins JN, Acerbi I, et al. Tissue mechanics modulate microRNA-dependent PTEN expression to regulate malignant progression. Nat Med. 2014 Apr;20(4):360-7. PubMed PMID: 24633304. PMCID: PMC3981899. eng.
47. Masuzaki R, Tateishi R, Yoshida H, Goto E, Sato T, Ohki T, et al. Prospective risk assessment for hepatocellular carcinoma development in patients with chronic hepatitis C by transient elastography. Hepatology. 2009 Jun;49(6):1954-61. PubMed PMID: 19434742. eng.
48. Masuzaki R, Tateishi R, Yoshida H, Sato T, Ohki T, Goto T, et al. Assessing liver tumor stiffness by transient elastography. Hepatol Int. 2007 Sep;1(3):394-7. PubMed PMID: 19669335. PMCID: PMC2716830. eng.
49. Schrader J, Gordon-Walker TT, Aucott RL, van Deemter M, Quaas A, Walsh S, et al. Matrix stiffness modulates proliferation, chemotherapeutic response, and dormancy in hepatocellular carcinoma cells. Hepatology. 2011 Apr;53(4):1192-205. PubMed PMID: 21442631. PMCID: PMC3076070. eng.

50. Chaffer CL, Weinberg RA. A perspective on cancer cell metastasis. Science. 2011 Mar;331(6024):1559-64. PubMed PMID: 21436443. eng.
51. Erler JT, Bennewith KL, Cox TR, Lang G, Bird D, Koong A, et al. Hypoxia-induced lysyl oxidase is a critical mediator of bone marrow cell recruitment to form the premetastatic niche. Cancer Cell. 2009 Jan;15(1):35-44. PubMed PMID: 19111879. PMCID: PMC3050620. eng.
52. Guck J, Schinkinger S, Lincoln B, Wottawah F, Ebert S, Romeyke M, et al. Optical deformability as an inherent cell marker for testing malignant transformation and metastatic competence. Biophys J. 2005 May;88(5):3689-98. PubMed PMID: 15722433. PMCID: PMC1305515. eng.
53. Burdick MM, McCaffery JM, Kim YS, Bochner BS, Konstantopoulos K. Colon carcinoma cell glycolipids, integrins, and other glycoproteins mediate adhesion to HUVECs under flow. Am J Physiol Cell Physiol. 2003 Apr;284(4):C977-87. PubMed PMID: 12477667. eng.

CHAPTER III

Evaluation of the Effects of Decellularization on Liver Tissue Mechanics*

Emma C. Moran

* This chapter is a compilation of three published manuscripts, all focusing on different aspects of characterizing liver tissue biomechanics. Therefore, this chapter consists of three sub-chapters, 3.1, 3.2 and 3.3. There is an introduction and conclusion introducing and summarizing, respectively, the overall findings of this chapter.

Contents

CHAPTER 3 INTRODUCTION

This chapter is a compilation of three published peer-reviewed manuscripts that have investigated the biomechanical properties of liver tissue and the influence of tissue decellularization on these properties. The first paper is experimental work measuring parenchymal fluid pressure (PFP), also known as interstitial fluid pressure in other tissue types, both in *in vivo* and *in vitro* native and decellularized livers at different flow rates. These measurements were taken in order to optimize the flow rate of perfusion bioreactor systems used in the generation of bioengineered livers. We aimed to deliver physiological values of PFP within the scaffold, due to the influence of PFP in hepatic cell behavior (1). Additionally, these results were used as experimental inputs in the development of poroviscoelastic (PVE) finite element (FE) models of native and decellularized liver tissue in order to extract scaffold material properties, such as Young's Modulus. The second paper describes the development of a three-dimensional porohyperviscoelastic (PHVE) finite element model of bovine liver tissue developed in our lab that was critical towards our work characterizing the material properties of decellularized ferret liver, detailed in the third paper. The biphasic modeling approach allows for the characterization of both intrinsic solid matrix mechanical behavior as well as fluid flow dependent PFP with a single model. The third paper uses experimental and finite element modeling approaches to characterize the biomechanical properties of tissue following decellularization. Up to this point, this information was lacking from literature and is critically important due to the mechanosensitivity of both hepatic and non-hepatic cell types. The 3D PHVE model developed in the second manuscript was transformed into a simpler two-dimensional, axisymmetric FE model that allowed us to study the biomechanical properties of liver

tissue in a variety of states, including decellularization, perfusion, and at both the macro- and nano-scales.

CHAPTER 3.1

Evaluation of Parenchymal Fluid Pressure in Native and Decellularized Liver Tissue

Emma C. Moran, Pedro M. Baptista, Douglas W. Evans, Shay Soker, Jessica L. Sparks

Experiments and manuscript were completed by Emma C. Moran. Jessica L. Sparks and Shay Soker served in an advisory capacity and Pedro M. Baptista and Douglas W. Evans aided in experiments and served in an editing capacity. Text and figure formatting variations are due to journal guidelines. The work was published in *Biomed Sci Instrum*. 2012;48:303-9.

Abstract

One strategy for tissue engineering of bioartificial livers is the use of decellularized liver scaffolds, which contain a functional vascular network and intact extracellular matrix components. Due to the known mechanosensitivity of liver cells, particularly the response of hepatocytes to changes in parenchymal fluid pressure (PFP), it is necessary to evaluate the biomechanical environment within decellularized scaffolds. The objective of this study was to characterize the dependence of PFP on perfusion flow rate, in native and decellularized liver. Needle-guided Millar SPR-524 (3.5F) pressure sensors were inserted into liver parenchyma to measure PFP *in-situ* in rat (n=5) and *ex-situ* in portal vein-perfused native (n=5) and decellularized (n=7) liver tissue. Average *in-situ* PFP, measured in the left, central and right lobes, was found to be 2.86 ± 1.04 mmHg. PFP measured in *ex-situ* liver perfused at 3, 6, 9, and 12 ml/min was found to increase linearly with flow rate. Decellularized liver PFP ranged from 0.68 mmHg at 3ml/min to 2.42 mmHg at 12 ml/min, while native liver ranged from 4.32 – 11.93 mmHg. Results demonstrate that PFP in decellularized scaffolds can be controlled by varying flow rate. These results will be implemented in a poroviscoelastic finite element model of liver perfusion, developed by the authors, to predict PFP distribution in three-dimensional scaffolds for known flow rates. This computationally efficient model can be used to optimize perfusion bioreactor conditions throughout the scaffold, to aid in the engineering of functional liver tissue from a decellularized liver organoid.

Keywords: parenchymal fluid pressure, liver, decellularization, liver biomechanics, liver regenerative medicine

Introduction

In the United States there is a severe donor organ shortage, with demand far exceeding supply. There are currently 16,250 people on the waiting list for liver transplantations and only 6,291 liver transplantations were performed in 2010 (2). This need has driven research into alternatives for liver organ transplantation. The emerging fields of tissue engineering and regenerative medicine attempt to alleviate donor organ shortage by engineering artificial organs. The process begins with a biomaterial-derived scaffold to which cells are added. This process generally takes place in a bioreactor, which mimics the physiological environment for the purpose of tissue formation. One source of scaffolds for liver tissue engineering is acellular liver tissue. The decellularization process removes all of the cellular material from a native liver, leaving behind an intact and bioactive extracellular matrix (ECM). In addition, the microvasculature of the liver is preserved, allowing for physiological perfusion of the tissue and therefore adequate oxygen and nutrient delivery to cells (3). The decellularized organ scaffold is then placed in a perfusion bioreactor, where cells and media are perfused through the vasculature of the tissue. Perfusion flow rate can be adjusted to change the rate at which the cells and media are delivered into the scaffold in order to optimize liver tissue formation inside the acellular liver.

Inside the acellular scaffold within the perfusion bioreactor system, there are a number of forces acting on the cells, one of which is hydrostatic pressure. It is known that hepatocytes (mature liver cells) are responsive to changes in parenchymal fluid pressure (PFP), the hydrostatic pressure due to the presence of fluid in the liver interstitium (1). Therefore, characterizing this force is necessary to optimizing bioreactor conditions,

particularly flow rates. Previous studies have used polyurethane transducer-tipped catheters (Millar SPC 320, Millar Instruments Inc.) to measure interstitial fluid pressure in brain tumors (4). To our knowledge, the PFP in the liver has not been evaluated using this methodology, although an average PFP of liver tissue is reported to be 0 – 5 mmHg (5).

The liver is a highly vascularized organ, receiving 27% of the cardiac output (6) with a hepatic blood flow of 1.2 ± 0.3 ml/min per gram of liver in rats (7). The rat liver, and similarly the ferret liver, is divided into four hepatic lobes, the left, middle, right and caudate lobes (8). The middle lobe contains a deep notch that divides it into two components, which can be referred to as the middle right and middle left lobes. Each of the four lobes contains its own vascular supply, containing branches from the portal vein and hepatic artery (8). In the recellularization technique used by Baptista *et al.*, the right lobe is dissected from the entire organ in order to minimize the number of cells seeded into the scaffold (3). Due to the lobular nature of the rodent liver, the dissected right lobe still contains a functional vascular network.

The aim of this research was to evaluate the dependence of PFP on perfusion flow rate in decellularized livers and compare these findings to both *ex-situ* and *in-situ* measurements in native livers. *Ex-situ* measurements are applicable to the regeneration of liver tissue in a perfusion bioreactor system, in which the right lobe of a decellularized ferret liver is perfused with cells and media by a peristaltic pump. *In-situ* measurements allow for the comparison of the *ex-situ* perfusion system pressures to physiological PFP. The results from this work will ultimately be implemented in a poroviscoelastic finite element model of liver tissue in order to predict PFP distribution in three-dimensional scaffolds for known flow rates (9).

Methods

The right lobes of cadaveric ferret livers were used in the *ex-situ* experiments, to analyze PFP in conditions mimicking the perfusion bioreactor system. *In-situ* measurements were then performed in rats, which have a similar anatomy and size to the ferret livers. These measurements were taken in six locations across three lobes to study the effects of location on PFP. All animal studies were conducted in accordance with an IACUC approved protocol.

Ex-situ Testing: Liver specimens were obtained from 12 cadaveric ferrets ranging in age from 3-6 weeks. An abdominal incision was made and the liver was visualized. The inferior vena cava and portal vein were transected, all other vessels were ligated, and all ligaments and attachments were dissected. Following removal, the portal vein was cannulated with a 16-gauge (16G) cannula, leaving all samples with one central input (portal vein) and one output (inferior vena cava). Next, the right lobe of the liver was isolated to mimic the samples currently used in reseeding decellularized scaffolds (3). The right lobe was isolated by dissection, maintaining the perfusion of the lobe. Five of these samples in the native tissue state were tested within 6 hours of harvest. The remaining seven samples were decellularized through perfusion of 1% Triton-X 100 with 0.1% Ammonium Hydroxide (Sigma-Aldrich), as described by Baptista *et al* (3). The decellularized samples were testing following the completion of the decellularization, which includes perfusion of deionized water to remove any remnants of detergent. All liver samples were perfused with saline through the portal vein using a peristaltic pump (Masterflex 7523-70, Cole-Parmer) and pulse dampener (Cole-Parmer) to create a steady flow. A needle-guided transducer tipped catheter (Millar SPR-524 [3.5F], Millar Instruments Inc.) and MPVS-400 signal

conditioning hardware (Millar Instruments Inc.) with integrated DAQ technology (Powerlab, ADInstruments) was used to measure and record PFP in five native and seven decellularized liver samples. The pressure probe was inserted into the same relative location in each of the samples and the PFP was measured at flow rates of 3, 6, 9, and 12 ml/min (Fig.1).

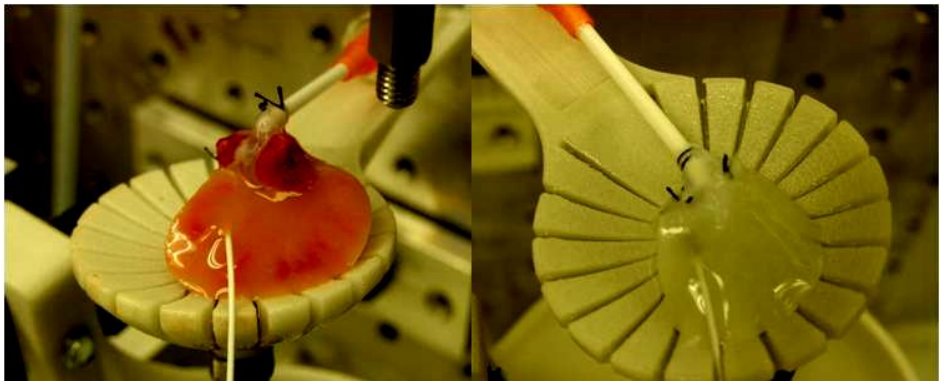

Figure 1: Native (left) and decellularized (right) *ex-situ* pressure measurements. The probe can be seen inserted into the right lobe of liver tissue and both samples are cannulated via the portal vein and perfused with saline.

***In-situ Testing*:** Five Sprague-Dawley rats (Charles River Laboratories, Inc., Wilmington, MA) were used to measure *in-situ* PFP and were kept under isoflurane gas anaesthesia throughout the procedure. Three of the rats were aged 5 months, while two of them were 5-6 weeks. It was found that the size of the livers in all rats was similar, so the samples were grouped together. A longitudinal abdominal incision was made and the four lobes of the liver were visualized (left, middle left, middle right, right). The maximum widths of each of these lobes was measured and recorded in each rat (Table 1). Six PFP measurements were taken in each rat: three measurements in the left lobe, and one each in the middle left lobe, middle right lobe, and right lobe (Fig. 2). Of the three measurements

in the left lobe, one measurement was taken at the midpoint of the width, one measurement was 1cm from the left and one was 1cm from the right. All other lobe measurements were taken at the midpoint of the width and all measurements were taken 1cm above the bottom of the lobe. A needle-guided transducer tipped catheter was inserted into the tissue a depth of 5-6mm from the tip of the probe and PFP was measured and recorded as described in the previous section. The probe was withdrawn when the pressure stabilized and the next measurement was not taken until complete clotting occurred in the previous measurement wound. The animals were sacrificed following the six PFP measurements.

Table 1: Parametric data of rats used for *in-situ* PFP measurements

Sample	Age/ Sex	Animal Weight (g)	Maximum Liver Lobe Width (cm)			
			Left Lobe	Central Left	Central Right	Right
1	5 month/ F	375	4.0	2.8	1.8	2.0
2	5 month/ F	355	4.0	2.4	1.5	2.0
3	5 month/ F	370	4.5	1.5	2.2	2.2
4	5-6 week/ M	200	4.0	1.4	2.5	2.1
5	5-6 week/ M	172	3.6	1.2	2.3	2.0

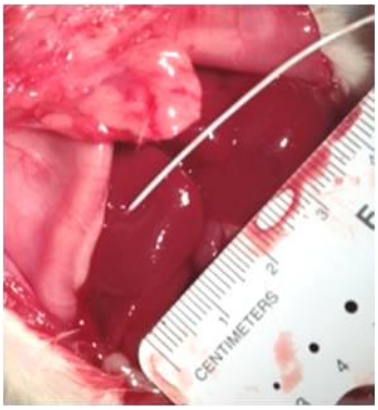

Figure 2: *In-situ* pressure measurement. Middle right lobe pressure measurement.

Results

Ex-situ Measurements: PFP in native liver ranged from 4.43 mmHg at 3ml/min to 11.93 mmHg at 12ml/min, while PFP of decellularized liver ranged from 0.68 mmHg at 3ml/min to 2.42 mmHg at 12ml/min. Both native and decellularized liver PFP increased linearly with flow rate (Fig. 3).

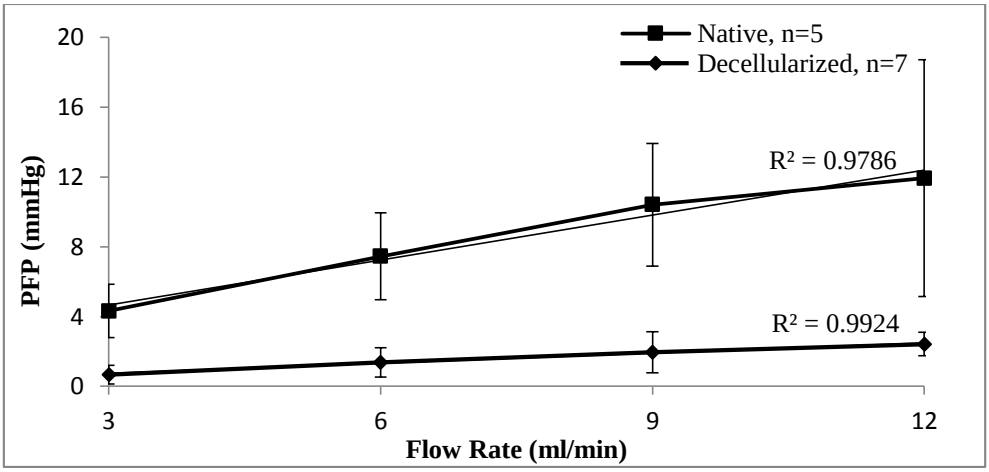

Figure 3: *Ex-situ* PFP as a function of perfusion flow rate in the right lobe of both native ($R^2 = 0.9786$) and decellularized ($R^2 = 0.9924$) liver tissue. Error bars indicate one standard deviation from the mean.

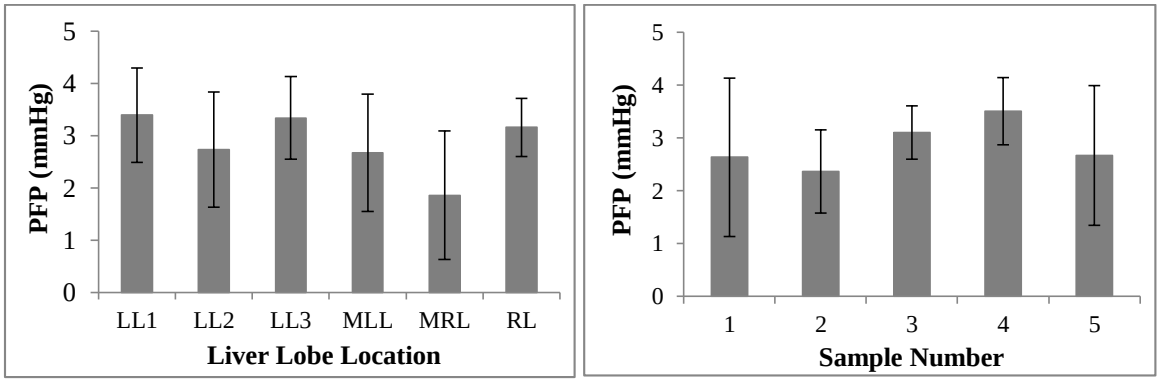

Figure 4: *In-situ* mean PFP measurements with standard deviation error bars as a function of location of pressure measurement (left) and sample number (right). The liver lobe locations are as follows: left lobe locations 1-3 (LL1-3), middle left lobe (MLL), middle right lobe (MRL), and right lobe (RL).

***In-situ Measurements*:** Mean PFP across all samples and locations was found to be 2.86 ± 1.04mmHg. One-way ANOVA identified no statistically significant difference between PFP measurements due to measurement location ($p=0.16$) or sample number ($p=0.35$). The mean PFP measurements sorted for location and sample can be seen in Fig. 4.

Ex-situ vs. Right Lobe In-situ Measurements: *In-situ* measurements in the right lobe and all eight *ex-situ* test groups were compared using a one-way ANOVA, which found that there is a statistical significance between groups ($p<0.05$). Pos-hoc analysis was conducted using the Fisher's least significant difference (LSD) correction, to determine which means are statistically different from one-another. Of particular interest was the statistical difference between the *in-situ* results and each of the *ex-situ* conditions. Results show that there is no statistically significant difference between right lobe *in-situ* PFP and native *ex-situ* PFP at 3 ml/min and decellularized *ex-situ* PFP at 6, 9, and 12 ml/min.

Table 2: Comparisons between right lobe *in-situ* measurements and *ex-situ* measurements. P-value < 0.05 (*) indicates a statistically significance difference between groups.

***In-situ* Group**	***Ex-situ* Group**	**p-value**
Right lobe *in-situ*	Native *ex-situ*: 3 ml/min	.372
	Native *ex-situ*: 6 ml/min	.002*
	Native *ex-situ*: 9 ml/min	.000*
	Native *ex-situ*: 12 ml/min	.000*
	Decellularized *ex-situ*: 3 ml/min	.034*
	Decellularized *ex-situ*: 6 ml/min	.122
	Decellularized *ex-situ*: 9 ml/min	.292

Discussion

In both native and decellularized liver, we found a positive correlation between PFP and perfusion flow rate. This finding is particularly important for the recellularization of decellularized liver scaffolds because it will allow us to adjust the perfusion flow rate to physiological PFP. We found that decellularized liver PFP measurements were much lower than their native counterparts, for comparable flow rates. This finding is not surprising, considering the removal of all cellular components in the decellularization process. These results are consistent with our previous work that found that the elastic modulus of decellularized liver is much lower than native liver (10). Future work will include measuring PFP in reseeded liver scaffolds, to evaluate if the redistribution of cells into the matrix results in higher pressures than in the decellularized liver and how that data compares to PFP in native livers.

In-situ PFP in rats was measured to be 2.86 ± 1.04mmHg, with no statistical difference due to measurements taken at different locations within a single liver or between samples. This value is consistent with the estimated published values of liver PFP, 0 – 5 mmHg (5). There was a relatively large range of measured PFP in *in-situ* liver (0.55 – 4.49 mmHg), indicating that there is some variability in PFP across different areas of the liver. This variability in PFP also occurred in *ex-situ* PFP measurements, particularly the native liver at higher flow rates. These observations were expected due to the known heterogeneity of flow rate throughout the liver (7). Although care was taken to insert the pressure probe in the same relative location each time in order to decrease variability across measurements, there is the possibility of error in this method. To further reduce the variations, measurements were taken as superficially as possible in order to ensure that the

probe was not invading larger vessels, which could lead to artificially high measurements. The methodology of using transducer tipped pressure catheters (Millar SPR-524 [3.5F], Millar Instruments Inc.) to measure small organ PFP could be improved with the use of a smaller probe. The probe diameter used in this study was 3.5F (1.2mm), however 1F (.33mm) probes are commercially available. The use of a smaller probe would cause less damage to the tissue upon its insertion and minimize the chances that measurements are taken in the vasculature, and not the parenchyma, of the tissue.

The results of this study demonstrate that the flow rates currently used in the perfusion bioreactors, 6 ml/min and above (3), correspond to *ex-situ* decellularized liver PFP that is similar to *in-situ* PFP measurements in the right lobe of native liver. This finding is important because it indicates that physiological mechanical cues are being delivered to the regenerating tissue. However, future work could involve directly measuring hepatic blood flow during *in-situ* PFP measurements in order to directly compare both physiological flow rates and PFP to the bioreactor parameters. *Ex-situ* PFP measurements in native tissue at the faster flow rates were higher than *ex-situ* decellularized liver and *in-situ* values. These results suggest that PFP may increase in the reseeding process, which could be accounted for by lowering the flow rate as cells are seeded in order to maintain physiological pressures. PFP measurements from these experiments can be implemented as input conditions or used for validation studies in poroviscoelastic (PVE) finite element models of liver tissue (9). Finite element modeling is an efficient and cost-effective way to optimize bioreactor conditions, such as flow rate, that will effect tissue formation.

Conclusions

The present study successfully measured PFP *ex-situ* in both decellularized and native livers and compared these values to *in-situ* measurements of native liver PFP. This work is particularly important to the field of liver bioengineering due to the known mechanosensitivity of liver cells. Methodology from this work can be applied to different organs over a range of sizes to simply and effectively evaluate PFP.

Acknowledgements

This research was funded by a seed grant from the Wake Forest Institute for Regenerative Medicine.

CHAPTER 3.2

Porohyperviscoelastic Model Simutaneously Predicts Parenchymal Fluid Pressure and Reaction Force in Perfused Liver

Emma C. Moran, Smitha Raghunathan, Douglas W. Evans, Nicholas A. Vavalle, Tanya LeRoith, Thomas L. Smith, Jessica L. Sparks

Manuscript was written and prepared by Emma C. Moran. Smitha, Douglas and Nicholas helped with experimental studies, model development and editing. Tanya provided histological analysis, Thomas provided experimental guidance and Jessica served in an advisory capacity. Text and figure formatting variations are due to journal guidelines. The work was published in *Journal of Biomechanical Engineering* 2012; 134(9):091002.

Abstract

Porohyperviscoelastic (PHVE) modeling gives a simplified continuum approximation of pore fluid behavior within the parenchyma of liver tissue. This modeling approach is particularly applicable to tissue engineering of artificial livers, where the inherent complexity of the engineered scaffolds prevents the use of computational fluid dynamics. The objectives of this study were to simultaneously predict experimental parenchymal fluid pressure (PFP) and compression response in a PHVE liver model. Model PFP matched experimental measurements (318 Pa) to within 1.5%. Linear regression of both phases of compression, ramp and hold, demonstrated strong correlation between model and experimental reaction force ($p<0.5$). The ability of this PVE model to accurately predict both fluid and solid behavior is important due to the highly vascularized nature of liver tissue and the mechanosensitivity of liver cells to solid matrix and fluid flow properties.

Introduction

Chronic liver disease, including cirrhosis, hepatitis and hepatocellular carcinoma, is a tremendous problem in the United States with an economic burden of 1.6 billion dollars per year (11). This condition usually results in the need for a transplanted organ, which is the gold standard of treatment for patients with end stage liver failure. However, the demand for transplantation greatly exceeds the supply, with 16,250 people on the waiting list and only 6,291 liver transplantation procedures being performed in 2010 (2). This need has driven biomedical research into alternatives to whole liver transplantation. One such

approach is the engineering of bioartificial livers using tissue engineering and regenerative medicine techniques.

Decellularization is one technique used in the tissue engineering of artificial livers (3-7). The decellularization process removes all of the cellular components of native liver while retaining the bioactive extracellular matrix (ECM), which is necessary to regulate cell differentiation and function. In addition, the decellularized liver contains an intact microvasculature that allows for perfusion of the tissue (3, 12-15). Following decellularization, native liver cells can be introduced into the scaffold in a perfusion bioreactor which mimics the physiological environment for the purpose of cell growth (3). This recellularization process contains two steps: seeding of the cells into the scaffold followed by maintenance of the forming tissue through perfusion of media. The intact vasculature of the scaffold is crucial for both steps. The retention of microvasculature and resulting fluid transport allows for both delivery of cells into the liver matrix and adequate oxygen and nutrient supply, a process necessary for cell survival and tissue growth.

While the intrinsic vascular system in decellularized scaffolds is necessary for tissue regeneration, it is inherently complex. In geometrically simpler scaffolding designs, computational fluid dynamics (CFD) can be used to predict fluid stresses acting on the cells in perfusion bioreactors (16, 17). Knowledge of these forces is particularly important in liver tissue engineering because it has recently been shown that microenvironment mechanical properties regulate the phenotype of hepatic stem and progenitor cells (18) and that hepatocytes, portal fibroblasts and stellate cells exhibit mechanosensitivity as well (19). In addition to matrix stiffness, hepatocytes have also been shown to respond to changes in parenchymal fluid pressure (PFP) (1). However, applying CFD to bioengineered

scaffolds requires detailed knowledge of the 3-D porous structures in which fluid flows, information that is not feasible to obtain in liver.

Porohyperviscoelastic (PHVE) modeling gives a simplified continuum approximation of pore fluid behavior within the parenchyma of liver tissue. PHVE is an extension of biphasic theory, which models the material to be a porous-fluid saturated solid, in which the fluid flows relative to the deforming solid (20). Hyperelasticity and viscoelasticity are integrated into this theory to account for the non-linear elastic behavior and inherent viscoelasticity of the liver solid matrix, respectively. In the liver, the space of Disse (or interstitium) is continuous with the sinusoidal space, with free passage of fluid from one compartment to the other. Therefore, the term "parenchymal fluid" is used throughout this study, rather than "interstitial fluid". The experimental and PHVE modeling work described in this paper successfully characterized intrinsic solid matrix mechanical behavior and fluid flow-dependent parenchymal fluid pressure (PFP) in perfused liver tissue with a single computational model. In the future, calculating these biomechanical conditions throughout the parenchyma of seeded decellularized scaffolds is essential for optimizing both cell seeding and maintenance in perfusion bioreactor designs for liver regeneration. This study represents a step toward that goal, by demonstrating that a three-dimensional PHVE liver model can accurately predict reaction force and PFP in perfused native liver tissue, using a single set of model parameters.

Other studies have used extensions of poroelastic modeling, such as poroviscoelastic (PVE) and porohyperelastic (PHE), to characterize numerous soft biological tissues, including cartilage (21-25), intervertebral discs (26), lung (27), heart (28), brain (29, 30), and aorta (31). The authors of the present study previously reported an

application of PHVE theory to liver tissue (9), with the development of a two-dimensional axisymmetric PHVE model that accurately simulated liver tissue stress relaxation response in unperfused liver specimens. More recently, hyperelastic, viscous and porous components of liver biomechanics were applied in a soft tissue model for surgery simulation (32). Since a PHVE model is capable of predicting pore fluid response in addition to solid matrix stress, this modeling strategy can be extended to three-dimensions to examine the behavior of perfused native liver tissue.

Previous work in liver perfusion has investigated modeling the hepatic circulation on a microscale level to examine the interactions between fluid and solid phases (33, 34). Wu *et al.* used a tumor microcirculation model to examine the interactions between intravascular and interstitial flow dynamics (35). The present work focuses on the relationship between macroscale fluid input and microscale flow. To the authors' knowledge, this is the first study to report a validated three-dimensional PHVE model of liver perfusion. The objective of this study was to model perfused liver tissue using finite element methods to:

1) Simultaneously predict experimental parenchymal fluid pressure and compression response in an avascular model of liver tissue.
2) Apply these optimized solid matrix and fluid properties to a model of liver containing a portal vein to analyze the effect of fluid input geometry on parenchymal fluid pressure.

Future research will couple this PHVE modeling strategy with mass transport and predictive cell behavior models to optimize biomechanical conditions for effective liver tissue formation in the field of regenerative medicine.

Materials and Methods

Specimen Preparation. Bovine livers from female cows, average weight of 1,100 pounds and age eight to eleven years, were acquired from a local abattoir. The tissue was placed on ice immediately after animal sacrifice and kept on ice for transport to the laboratory, where samples were isolated as described below. A novel method was developed in order to achieve regular, repeatable-geometry tissue samples near the terminal branches of each vascular segment (Fig. 1). Extraneous fat and connective tissue were removed from the porta hepatis region in order to trace the portal vein, and a probe was then used to follow the vessel to terminal branches where vasculature had reached a diameter less than 2mm. The capsule was then removed from the area of interest and samples were harvested using a surgical blade and template. Samples were then trimmed to appropriate heights and dimensions, yielding a total of 14 discs with attached portal vein from five different livers. Samples were nominally 26.5mm in height with a surface area of 5150.8mm^2. After harvest, samples were stored in Dulbecco's Modified Eagle Medium (DMEM) and refrigerated until testing the next day. All samples were tested between 24 and 44 hours post mortem. Histological sections were obtained at sample harvest and again at sample testing to investigate the effect of storage time on tissue integrity.

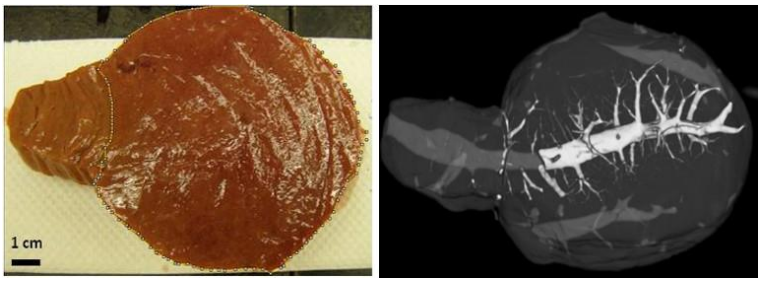

Figure 1: Left: Cylindrical sample of bovine tissue used in experimental testing. Right: Micro-CT image of perfused sample showing the portal vein with branching

The final step of specimen preparation involved placing a foley catheter in the portal vein entrance to the sample. The tip of the catheter was inflated to prevent back-flow of perfusate. The samples were then placed in the test chamber with the foley catheter secured to the chamber wall (Fig. 2).

Histology: Histology specimens were acquired at sample harvest and again immediately before the commencement of mechanical testing. Samples were fixed in 10% neutral buffered formalin and stained with hematoxylin and eosin (H&E), allowing the investigation of tissue degradation between sample harvest and testing. Tissue degradation of each sample was evaluated by a board certified veterinary pathologist, using a numeric scale (Table 1) in which cell swelling, dissociation and nuclear dissolution were evaluated. A two sample non-parametric T-test (Mann-Whitney) was conducted on histology sets to determine if there was a significant difference between sample integrity at harvest and at testing. Also, a correlation study was performed between histology rating and sample peak reaction force, attempting to determine whether or not tissue rating influenced mechanical response.

Table 1: Histology rating scale detailing examination of cell swelling, dissociation and nuclear dissolution.

0	Normal
1	Mild cell swelling
2	Moderate cell swelling
3	Moderate cell swelling and dissociation (>25%)
4	Moderate cell swelling with nuclear dissolution (>25%)
5	Severe cell swelling, nuclear dissolution, and tissue degradation

Test Configuration: Unconfined compression testing was conducted on a Bose Test Bench mechanical characterization system with enclosed environmental chamber (Fig. 2)

(Bose Electroforce, Eden Prairie, MN). During testing, the load cell (10N, ±.0098N resolution, submersible, Honeywell Model 31) was submerged in room temperature saline in order to minimize reaction force artifacts created by perfusate exiting tissue. Continual perfusion of specimens during testing maintained a layer of saline between sample and platen. This significantly reduced the interface friction between sample and platen, allowing the selection of a frictionless boundary condition during modeling.

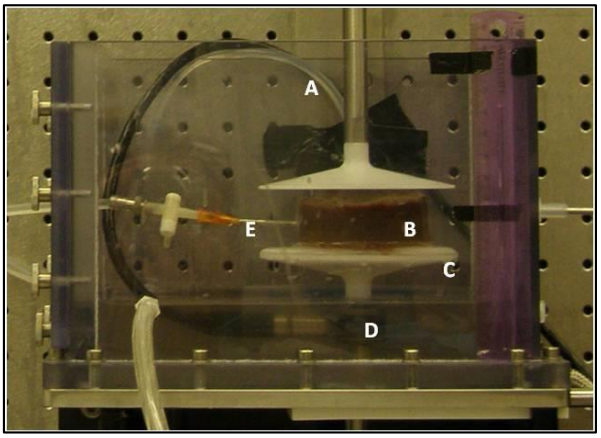

Figure 2: Mechanical testing configuration for perfused bovine liver testing depicting perfusion input tubing (A), specimen (B), saline boundary between sample and platen (C), load cell (D), and wick-catheter parenchymal fluid pressure measurement system (E). Environmental chamber dimensions 20cm x 15cm x 15cm.

Parenchymal Fluid Pressure Measurement: PFP measurements were made using the wick-catheter method [22] (Fig. 3). The wick-catheter method works on the principle of creating a continuous column of fluid between hydrated tissue and a distal pressure transducer, connected by flexible tubing. This arrangement eliminates the contribution of solid-phase mechanical stress in pressure readings, allowing isolated measurement of only the fluid pressure response. The catheter was created using the flexible tip of a shielded I.V. catheter (14 gauge). Absorbable dexon suture (0.35mm diameter) was used to create the wick, and inserted in the catheter tip with approximately 1-2mm protruding to facilitate fluid entry into the small diameter catheter (Fig. 3). The catheter was then connected to a

pressure transducer (Micro Switch, Freeport, IL) via 3.5mm flexible medical tubing and filled with vacuum-treated water. The water was exposed to negative pressure for at least 24 hours prior to use in order to minimize compressible gasses coming out of solution during testing. This allowed the water to act as an incompressible medium to transmit interstitial fluid pressure changes from the catheter tip to the remote pressure sensor. System calibration, or the conversion of sensor output from mV to mmHg, was conducted by measuring sensor voltage output when the catheter tip was inserted at the base of water columns of variable heights. Once a liver sample was prepared for testing, a syringe tip was placed on the catheter and the device was inserted 15mm into the parenchyma of the tissue. The syringe tip was then withdrawn from the tissue, leaving only the flexible catheter to transmit pressure measurements. Since the catheter was inserted into the parenchyma, and not the vasculature, of the liver tissue, the catheter measured pore fluid gauge pressure. In this work, the term parenchymal fluid pressure is used to describe this measurement. Pressure measurements were filtered using a low-pass Butterworth filter. Threshold frequencies selected were unique to each data set. Noise data was then integrated and normalized to yield data centered at 0 ± .25 with a regression slope of less than 7E-05.

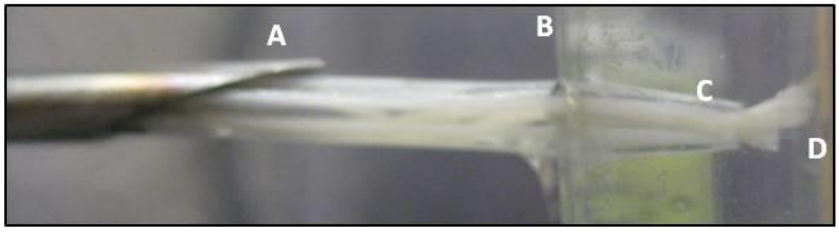

Figure 3: Wick catheter system with syringe tip (A) withdrawn, shown inserted into a water column calibration device (B). Note soluble dexon suture (D) extending past catheter tip (C).

Sample Perfusion Experiments: Prior to the compression experiments, all liver samples were perfused to steady-state in order to simulate physiological parenchymal fluid conditions. Samples were perfused to normal PFP (~3 mmHg) (6) with room temperature normal saline solution using a gravity perfusion system. The perfusate reservoir was placed 0.66m above the sample and a pump was used to maintain a constant perfusate level in the reservoir. This reservoir was then connected to the foley catheter at the portal vein entrance of each sample using flexible 5mm tubing. Samples were perfused for 10 minutes until mechanical equilibrium (steady state perfused mass) was achieved. Sample mass and PFP were monitored throughout the equilibration period. Specimens were continually perfused for all remaining experiments (unconfined compression and equlibrium stress-strain testing).

Unconfined Compression Experiments: After equilibrium (steady-state perfused mass) was achieved, perfused specimens were then preloaded to 1g and allowed to relax for 900 seconds until relaxation fell below .01g/s for the final 100 seconds of the test [12]. The preloading protocol and subsequent relaxation time were selected based on preliminary tests, in order to achieve consistent baseline conditions in all samples (average pre-test equilibrium load of .5g). After preloading, samples were subjected to unconfined compression to 15% strain at a rate of $0.001s^{-1}$. Reaction force was measured with a 10N submersible load cell (Honeywell Model 31) while interstitial pressure was monitored via the wick-catheter pressure measurement system. At peak compression, samples were allowed to relax for approximately 3000 seconds, until relaxation fell below .01g/s for the final 100 seconds of the test [12].

Equilibrium Stress-Strain Experiments: Equilibrium stress-strain testing was conducted on a separate set of four bovine liver samples (from two livers) in unconfined compression. These tests were conducted in order to assess the time-independent behavior of the tissue (23), allowing the selection of either a linear elastic or hyperelastic material model. Successive ramp displacements to 5, 15 and 25% strain were applied to each sample at a rate of $0.001s^{-1}$. After each compression ramp, samples were allowed to equilibrate for 3000 seconds before the application of the next strain level. Relaxation was achieved when the change in tissue load was less than .01g/s for the final 100 seconds of equilibration. Lagrangian stress was calculated by dividing equilibrium reaction force by average initial surface area.

Porohyperviscoelastic Material Model: PHVE theory is an extension of biphasic theory, which states that a material is comprised of an incompressible solid substance and an incompressible liquid, where the relative motion between these two phases creates rate-dependent behavior (21). When the liquid phase is inviscid, it has been shown that biphasic theory is equivalent to poroelasticity (20). Poroelasticity is widely used in finite-element modeling programs, such as Abaqus, to study soil mechanics and more recently this methodology has been extended to PVE, to include the inherent viscoelasticity of the solid matrix (9, 22, 29, 36).

As adapted from Evans *et al* (10), the equations governing biphasic theory were first proposed by Mow (21) and are given by Eqs. (1-7) [15, 18, 32, 35]. In linear biphasic theory, it is assumed that the solid phase and fluid phase are both intrinsically incompressible; however the drained response of the tissue is compressible due to exudation of fluid (37). Using this assumption, the conservation of mass can be written as:

$$\underline{\nabla} \cdot (\Phi^s \underline{v}^s + \Phi^f \underline{v}^f) = \underline{0} \tag{1}$$

where *s* and *f* stand for solid and fluid phase respectively, Φ is volume ratio, $\underline{v}$ is velocity. It is assumed that $\Phi^f + \Phi^s = 1 (37)$. Assuming inertial forces to be much smaller in magnitude than internal frictional forces, the conservation of linear momentum can be written as:

$$\underline{\nabla} \cdot \underline{\underline{\sigma}}^s + \underline{\pi}^s = \underline{0} \tag{2}$$

$$\underline{\nabla} \cdot \underline{\underline{\sigma}}^f + \underline{\pi}^f = \underline{0} \tag{3}$$

where $\underline{\underline{\sigma}}$ are Cauchy stress tensors of each phase and $\underline{\pi}$ are frictional body forces (units: F L^{-3}). The frictional body forces are assumed to be proportional to their relative velocities and inversely proportional to the hydraulic permeability k'(units: L^4 F^{-1} T^{-1}) so that:

$$\underline{\pi}^s = -\underline{\pi}^f = \frac{(\Phi^f)^2}{k'} (\underline{v}^f - \underline{v}^s) \tag{4}$$

Finally, the stress in each phase can be written as:

$$\underline{\underline{\sigma}}^f = -\Phi^f p \underline{\underline{I}} \tag{5}$$

$$\underline{\underline{\sigma}}^s = -\Phi^s p \underline{\underline{I}} + \underline{\underline{\sigma}}^s \tag{6}$$

where p is pore fluid pressure and $\underline{\underline{\sigma}}^s$ is the apparent solid stress due to deformation of the solid matrix. Thus, the total stress is given as:

$$\underline{\underline{\sigma}} = \underline{\underline{\sigma}}^s + \underline{\underline{\sigma}}^f \tag{7}$$

In PHVE theory the effective solid stress tensor $\underline{\underline{\sigma}}^{s}$ is replaced with:

$$\underline{\underline{\sigma}}^{s} = \int_0^t 2G(\tau-\tau')\dot{\underline{\underline{e}}}dt' + \underline{\underline{I}}\int_0^t K(\tau-\tau')\dot{\phi}dt' \tag{8}$$

where *G* and *K* are the elastic shear and bulk relaxation functions, $\underline{\underline{e}}$ is the mechanical deviatoric strain and ϕ is the volumetric strain (22, 25). The relaxation function implemented in this work was a three-term Prony series expansion:

$$R(t) = \frac{R_\infty}{1-\sum_{i=1}^{n} r_i}\left[1-\sum_{i=1}^{n} r_i\left(1-e^{-t/\tau_i}\right)\right], n=3 \tag{9}$$

where R is the time-dependent modulus, R_∞ is the long-term modulus, and the Prony series parameters (n, r_i, and τ_i, i=1,2,…,n) are material constants (38).

In this work, a hyperelastic material model was used to model the rate-independent behavior of the solid matrix based on the non-linearity of the equilibrium stress-strain curve (Fig. 5). A 2nd order reduced polynomial hyperelastic model was chosen based on stability and fit analysis. The reduced polynomial model is a particular form of the general polynomial model in which the second invariant is assumed to be zero $(C_{ij} \to C_{i0})$. This assumption is justified through the observations that the sensitivity of the strain energy function to the second invariant is generally much smaller than that to the first invariant [34]. Additionally, the second invariant dependence is difficult to measure and therefore based on potentially inaccurate measurements (39). This reduced polynomial material model is given in Eq. (9) where *U* is the strain energy per unit reference volume, $\bar{I}_1$ is the

first deviatoric strain invariant, J^{el} is the elastic volume ratio, and N is the polynomial order (38). The remaining coefficients C_{i0} and D_i are material parameters.

$$U = \sum_{i=1}^{N} C_{i0}\left(\bar{I}_1 - 3\right)^i + \sum_{i=1}^{N} \frac{1}{D_i}\left(J^{el} - 1\right)^{2i}, N = 2 \tag{10}$$

C_{i0} and D_i are related to the initial shear modulus (μ_0), bulk modulus (K_0), and Poisson's ratio (ν) through Eqns. 10 and 11:

$$\mu_0 = 2C_{10} \tag{11}$$

$$D_1 = \frac{2}{K_0} = \frac{2(1-2\nu)}{\mu_0(1+\nu)} \tag{12}$$

In Abaqus SOIL analysis, Darcy's law governs the rate of fluid transport through the solid matrix:

$$\underline{f} = -\frac{\underline{k}}{\gamma_w}\left(\frac{\partial p}{\partial \underline{x}} - \rho_w \underline{g}\right) \tag{13}$$

Where $\underline{f}$ is the volumetric flow rate of wetting liquid per unit area of porous medium, $\underline{k}$ is material permeability, γ_w is the specific weight of the wetting liquid, ρ_w is the density of the fluid, and $\underline{g}$ is gravitational acceleration. Note that Abaqus defines permeability $\underline{k}$ (units: LT^{-1}), which many authors refer to as hydraulic conductivity. Abaqus permeability is related to hydraulic permeability k' seen in Eq. 4 (units: $L^4 F^{-1} T^{-1}$) by:

$$k\left(\frac{m}{s}\right) = k'\left(\frac{m^4}{Ns}\right) * \gamma_w\left(\frac{kg}{m^3} * \frac{m}{s^2}\right) \tag{14}$$

Finite Element Models: Geometry, Mesh and Boundary Conditions: Two three-dimensional porohyperviscoelastic finite element models were created using Abaqus SOIL analysis (Abaqus v6.10). The geometry of both models mimics the cylindrical liver stamps used in experimental testing (diameter = 80mm, height = 27mm). The first model, termed the avascular model, is a uniform cylinder in which perfusion is simulated by applying the fluid load to a small area at the surface of the tissue (Fig. 4). The second, or portal, model contains a simulated portal vein and the fluid load is applied throughout the vein to simulate distributed tissue perfusion (Fig. 4). The portal vein was represented as a truncated cone where the dimensions were found from microCT images of an experimental sample (Fig. 1).

Experimental flow rate (1 liter/ 2.25 min) allowed for the normalization of fluid velocity based on the surface area over which it was applied. The avascular model surface area was 6.28E-5m^2 and the portal surface area was 1.18E-03m^2. Using these values, the avascular model surface pore fluid load calculated was -.118m/s and the portal model load was -.00627m/s, where the negative sign indicates movement of the fluid into the tissue. The boundary condition of drainage-only flow was applied to the lateral surfaces of both models using the parameter SFLOW (5E-06m^4/Ns), so that fluid flow only occurs from the interior to the exterior region of the model, and the bottom surfaces were constrained from moving vertically in all steps. Initial void ratio was specified to be 0.2, based on histological analysis (Fig. 5). Both parts were meshed in Hypermesh and contain 3840 8-node elements with trilinear displacement, pore pressure and reduced integration type (C3D8RP). Mesh convergence studies confirmed an appropriate mesh density.

Finite Element Simulations: The open channel geometry of the portal model prevented the simulation of 15% compression in this model, so only the avascular model was used to simulate unconfined compression experiments. Both models were used to simulate perfusion, which consisted of perfusing fluid for 200 seconds to allow the parenchymal pressure in the model to reach equilibrium. Following the 200 second perfusion equilibration period, compression of the perfused avascular model was performed through displacement of the top nodes to 15% strain at a rate of $.001s^{-1}$. A 3000 second hold step followed the compression to allow for relaxation of the tissue.

The output variables used to compare experimental and model results were parenchymal fluid pressure at equilibrium following the perfusion step and reaction force throughout the compression and hold periods. Parenchymal fluid pressure was calculated by averaging 77 nodes over an area that the mimicked the location of the experimental wick-in-catheter measurement (Fig. 4). Reaction force was found by summing all of the nodes on the bottom of the sample.

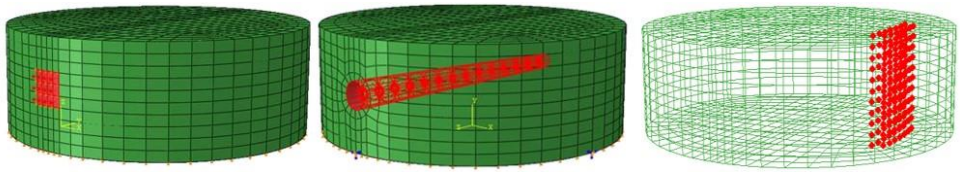

Figure 4: Left: Avascular model showing surface area over which the surface fluid load was applied. Middle: Portal model with simulated portal vein. The surface area of the fluid load is shaded and was directed into the tissue from the sides of the portal vein. Right: Red nodes indicate those included in the calculation for parenchymal fluid pressure.

Finite Element Model Optimization: The model optimization was performed on the avascular liver model to identify a set of material properties to accurately predict both steady-state parenchymal fluid pressure and reaction force during compression/relaxation. These parameters were then applied directly to the portal liver model in simulation of

distributed perfusion. Material properties were optimized using commercial optimization software (Isight Design Gateway 5.0) using a Pointer algorithm. Pointer is an automatic optimization that controls an evolutionary algorithm (40, 41), the Nelder and Mead downhill simplex method (42), sequential quadratic programming (NPQL) (43), and a linear simplex method (41). During the optimization procedure, the program determines which algorithms are most successful in converging on the objective and controls the optimization scheme accordingly. The most feasible design is one that satisfies all constraints and best minimizes the objective function, which calculates distance between the model value and experimental value.

Baseline material properties were selected based on previous PHVE liver modeling by the authors (9). SFLOW, or the drainage only boundary condition, was varied until the PFP and reaction force outputs were within the correct order of magnitude. The sum of the relaxation Prony coefficients ($g_1+g_2+g_3$), which control the equilibrium force of the relaxed tissue, were manually fit to the mean experimental equilibrium force. The Pointer algorithm was then used to optimize for PFP, with permeability (k) set as a variable and confined to a specific range. Once this optimization converged on a feasible design, a second optimization was run, with the already optimized PFP value set as the constraint of the optimization. Peak reaction force was the objective and hyperelastic parameters (C_{10}, C_{20}, D_1) were variables. Following this second optimization, final Prony series parameters were obtained by manually fitting mean relaxation time-history data to model relaxation output, keeping the sum of the g terms constant.

Results

Histology: A representative H&E image of bovine liver can be seen in Figure 5. The average histological tissue degradation ratings were 1.3 (S.E.M = 0.05) and 1.7 (S.E.M = 0.08) for samples taken at harvest and test time respectively. A two sample non-parametric T-test (Mann-Whitney) was conducted to compare specimens from harvest versus test time. Tissue integrity was shown to be significantly different between these two data sets ($p < .05$), based upon the assessment of cell swelling, cell wall integrity and nuclear dissolution (Table 1). However, there was no statistically significant correlation between peak reaction force during compression testing and histological grading ($p > .05$). This suggests that while there was some sample degradation during refrigerated storage time, it was not enough to cause a statistically significant influence on tissue reaction force during compression.

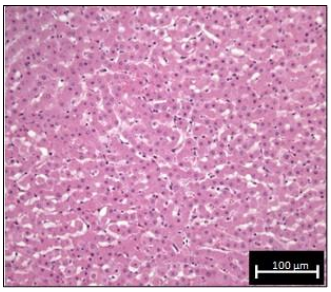

Figure 5: A representative H&E image of bovine liver. Void volume was determined from histological images using the methodology reported in Raghunathan *et al.* Void ratio was calculated to be 0.2, according to the equation e = n/(1-n), where n=void volume/total volume.

Equilibrium Stress-Strain Relationship: Average equilibrium stress-strain results showed a slightly nonlinear relationship over the range of strains tested (Fig. 6), which is consistent with previous studies on liver tissue (9). Two of the four samples were unable to be

compressed to 25% strain due to concern over exceeding the load cell capacity (10N). These samples were instead compressed to 20% and 23% strain.

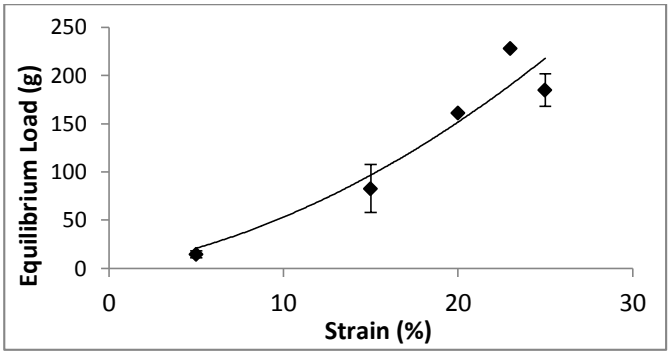

Figure 6: Equilibrium load versus strain results for perfused bovine liver samples (95% confidence intervals shown)

Model Parameters: Optimized hyperelastic parameters, Prony series parameters, and permeability can be seen in Table 2. From hyperelastic terms, the initial shear modulus, bulk modulus and Poisson's ratio were calculated to be $\mu_0 = 200.6Pa$, $K_0 = 606.1Pa$, and $\nu = .35$.

Table 2: Material properties of optimized PHVE model

Solid Phase							Fluid Phase	
Hyperelasticity: Reduced order polynomial				Viscoelasticity: Prony Series			Permeability	Specific Weight
C_{10}	C_{20}	D_1	D_2	g_1/τ_1	g_2/τ_2	g_3/τ_3	k	γ
100.3 Pa	376.4 Pa	.0033	0	.12/ 5sec	.4/ 50sec	.28/ 600sec	.00401 m/s	9855 N/m³

Perfusion Results: The experimental average steady-state parenchymal fluid pressure (PFP) following tissue perfusion was 318 Pa (S.E.M. = 69 Pa). The avascular model, optimized to the experimental data, was within 1.5%, predicting a value of 313 Pa. Using the optimized material properties from the avascular model, the portal model underpredicted experimental PFP by 29%, a value of 225 Pa. Contour maps of the pore pressure (PFP) and fluid velocity following perfusion also revealed different patterns of fluid flow between the two models (Fig. 7).

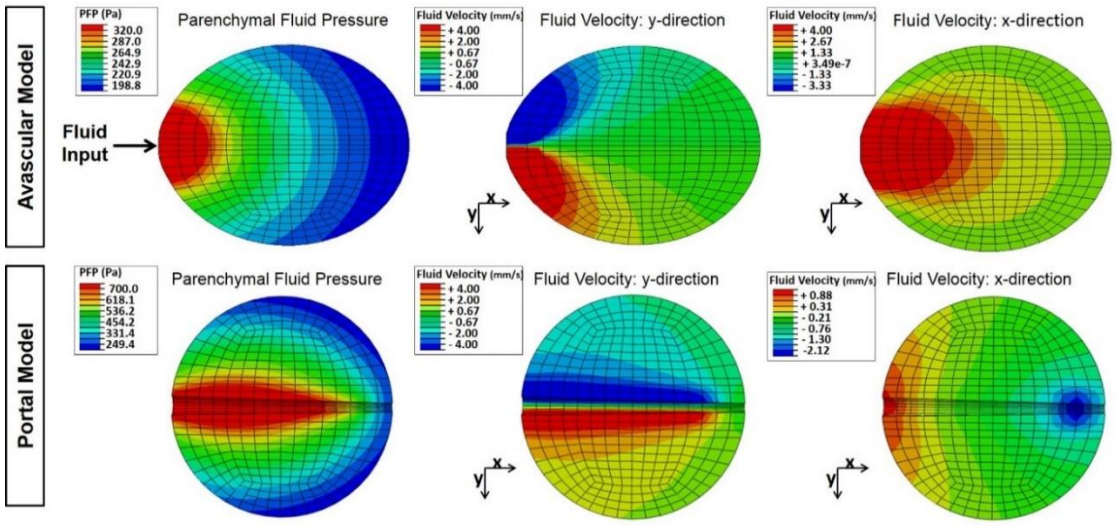

Figure 7: The avascular models (top) and portal models (bottom) are cut in half, horizontally, displaying the middle of the tissue. Left: parenchymal fluid pressure (PFP), Middle: fluid velocity in the y-direction, Right: fluid velocity in the x-direction.

Compression Results: The avascular finite element model showed strong similarity to experimental compression and relaxation (Fig. 8). Validation was carried out using linear regression techniques (44). Linear regression of the model vs. experimental ramp phase reaction force demonstrated strong correlation, yielding an R^2 value of .989 with a slope of .989 ($p<.05$). Linear regression of the relaxation phase similarly showed strong correlation, with an R^2 value of .990 and a slope of .962 ($p<.05$) (Fig. 9). During compression, the average experimental increase in PFP was minimal (7.5% of steady-state PFP). Similarly, avascular model output from the nodes simulating experimental measurements (Fig. 4) showed no significant change in pressure with compression (1.2% of steady-state PFP) (Fig. 10).

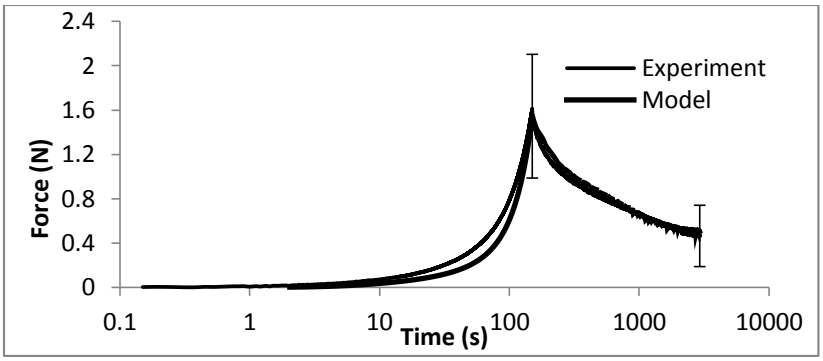

Figure 8: Reaction force of the ramp and hold of average experimental data and PVE model prediction with error bars indicating standard deviation of the liver sample's peak and relaxed reaction force.

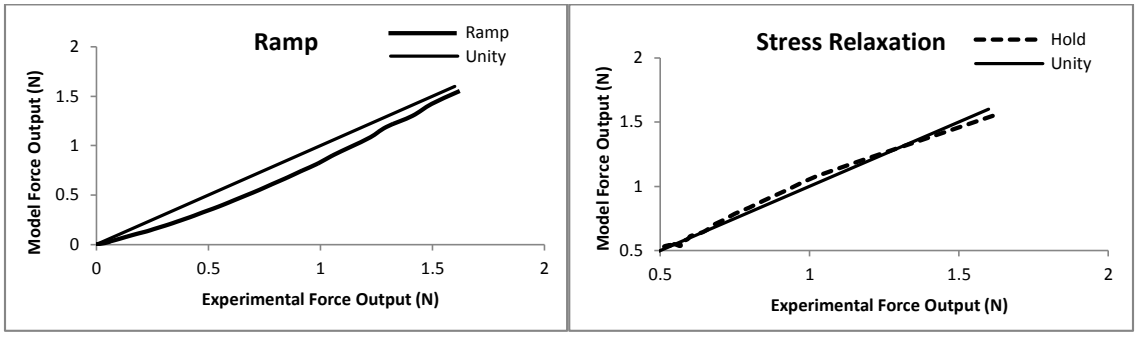

Figure 9: Linear regression comparing experimental ramp phase data (left) and hold phase data (right) to their PVE model simulations.

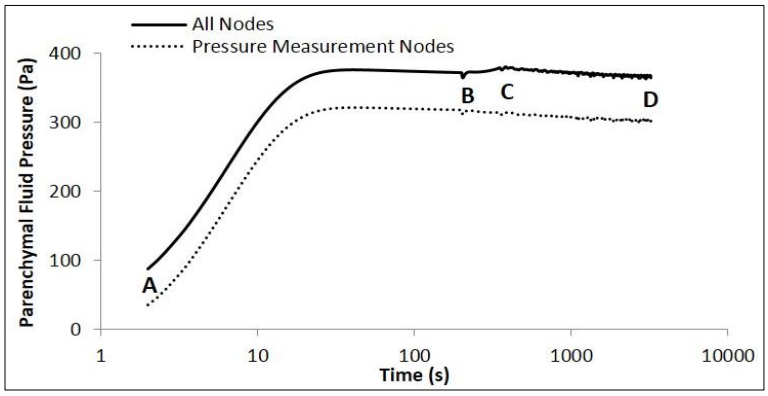

Figure 10: Parenchymal Fluid Pressure (PFP) as a function of time for perfusion (A→B), compression (B→C), and hold (C→D). Measurements are shown as both the average of nodes from the entire model (solid line) and the area of 77 nodes used to optimize PFP (dashed line) (refer to Fig. 4). Small oscillations in pressure during the hold phase can be attributed to instability in PE finite element modeling in Abaqus, as described by Stokes, *et al*. (45). For comparison, experimental steady state pressure was 318 Pa, increasing 7.5% during compression.

Discussion

The three-dimensional PHVE liver model developed in this study successfully predicted both experimental parenchymal fluid pressure and reaction force during stress relaxation testing in the avascular geometry model. PFP was predicted to within 1.5% of experimental measurements and the stress relaxation displayed high linear correlation (R^2>0.98) between model and experiment. While a two-dimensional PHVE model can accurately simulate the mechanical response of liver tissue under compression, as demonstrated by Raghunathan *et al.*, a three-dimensional model is needed to examine the effects of portal vein perfusion on both parenchymal fluid pressure and mechanical response. The ability of this model to predict both fluid and solid behavior is important due to the highly vascularized nature of liver tissue and the effects of fluid flow and solid matrix characteristics on the behavior of liver cells. This modeling technique ultimately can be used in conjunction with mass transport, such as Vande Geest *et al.* (46), and predictive cell behavior models, as described in *Stops et al.* (47, 48), to optimize the growth of functional liver tissue using decellularized whole organ scaffolds.

The development of a liver finite element model that includes perfusion and accurately predicts PFP is also important due to the known effects of perfusion on mechanical properties (49). In addition, previous work by the authors has shown that perfusion acts to standardize soft tissue materials being tested, leading to less variability in mechanical testing results (10). However, the present study showed that the geometry of the model influenced the resulting pore pressure, despite normalization of fluid flow velocity to surface area. Using the optimized material properties from the avascular model, the portal model under-predicted the experimental pore pressure by 93 Pa (29%). This

underestimation of pressure could be due to the fact that the fluid load in the portal model was applied closer to the boundaries of the model, specifically in the area in which the pressure was measured. This finding highlights the importance of fluid flow input distribution geometry in PVE model pressure response. Pressure measurements from both perfusion and compression of the avascular model demonstrate that most of the increase in pressure occurs during the perfusion step, as seen in Figure 10. There is a slight increase in PFP during compression in the average of the nodes used to simulate experimental measurements (1.2% increase) and the average of all of the nodes (3.8% increase). This discrepancy in pressure increase between the two measurements methods is not surprising considering the pore pressure distribution (Fig. 7), noting that the pressure measurement node subset is closer to the periphery of the model (Fig. 4). Finally, there is a mild decrease in PFP during the hold period, indicating that the contribution of fluid exudation to relaxation of the tissue is minimal.

The governing behavior of fluid was modeled using Darcy's law, with the assumption of isotropic, constant permeability and full saturation throughout perfusion and compression. In this model, permeability is an optimized material property, due to lack of experimental data on liver permeability. Thus, permeability is assumed constant in the model. As a result of this assumption and the lack of a defined porous bulk modulus, it was found that the calculated pore pressure and reaction forces were independent of specified initial void ratio. Void ratio values can have an influence on pore pressure and reaction force if the permeability is specified as a function of void ratio (50). Future work will include experimentally determining liver permeability and its changes with void ratio, and then implementing these results in a finite element model. Modeling void ratio changes

with tissue permeability will lead to more accurate fluid behavior in the computational model. The optimized permeability in this model is .00401 m/s, which is within the estimated range of values found from swelling tests of liver tissue (51). This indicates that permeability in liver may be much higher than experimentally measured values for articular cartilage and intervertebral discs (52), and using those values in PHVE modeling of liver tissue may not be appropriate. More information on experimental values of liver tissue permeability and the relationship between permeability and changes in void ratio would improve the accuracy of the model and may allow for fewer assumptions in the fluid behavior.

In poroviscoelastic theory, the time-dependent relaxation response of the tissue is a result of both the inherent viscoelasticity of the solid matrix and exudation of the fluid from the solid matrix. In order to investigate the contributions of these two mechanisms within the PHVE model, porohyperelastic (PHE) and viscohyperelastic (VHE) models were developed. The PHE model excluded the inherent viscoelasticity of the solid matrix, while the VHE omitted tissue perfusion and fluid components. The material parameters used in these models were the optimized material properties from the PHVE model (Table 2). The results from the ramp and hold simulations of all three models are shown in Figure 11. It can be seen from this figure that there is no relaxation of the tissue in the PHE model, suggesting that all of the relaxation response is due to the viscoelasticity of the solid matrix, as seen in the stress relaxation of the VHE material. It is believed that this is due to the extremely high permeability of liver tissue and slow compression rate used in this testing. The high permeability and slow rate of compression allow for most of the fluid to escape during compression and reach equilibrium within the tissue before the hold period begins.

Effective fluid velocities reaching 4mm/s were observed in the PHVE model (Fig. 7), providing evidence that the fluid is moving through the solid matrix at a fast rate. This theory is supported by the fact that there was minimal (7.5%) increase in experimental pressure during compression.

Large differences in peak force were also observed between the PHVE, PHE, and VHE models. The PHE model demonstrated a higher peak force than the PHVE, because the inherent viscoelasticity of the solid matrix caused the PHVE model to begin relaxing during the long compression time. The VHE model demonstrated a much lower peak force than both models, indicating that the fluid greatly contributes to the stiffness of the tissue. Hyperelastic material constants were chosen instead of linear elastic constants due to the non-linearity of the equilibrium stress-strain curve (Fig. 6). To demonstrate the effect of the non-linear elastic material parameters, a poroviscoelastic (PVE) model was developed for comparision, which used a linear elastic model to define the time-independent behavior. Young's Modulus in the PVE model was 2500Pa, with a Poisson's ratio of 0.35. Results from this analysis are shown in Figure 12. This graph demonstrates that the hyperelastic model better fits the experimental data than the linear elastic model. Due to the large experimental strain, the hyperelastic model was restricted to the use of a 2^{nd} order reduced polynomial model. Higher order material models fit the experimental data more accurately, but were unstable in this degree of compression. This could account for the weaker linear regression of the ramp phase versus the hold phase of the model.

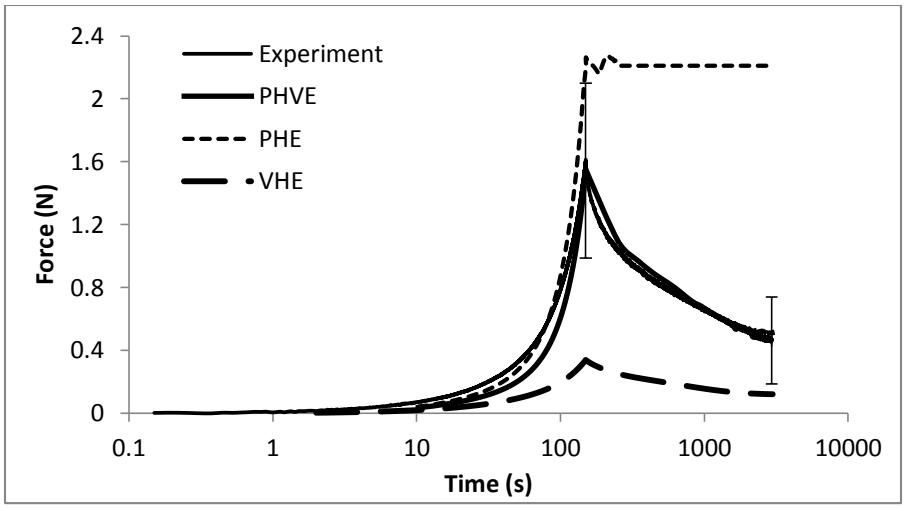

Figure 11: Stress relaxation response of (1) porohyperviscoelastic (PHVE) model that was optimized to experimental pressure and reaction force, (2) porohyperelastic (PHE) model in which the viscoelastic Prony series was removed, and (3) viscohyperelastic (VHE) model in which all fluid components were removed. Note the small oscillations during the hold phase in the PHE model, which may be attributed to instability in PE finite element modeling in Abaqus, as described by Stokes, *et al*. (45). The first two of these oscillations are shown, but the rest were removed for clarity.

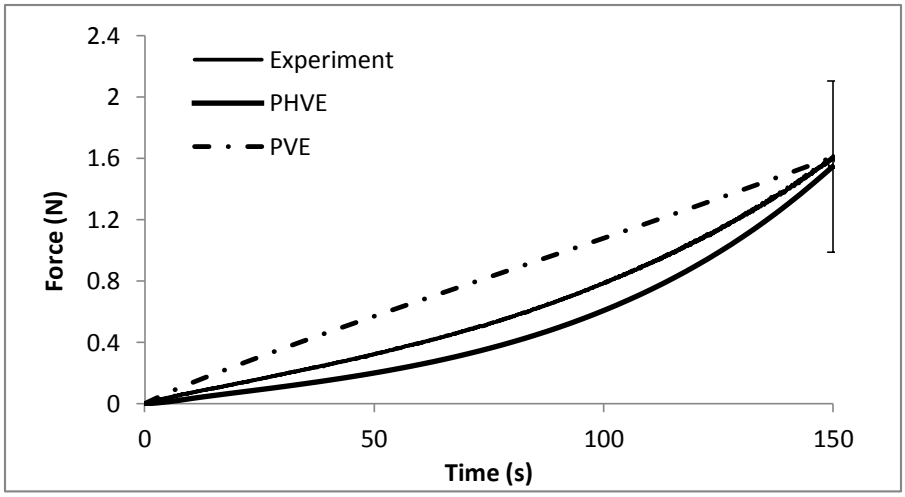

Figure 12: Compression response of porohyperviscoelastic (PHVE) versus (hyperelastic constants) poroviscoelastic (PVE) model (linear elastic constants). The relaxation response is the same in both models, so only the compression portion of the curve is shown.

The model was found to have initial shear and bulk moduli of 200 Pa and 606 Pa, respectively. These values are in the low end of the wide range of liver tissue moduli reported in the literature (9, 32, 53-56); however they are comparable to the modulus reported in Liu *et al.* for liver testing at a low shear rate (E<100Pa). One possible explanation for the softer moduli found in this work is that, since the moduli are being implemented in a perfused PHVE model, they are representative of the solid phase only. The overall stiffness of the entire liver has additional contributions from the incompressible fluid and would therefore be much higher. Thus, some literature values may be reporting this overall tissue stiffness, rather than just that of the solid matrix. Another explanation is that the current study used cylindrical stamps of liver tissue that were not completely surrounded by the Glisson's capsule, a fibrous encasement normally surrounding the entire liver. The lack of this encasement allows for increased expansion of the tissue during compression, which could account for some of decrease in stiffness. A three-term Prony series was sufficient to model the relaxation response of the tissue, allowing a single relaxation term for each logarithmic decade of relaxation (38).

Future developments of this research would integrate the parenchymal PHVE model developed in this work with realistic modeling of liver vasculature. The perfused PHVE model in this paper is a good representation of flow in the parenchyma of the tissue. More realistic modeling of the portal vein, hepatic artery, and their larger branches would improve the integration of this model with computational fluid dynamics simulations of flow in large vessels. This would allow for studying of shear stresses within the liver vasculature in addition to the already modeled PFP and solid matrix stiffness.

While the experimental and modeling work in this paper was based on native liver, the techniques can easily be translated to decellularized liver. The authors have recently developed an axi-symmetric PVE model of decellularized liver and found that both fluid and solid material properties change as a result of the decellularization process (10). Therefore, developing a 3-D PVE model of perfused decellularized liver tissue could be readily accomplished by altering the model material properties. The ability of the model presented in this paper to accurately simulate tissue perfusion is crucial to the translation to decellularized liver because it was found that this material can only undergo mechanical testing while perfused; otherwise the tissue will collapse due to the lack of cellular substance (10). 3-D modeling is especially important in the application of this technique to the perfusion bioreactor system used in regenerative medicine because it allows for a more complete description of flow and pressure throughout the organ-scale scaffold. In conclusion, the PHVE model described in this work is a valuable tool that can be applied to regenerative medicine to accurately analyze both fluid and solid components of liver tissue.

Acknowledgements

This research was funded through support from the Biomedical Engineering Department of Wake Forest University School of Medicine. Assistance with micro-CT was provided by Josh Tan of the Center for Biomolecular Imaging.

CHAPTER 3.3

Scale Dependent Properties of Native and Decellularized Liver Tissue

Douglas W. Evans, Emma C. Moran, Pedro Baptista, Shay Soker, Jessica L. Sparks

Manuscript was written and prepared by Douglas W. Evans. Emma C. Moran assisted in experimental and modeling work and served in an editing capacity. Jessica L. Sparks and Shay Soker served in an advisory capacity and Pedro M. Baptista served in an editing capacity. Text and figure formatting variations are due to journal guidelines. The work was published in *Biomech Model Mechanobiol.* 2013 Jun;12(3):569-80.

Abstract

Decellularization, one technique used in liver regenerative medicine, is the removal of the native cells from an organ leaving behind an intact structure of extracellular material. The biomechanical properties of this novel scaffold material are currently unknown and are important due the mechanosensitivity of liver cells. Characterizing this material is important for engineering liver tissue from this decellularized scaffold as well as creating new 3-dimensional mimetic structures of liver extracellular matrix. This study set out to characterize the biomechanical properties of perfused liver tissue in its native and decellularized states on both a macro and nano-scale. Poroviscoelastic finite element models were then used to extract the fluid and solid mechanical properties from the experimental data. Tissue-level spherical indentation-relaxation tests were performed on 5 native livers and 8 decellularized livers at two indentation rates and at multiple perfusion rates. Cellular-level spherical nanoindentation was performed on 2 native livers and 1 decellularized liver. Tissue-level results found native liver tissue to possess a Young's modulus of 10.5 kPa and decellularized tissue a modulus of 1.18 kPa. Cellular-level testing found native tissue to have a Young's modulus of 4.40 kPa and decellularized tissue to have a modulus of 0.91 kPa. These results are important for regenerative medicine and tissue engineering where cellular response is dependent on the mechanical properties of the engineered scaffold.

Introduction

Liver diseases including cirrhosis, hepatitis, and hepatocellular carcinoma affect nearly 30 million Americans with organ transplantation as the only long-term treatment

currently available (57). In the United States the number of liver transplantations has been steadily increasing each year reaching 6,291 in 2010 (58). This number is expected to climb to nearly 8,000 procedures in 2020 (59). However, the demand for transplantation annually surpasses the supply with the current waiting list at 16,250 (58). One way to address the deficit in organ supply is through regenerative medicine by creating alternative transplantation materials (60, 61).

Decellularization, one technique in regenerative medicine, is the removal of the native cells from an organ leaving behind an intact structure of extracellular material (62). This technique takes advantage of the native bioactive extracellular matrix (ECM), primarily composed of various types of collagen with embedded signaling proteins, which is necessary to regulate cell differentiation and function. Decellularization also leaves behind an intact de-endothelialized vasculature, which preserves the natural method of supplying cells with blood and oxygen (62). To recellularize an organ scaffold, perfusion bioreactors are employed to deliver cells and cell culture media back through the intact vasculature (63).

Microvasculature and blood flow are especially important in the liver which at any time holds 10-15% of the body's total supply and receives nearly 30% of the resting cardiac output (64). In such a vascular organ it is not surprising that parenchymal fluid pressure has recently been shown to effect viability and function of hepatocytes, the primary cell type of the liver (65). In addition to responding to pressure, hepatocytes have been shown to react to the mechanical environment by altering differentiation and proliferation.(66) Other liver cells including stellate cells, portal fibroblasts, and hepatic stem and progenitor cells have also been shown to exhibit mechanosensitivity and alter behavior based on the

stiffness of their substrates (67, 68). Complicating the cellular response to pressure and substrate stiffness is an underlying organ dependent perfusion-stiffness relationship (69).

The mechanosensitivity of the cells populating the liver, and specifically of the cells repopulating a decellularized liver scaffold, highlights the importance of characterizing the biomechanical properties of the scaffold at the cellular scale. In addition, characterizing decellularized liver scaffolds allows for isolation of the matrix contribution to the overall mechanical behavior of the liver. In the emerging field of multi-scale modeling an effort is being made to integrate the small fundamental scales with the large functional scales that exist in the hierarchical structure of biologic systems (70). While the ECM of the entire liver is a complicated network of interconnected bands of collagen and other proteins, individual cells are only in direct contact with some of these matrix supports and therefore may sense a substrate stiffness much different from the stiffness of the entire organ. To our knowledge, the mechanical properties of decellularized liver tissue have never been reported, for any length scale. To this end, this study set out to characterize the biomechanical properties of perfused liver tissue in its decellularized and native states on both tissue-level and cell-level length scales.

In this work, liver biomechanical properties were quantified using poroviscoelastic constitutive models in finite element simulations of conventional indentation and nano-indentation experiments. The liver is composed of cells embedded on a saturated hydrated porous ECM and is therefore modeled well using poroviscoelasticity (PVE). PVE, a descendant of biphasic theory, has previously successfully been used to model liver tissue(9) as well as brain(71), heart(72), lung(73), cartilage(74), aorta(75), and intervertebral discs(76). The strength of a PVE model is its ability to simultaneously

predict the internal fluid and solid properties of biphasic materials. In this study, we report the development of PVE models for native and decellularized liver at the tissue and cellular scales, using macro and nano-indentation testing of perfused tissue.

Materials and Methods

Experiments

Specimens: Liver specimens were obtained from 16 cadaveric ferrets ranging in age from 3-6 weeks. The intact liver was removed through an abdominal incision in which the inferior vena cava, superior vena cava and portal vein were transected while the capsule remained intact. The right lobe was isolated by dissection and the superior vena cava was ligated. The portal vein was cannulated with a 16G cannula, leaving an ex-vivo section of liver tissue with one central input (portal vein) and one output (inferior vena cava). Seven of these samples in this native tissue state were tested within 12 hours of harvest. The remaining 9 ex-vivo sections were then decellularized through perfusion of 1% Triton-X 100 with 0.1% Ammonium Hydroxide (Sigma-Aldrich), as reported by Baptista et al (62). The decellularized samples were then tested after the decellularization process.

Macro-scale Testing: Macro-indentation experiments were performed on native and decellularized livers using a Bose ElectroForceTestBench mechanical testing system equipped with a 1000-gram load cell (Bose ElectroForce), Fig 1. Spherical indenters were created by attaching steel balls (McMaster-Carr) to cup-point set screws (McMaster-Carr) that directly coupled to the load cell. The indenters were 4mm in diameter for the native livers and 8mm in diameter for the decellularized livers. Preliminary results indicated that

to maintain an adequate signal to noise ratio, a larger indenter was required to test decellularized liver samples. The livers were supported by a custom articulating drainage platform (Solid Concepts) and attached to a 2-axis manual position system (1/2" dovetail translation stage Thor labs). The setup allowed for liver samples to be perfused with saline using a peristaltic pump (MasterFlex 7523-70 Cole-Parmer) and pulse dampener (Cole-Parmer).

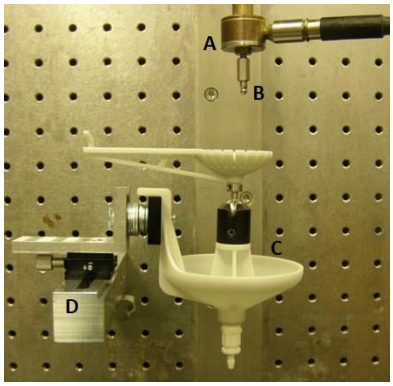

Figure 1: Macro-indentation setup showing: A) load cell, B) spherical indenter and set screw, C) custom-articulating drainage platform, D) 2-axis manual positioner

Macro-indentation tests were performed on 5 of the native and 8 of the decellularized liver samples. For native samples each liver was subjected to 4 tests: 1 test with an indentation rate of 0.01 mm/s perfused with 6 ml/min of saline and 3 tests with an indentation rate of 1 mm/s perfused with 0, 3, and 6 ml/min of saline (Table 1). Due to the larger indenter required for the decellularized samples, each decellularized liver was limited to only 2 indentations. Indentation sites on each sample were spaced approximately 10mm from one another. Decellularized samples were tested under 3 conditions: one test at an indentation rate of 0.01 mm/s perfused with 6 ml/min saline, and 2 tests with an indentation rate of 1 mm/s perfused with 3 and 6 ml/min saline respectively. Five indentations were performed for each of these test conditions totaling 15 decellularized

indentations randomly distributed across the 8 samples. For both native and decellularized tests indenter-sample contact was pre-established by a 2 mN load change followed by an indentation of 2mm for native tissue and 4mm for decellularized tissue and 360 s relaxation period.

Table 1: Test matrix for macro-indentation showing number of indentations performed

Macro-Indentation

	Perfusion [ml/min]	Indentation Rate [mm/s]		Indented Surface
		0.01	1.0	
Native	0	---	5	Capsule
	3	---	5	Capsule
	6	5	5	Capsule
Decell	3	---	5	Capsule
	6	5	5	Capsule

Nano-Scale Testing: Nano-indentation experiments were performed on native and decellularized livers using a custom cantilever based Nano Tissue Indenter (NTI), Fig 2. This device was developed and validated in previous work and can detect applied force and displacement with resolutions of 0.283 μN and 0.694 μm (77). The device uses segments of fiber optic cable to apply a force transmitted through a micro-sphere into a tissue. The force applied is proportional to the cable's stiffness and displacement. Cable stiffness is a function of its length and cable displacement stems from a 3-axis position-table raising a sample into contact with the indenter. The livers were held with the same custom articulating drainage platform as the macro tests. Due to the presence of a fluid film on the surface of the tissue, indenter-sample contact was established by the rest position following "jump-to-contact," the sudden downward pull caused by surface tension of the liquid when the layer is breached. Indentations consisted of raising the livers with a position table at a rate of 0.01 mm/s for 1 mm in the decellularized liver test and 0.05 and

0.01 mm/s for 2 mm in the native liver tests. All NTI based indentations in this study used a titanium indenter with a diameter of 793.75 μm.

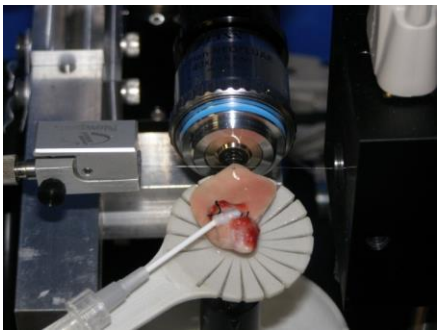

Figure 2: Perfused native tissue being nano-indented with NTI

A native liver and decellularized liver both perfused with 6 ml/min of saline were each indented in 10 locations (Table 2). Each indentation location was separated by 3 mm and was positioned 10-15 mm from the cannula perfusion source. A cantilever with a stiffness of 0.0183 μN/μm was used for the decellularized indentations and a second cantilever 0.1133 μN/μm stiff was used for the native liver. The stiffer cantilever was necessary after the softer cable failed indent the native liver a sufficient amount. A second native ferret liver was also tested with the softer cantilever, this time without perfusion. The unperfused native liver was indented 10 times through the capsule and another 7 times in the parenchyma of the tissue after a section of capsule had been removed.

Table 2: Test Matrix for nano-indentations showing number of indentations performed

Nano-Indentation

	Perfusion [ml/min]	**Table Rate [mm/s]**		**Indented Surface**
		0.05	**0.01**	
Native	0	10	---	Capsule
		7	---	Parenchyma
	6	---	10	Capsule
Decell	6	---	10	Capsule

Pressure Measurements: A needle guided Millar SPR-524 (3.5F) sensor and MPVS-400 signal conditioning hardware (Millar) with integrated ADInstruments Powerlab DAQ technology were used to measure and record parenchymal fluid pressure in the perfused native and decellularized livers following macro-indentation. The pressure probe was inserted into the same location in 7 decellularized livers and 5 native livers and parenchymal fluid pressure (PFP) was measured at perfusion flow rates of 3ml/min and 6ml/min.

Computational Modeling

PVE Theory: PVE theory is an extension of biphasic theory to include an inherent viscoelasticity of the solid component(78). The underlying biphasic model is a material comprised of a linear elastic incompressible solid and an incompressible liquid where the relative motion between these two phases creates rate-dependent behavior(79). When the liquid phase is inviscid, biphasic theory has been shown to be equivalent to an alternate theory of a liquid-solid material poroelasticity (20). Poroelasticity, widely used in soil mechanics, is a material model available in commercial finite-element packages such as Abaqus. The use of Abaqus in modeling soft biphasic tissue has been validated and extended to PVE (9, 71, 80, 81).

The equations governing biphasic theory are given by Eqns 1-6. Under the assumption that the solid phase and fluid phase are both intrinsically incompressible the conservation of mass can be written as:

$$\underline{\nabla} \cdot (\Phi^s \underline{v}^s + \Phi^f \underline{v}^f) = \underline{0} \qquad (1)$$

where *s* and *f* stand for solid and fluid phase respectively, Φ is volume ratio, $\underline{v}$ is velocity. Assuming inertial forces to be much smaller in magnitude than internal frictional forces, the conservation of linear momentum can be written as:

$$\underline{\nabla} \cdot \underline{\underline{\sigma}}^s + \underline{\pi}^s = \underline{0} \tag{2}$$

$$\underline{\nabla} \cdot \underline{\underline{\sigma}}^f + \underline{\pi}^f = \underline{0} \tag{3}$$

where $\underline{\underline{\sigma}}$ are Cauchy stress tensors of each phase and $\underline{\pi}$ are frictional body forces (units: F L^{-3}). The frictional body forces are assumed to be proportional to their relative velocities and inversely proportional to the hydraulic permeability k (units: L^4 F^{-1} T^{-1}) so that:

$$\underline{\pi}^s = -\underline{\pi}^f = \frac{(\Phi^f)^2}{k}(\underline{v}^f - \underline{v}^s) \tag{4}$$

Finally, the stress in each phase can be written as:

$$\underline{\underline{\sigma}}^f = -\Phi^f p \underline{\underline{I}} \tag{5}$$

$$\underline{\underline{\sigma}}^s = -\Phi^s p \underline{\underline{I}} + \underline{\underline{\sigma}}^s \tag{6}$$

where p is hydrostatic pressure and $\underline{\underline{\sigma}}^s$ is the apparent solid stress due to deformation of the solid matrix(20, 78, 79, 81, 82). In PVE theory the effective solid stress tensor $\underline{\underline{\sigma}}^s$ is replaced with:

$$\underline{\underline{\sigma}}^s = \int_0^t 2G(\tau - \tau')\underline{\underline{\dot{e}}}dt' + \underline{\underline{I}}\int_0^t K(\tau - \tau')\dot{\phi}dt' \tag{7}$$

where G and K are the elastic shear and bulk relaxation functions, $\underline{\underline{e}}$ is the mechanical deviatoric strain and ϕ is the volumetric strain(78, 82). Each relaxation function can be defined by the prony series expansion:

$$R(t) = \frac{R_\infty}{1-\sum_{i=1}^{n} r_i}\left[1-\sum r_i\left(1-e^{-t/\tau_i}\right)\right] \tag{8}$$

where R is the time-dependent modulus, R_∞ is the long-term modulus, and the prony series parameters (n, r_i, and τ_i, i=1,2,…,n) are material constants(83).

In this work, the material was defined by specifying the hydraulic conductivity (k'), the specific weight of the liquid (γ), prony series parameters, a long-term Young's modulus (E_∞) and Poisson's ratio (ν) so that:

$$G_\infty = \frac{E_\infty}{2(1+\nu)} \tag{9}$$

$$k = \frac{k'}{\gamma} \tag{10}$$

Finite Element Modeling: Macro and nano-scale models of the perfused native and decellularized liver tissue experiments were created in Abaqus (v10.1, Simulia Corp) using its internal soil analysis. The models were axisymmetric and consisted of a sphere indenting a disc of material (Fig 3). Since indentation experiments are ideally performed on an infinite half-space (84), the model height and width were 5x and 10x the indenter radii. The indenter was modeled as a deformable solid (type CAX4R) with $E_{ind} >> E_{mat}$. The tissue was modeled as a PVE material using a pore fluid element (type CAX4RP) and

by specifying the fluid components (Eqn 10), linear elastic components (Eqn 9), and viscoelastic components (Eqn 8). The model was perfused by specifying the pore pressure on the bottom nodes of the material to match the experimentally measured conditions and allowing the model to equilibrate for 5000 s.

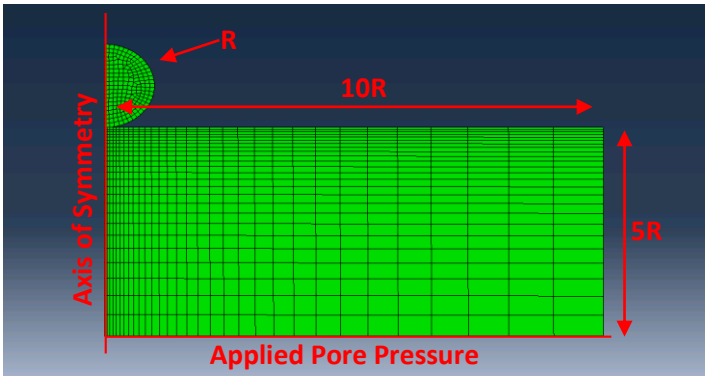

Figure 3: Generic finite element axisymmetric indentation model

PVE Parameters: The parameters necessary to define a PVE material are the fluid components, elastic components, and viscoelastic components. Fluid components were defined by specifying the hydraulic conductivity of the solid and the specific weight of the fluid. The elastic components were comprised of a long-term Young's modulus and a Poisson's ratio. The viscoelastic components were defined by a multi-term Prony series.

Macro-scale Element Models: The specific weight of the fluid was calculated as the specific weight of saline the perfusion liquid to be 9855 N/m^3. Poisson's Ratio was selected from literature to be 0.35 representing the inherent compressibility of the drained solid matrix(9, 71). The long-term Young's modulus was found by optimizing the model in the absense of viscoelastic terms to match the average fully relaxed force obtained from 6 $^{ml}/_{min}$ perfusion tests. The value for native tissue permeability (k=0.00337 m/s) was deduced from optimization of a PVE model of perfused bovine tissue developed by the authors. While

this value is much larger than previously reported values of articular cartilage and other dense soft tissues, it is in the range of estimated permeability of liver as reported in Kerdok *et al* through experimental swelling tests(71, 85-87). The permeability of the decellularized tissue was assumed to be one magnitude larger (k=0.0337 m/s) due to removal of cellular components from the tissue.

The prony series terms were then found by a two-step process (Appendix). A 4-term prony series was optimized to the average relaxation experimental data from the samples tested at 1 $^{mm}/_{s}$ with 6 $^{ml}/_{min}$ perfusion using a Hooke-Jeeves algorithm in Isight (v5.2 Simulia Corp). The shear relaxation prony series function can be viewed in terms of reaction force and assumes that loading has occurred in an instantaneous step occuring at t=0. An approximation to account for actual finite load ramp-time (t_{ramp}) was applied by shifting the relaxation data back by a factor of $t_{ramp}/2$. The first-term components were constrained to g_1=.5 and t_1=2E-5 making up a nearly instantaneous relaxation component to be used as a scaling variable in the second step. The remaining 3 terms (1 for every decade of relaxation data), were allowed to vary with the constraints in Table 3. Because the instantaneous modulus of the material is unknown and depends on the non-unique prony parameters, a fine tuning of the relaxation parameters is needed to fit model peak force to experimental peak force. Step 2 in the prony series optimization was manual tuning of the g_1 parameter so the model peak force was within 5% of experimental peak force.

Table 3: Constraints on Prony term optimization

Parameters	Constraints	
	min	max
g_2, g_3, g_4	.001	.99
t_1	.01	1
t_2	1	100
t_3	100	1000
$\sum g_n$	.001	.999

Nano-Scale Finite Element Models: The identical fluid components, Poisson's ratio, and viscoelastic parameters fit to the macro-scale experimental data were used in the nano-indentation finite element model. The long-term elastic modulus was found by fitting the model force-time curve to the average experimental force-time curve, using the average experimental indentation-time curve as an input.

Statistics: The results were analyzed using two-sample Student's T-tests assuming unequal variance and one-way ANOVAs performed with α=0.05. The Bonferoni method was applied when applicable to avoid compound type 1 error.

Results

Macro-scale Indentation Experiments

Native Livers: The average peak and equilibrium force results are shown for each test group of n=5 in Fig 4. Significant differences were found in the three perfusion test groups (0 ml/min, 3 ml/min, and 6 ml/min) indented at 1 mm/s and no significant difference was found between the peak and relaxed force in the slower 0.01 mm/s indentation group. P-values of .0006 for the peak force and .00007 for the equilibrium force indicated that a difference existed within the two force groups. The results show that the indentations

performed at 0.01 mm/s with perfusion of 6 ml/min had a statistically significant lower peak force then the indentations performed at 1 mm/s and perfused at 6 and 3 ml/min. No statistical difference could be determined between the mean peak force of the unperfused native liver with any other group due to the large variability in the data. With respect to the mean equilibrium force, the unperfused group was statistically different from the rest of the groups perfused at 3 and 6 ml/min.

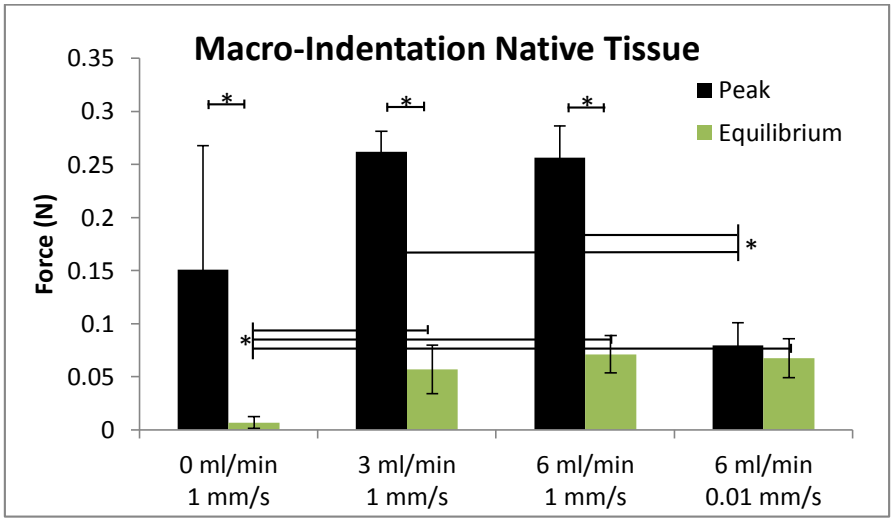

Figure 4: Mean peak and equilibrium force from native livers undergoing marco-indentation testing grouped by perfusion and indentation rate. 5 livers were each indented once per perfusion and indentation group totaling 20 indentation tests. A statistical mean difference $P<.05$ is indicated by (*). Bars indicate ± 1 standard deviation.

Decellularized Livers: The mean peak and relaxation force from the 15 macro-indentation tests on 8 decellularized livers are shown in Fig 5. A statistical difference between peak and equilibrium force within both test groups indented at 1 mm/s was found with no such difference being detected in the group indented at 0.01 mm/s. P-values of 0.0007 for the mean peak forces and .37198 for the mean equilibrium forces across each group indicated a difference in peak force between groups and no difference in equilibrium force between

groups. Further analysis revealed that the peak force from the tests run at the indentation rate of 0.01 mm/s were statistically different from the two tests run at 1 mm/s.

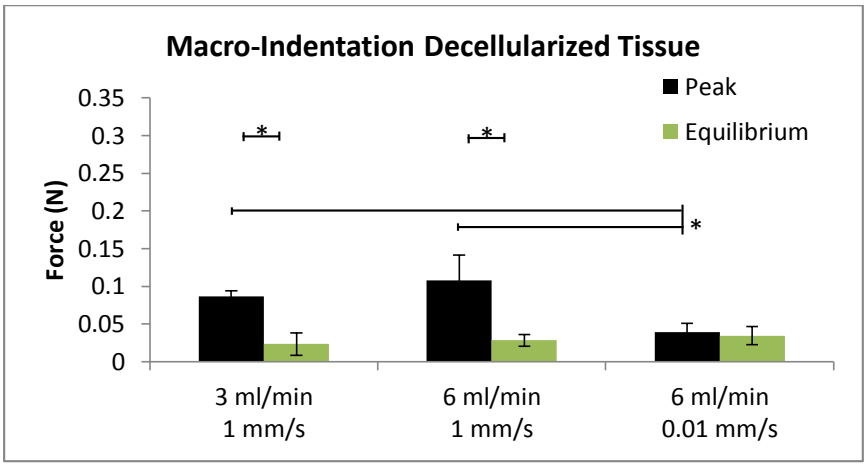

Figure 5: Mean peak and equilibrium force from decellularized livers undergoing macro-indentation testing grouped by perfusion and indentation rate. 8 livers were each indented a maximum of 2 times to randomly assigned groups totally 5 indentations per group. A statistical mean difference P<.05 is indicated by (*). Bars indicate ± 1 standard deviation.

Nano-Scale Indentation Experiments

Perfused Samples: The average indentation-force plot stemming from the 10 nano indentation tests performed on a native and decellularized liver are shown in Fig 6. The apparent stiffer perfused native liver required a stiffer cantilever than the decellularized tests. All other test conditions including perfusion rate, sample position rate, and indenter size were identical. The peak force and indentation obtained from each material is 108.7 ± 4.1 μN and 74.9 ± 20.6 μm for native liver and 19.0 ± 0.77 μN and 79.6 ± 22.9 μm for decellularized liver. There was no significant difference in indentation depth (p=.6349) but there is a significant difference in the applied force at this depth (p=1.6E-14).

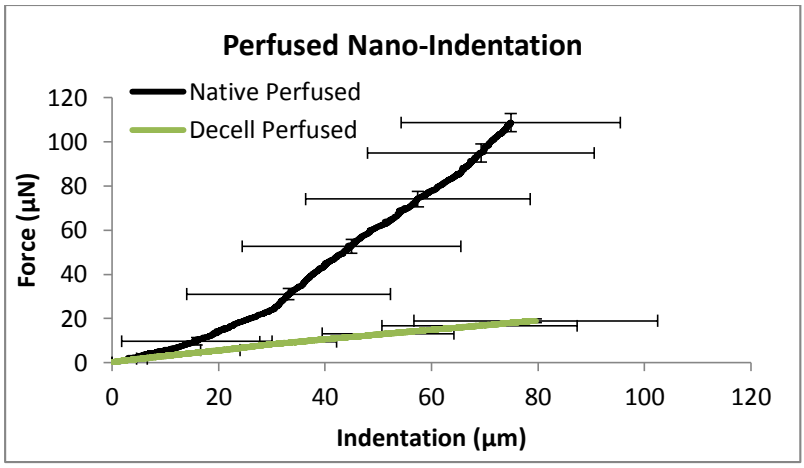

Figure 6: Average indentation-force curves for the perfused nano-indentation of native and decellularized liver. The tests were performed with a sample displacement rate of 0.01 mm/s and indentation lasted for 103 seconds.

Unperfused Samples: The average indentation-force plot from the 10 tests performed on the capsule and 7 tests in the parenchyma of an unperfused native liver are shown in Fig 7. These tests were performed with the identical indenter as the perfused samples however used a faster position-table displacement rate. The mean maximum force and indentation for these tests were 38.5 ± 1.2 μN and 53.9 ± 10.8 μm for the indentations performed through the capsule of the liver and 37.5 ± 0.58 μN and 33.6 ± 8.6 μm for the tests without the capsule of the tissue. There was no significant difference in the maximum force applied ($p=0.12$) but again there was a difference found in the indentation ($p=0.0006$).

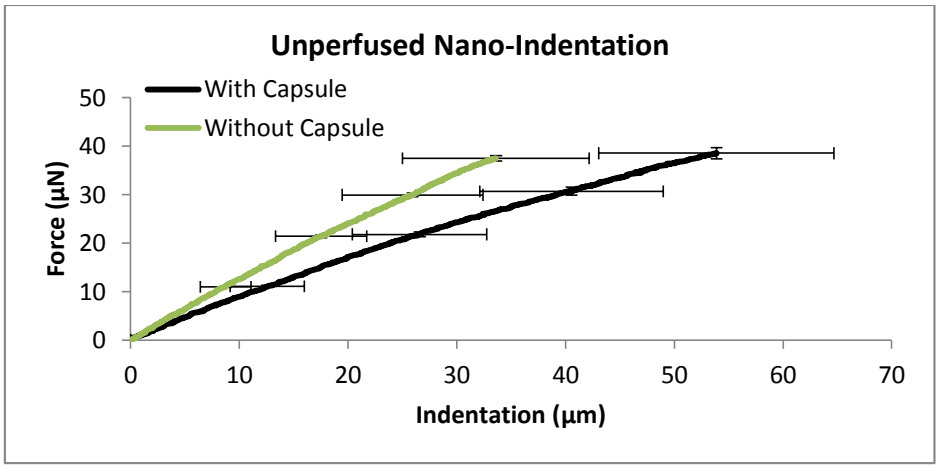

Figure 7: Average indentation-force curves for the unperfused nano-indentation of native liver through the capsule and within the parenchyma. The tests were performed with a sample displacement rate of 0.05 mm/s and indentation lasted for 40 seconds.

Pressure Measurements: The results of the pore fluid pressure measurements taken following the macro-indentation tests are shown in Fig 8. The mean pore pressures were calculated at each flow rate for both native and decellularized liver tissue. Native tissue had an average pore fluid pressure of 4.32 ± 1.52 mmHg and 7.44 ± 2.49 mmHg for the saline perfusion rates of 3 ml/min and 6 ml/min respectively. Decellularized tissue had an average pore fluid pressure of 0.68 ± 0.53 mmHg and 1.37 ± 0.85 mmHg for the saline perfusion rates of 3 ml/min and 6 ml/min respectively.

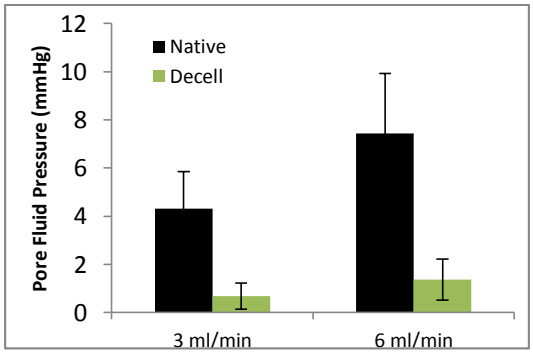

Figure 8: The average pore fluid pressure for native (n=5) and decellularized tissue (n=7) when perfused with 3 and 6 ml/min of saline.

PVE Models

PVE Parameters: The model parameters for the 6 finite element models created in this study are listed in table 4. The viscoelastic prony series parameters found from the macro-indentation of native and decellularized tissue were applied to their respective nano-indentation counterparts.

Table 4: Axi-symmetric PVE finite element model parameters

			Elastic Components		Fluid Components		Viscoelastic Components							
		Model	E (kPa)	v	k (m/s)	γ (kg/m³)	g_1	τ_1 (s)	g_2	τ_2 (s)	g_3	τ_3 (s)	g_4	τ_4 (s)
Perfused	Macro	Native	10.5	.35	.00337	9855	.53	2E-5	.376	1	.027	7.65	.01	100
		Decell	1.18	.35	.0337	9855	.481	2E-5	.480	.349	.017	.5	.001	100
	Nano	Native	4.40	.35	.00337	9855	.53	2E-5	.376	1	.027	7.65	.01	100
		Decell	.914	.35	.0337	9855	.481	2E-5	.480	.349	.017	.5	.001	100
Unperfused		Native with Capsule	2.62	.35	.00337	9855	.53	2E-5	.376	1	.027	7.65	.01	100
		Native without Capsule	5.05	.35	.00337	9855	.53	2E-5	.376	1	.027	7.65	.01	100

Macro-Indentations: The average force-time tissue response for the native and decellularized macro-indentations perfused at 6 ml/min and their corresponding finite element simulations are shown in Figs 9 and 10. Native liver tissue was determined to possess a Young's modulus of 10.5 kPa. This value along with the optimized prony series parameters were simultaneously able to match the peak force (4.89% error) and relaxed force (5.14% error) from the 1 mm/s indentation rate while predicting the peak (3.02% error) and relaxed force (4.82% error) from the slower 0.01 mm/s indentation rate. Decellularized liver was determined to be more compliant with a modulus of 1.18 kPa. The decellularized model matched the peak force (0.40% error) and the relaxed force (8.3%

error) for the faster indentation while predicting the slower indentation to 8.3% and 8.5% error respectively for peak and relaxed forces.

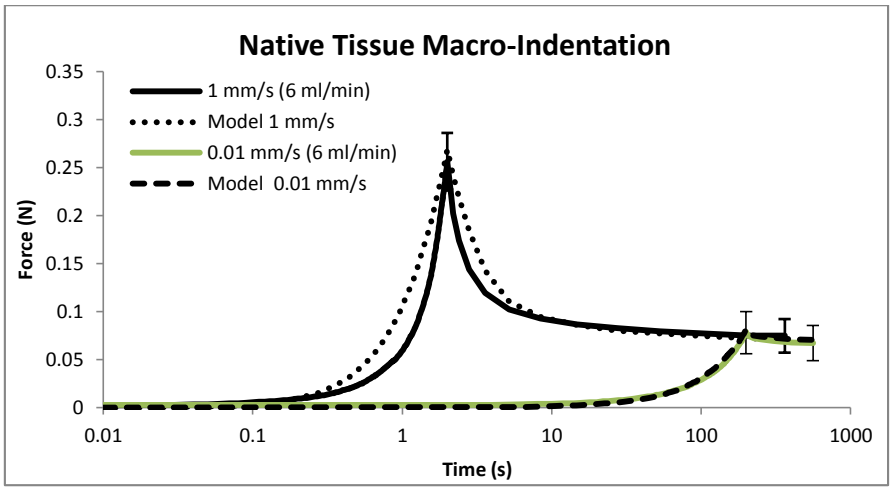

Figure 9: The average experimental tissue and model response from macro-indentations of native liver perfused with 6 ml/min saline.

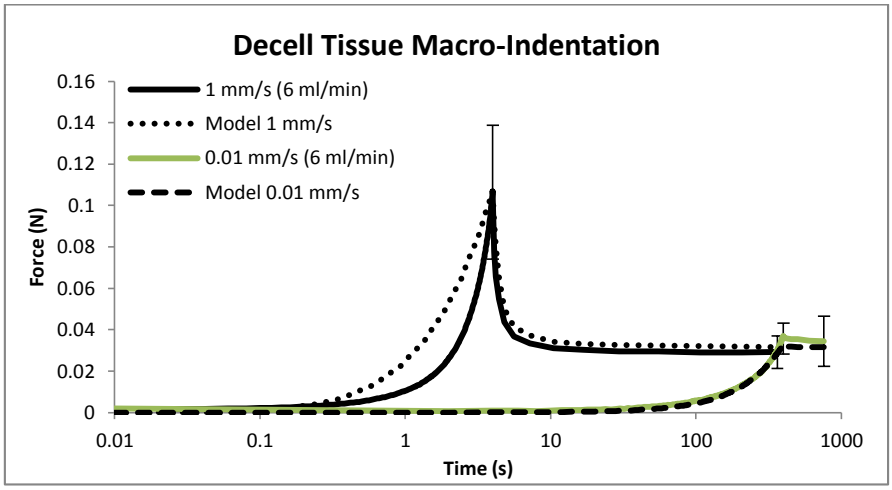

Figure 10: The average experimental tissue and model response from macro-indentations of decellularized liver perfused with 6 ml/min saline.

Nano-Indentations: In the four models created to simulate the nano-indentation experiments, the displacement of the indenter was assigned to follow the average

indentation-time curve for each group. A Young's modulus was found for each test by minimizing the sum of the residuals squared using a Hookes-Jeeves optimization algorithm (Isight v5.0 Simulia Corp). Figure 11 contains 4 force-time plots showing the mean experimental results for each test and the finite element model predictions with corridors indicating the variability in the experimental indention-time data. For the perfused tissue, native liver was found to have a Young's modulus of 4.40 kPa and decellularized liver was found to have a modulus of 914 Pa. The unperfused tests determined native liver with the capsule to have a modulus of 2.62 kPa and native tissue with the capsule removed to have a modulus of 5.05 kPa.

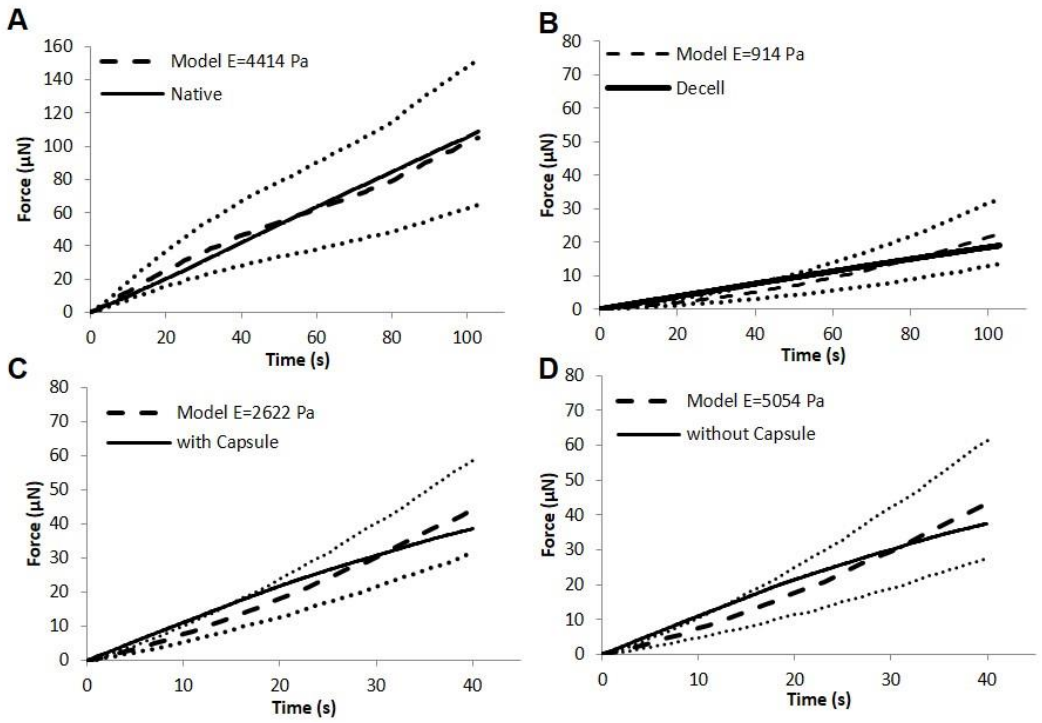

Figure 11: The nanoindentation average experimental force-time data and FE model with corridors representing the variability of the indentation data for: (A) perfused native tissue, (B) perfused decellularized tissue, (C) unperfused native tissue with capsule, and (D) unperfused native tissue without capsule

Discussion

It was found that native and decellularized tissue exhibit different mechanical properties on both the tissue and cellular levels. Macro indentation testing found native perfused liver to possess a Young's modulus of 10.5 kPa and decellularized perfused liver to possess a modulus of 1.18 kPa. Similarly, nanoindentation of the materials also found a difference in the properties with native tissue possessing a Young's modulus of 4.40 kPa and decellularized tissue a value of 0.91 kPa. These findings indicate that the inherent stiffness of liver tissue is lowered significantly from the decellularization process. This result should come as no surprise as the decellularization process removes all of the cellular components leaving behind primarily collagen which makes up 1.8-2.1% of a normal liver(88). This is an important finding due to the known mechanosensitivity of liver cells. In the engineering of liver tissue, cells being reseeded and adhering to the decellularized scaffold will therefore be subjected a different mechanical environment than that of native liver. These findings should be taken into account when considering the expected cellular behavior of cells reseeded into a decellularized scaffold.

The change in modulus found for native tissue between macro and nanoindentation was a difference of -58%. This drop in modulus may be partially explained by the number cells the indenter interacted with. The average hepatocyte has a cell diameter of ~30 μm and the maximum contact area of the indentations assuming Hertzian contact was 12.56 mm^2 and 0.201 mm^2 for macro and nanoindention respectively. This means that roughly 17,000 cells were directly contacted by the indenter in macro indentation and only 300 cells in nanoindentation. The Young's modulus of individual liver cells has be reported to be in the range of 1-2.5 kPa as determined by atomic force microscopy(89). The cellular-

scale tests performed in this study are in the upper end of the nanoindentation range and are at a larger scale. It stands to reason that as the scale of the test get closer to testing a single cell, the effective modulus of the cells and their underlying substrate will converge towards the modulus of the single cell. The change in modulus for decellularized tissue was less drastic falling only 23%. While the mechanism for this change in stiffness is unknown, the smaller change in modulus could be due to a similar mechanism as the native tissue. Collagen fibers are inherently smaller than hepatocytes and are made up of individual fibrils with diameters of ~150 nm(90). Therefore the magnitude of fibers contacted during cellular-level testing could still be significant which could explain the smaller drop in modulus seen in decellularized tissue compared with native tissue.

The macro PVE models fit to the experimental 1 mm/s indentation data were able to simultaneously capture the peak and equilibrium force while predicting the behavior for the slower tests in both native and decellularized tissue. The ramp, or indentation, portion of the experiments for both native and decellularized tissue exhibit a steeper curvature then the linear elastic PVE indentation model predicts. This discrepancy suggests that the inherent nature of the solid ECM with and without cells maybe better modeled as a hyperelastic material. The solid viscoelastic material properties, the prony series parameters, show that the native tissue relaxes at a slower rate than the decellularized tissue. The two largest shape-affecting terms of the prony series (g_2 and g_3) have time coefficients (τ_2 and τ_3) that are both greater than 1 for native tissue and less than 1 for decellularized tissue. The removal of cellular components of the decellularized material is in effect the removal of barriers to fluid flow. Therefore fluid is able to redistribute faster which explains the smaller prony series time coefficients.

The nanoindentation PVE models were used to determine the Young's moduli of perfused native and decellularized tissue as well as unperfused moduli of indentations occurring on the liver's fibrous capsule and in the parenchyma after the capsule had been removed. The expected findings were that liver parenchyma would be significantly more compliant than the capsulated tissue. The experimental data shows the opposite trend with parenchyma actually being stiffer than both unperfused capsulated tissue and perfused native tissue. One possible explanation of this finding lies in the experimental procedure. After completing the capsule indentations tests, a scalpel was used to remove a section of the tissue exposing the parenchyma. The act of cutting the tissue could have had the unintended effect of squeezing out liquid from the tissue. In this way, the unperfused de-capsulated tissue would have behaved like a pre-compressed material, exhibiting stiffer behavior.

The macro indentation-relaxation of perfused native tissue revealed a difference in reaction force between perfused samples and un-perfused samples. The unperfused tissue was anticipated to experience a lower peak and equilibrum force due to absence of a perfusate. This trend was documented in the significant difference seen between the equilibrium force measured between the perfused and unperfused tests. While a significant difference was not found in the measurement of peak force, the effect of perfusion was seen in the variability of the data. The unperfused peak force variability (0.1508 ± 0.1170 μN) was 4 times the maximum variability seen in the perfused data (0.2562 ± 0.0301 μN), with some samples peaking much lower than the perfused data as expected and surprisingly a few peaking higher than the perfused samples. The elevated peak force measurements are thought to again be an artifact of the experimental procedure. Any pre-test handling of

livers has the effect of squeezing fluid out of the tissue, and in the unperfused state this fluid was not replaced before testing. Perfusing the samples therefore had the effect of standardizing each sample, a step which was inherently absent in the unperfused tests.

Although perfusion made a difference in the force measurements, the two rates of perfusion tested in this study did not significantly change peak or equilibrium force for either native or decellularized tissue. Parenchymal fluid pressure measurements taken following macro indentation found the change in pressure between perfusion rates of 3 ml/min and 6 ml/min to be 3.12 and 0.695 mmHg for native and decellularized tissue respectively. The pressure change is difference in gage pressure of 72% and 105%, however the pressure actually acting on the tissue is absolute pressure, a difference of only 0.4% and 0.09%. The small actual change in absolute pressure may explain the absence of a reaction force dependence on flow-rate.

The time-dependent nature of native and decellularized tissue was confirmed by the results of the 2 indentation rates. The slower rate of 0.01 mm/s did not produce a significant difference in peak force compared with equilibrium force while the faster rate of 1 mm/s produced did produce a significant difference, between peak and equilibrium force for both native and decellularized tissue.

Conclusion

In conclusion, this work reports the difference in the mechanical properties between perfused decellularized and native liver on both the tissue and cellular scale. These results are relevant for regenerative medicine and tissue engineering where cellular response is

dependent on the mechanical properties of the engineered scaffold. In addition, PVE models were successfully created that modeled and predicted spherical macro and nanoindentation response. The strength of the PVE model is its ability to separate yet integrate the solid and fluid components of a biphasic material. This is particularly important in modeling biologic tissue such as the liver where perfusion plays an important role in the physiologic and mechanical response.

CHAPTER 3 CONCLUSIONS

Overall, the collective conclusions from the three manuscripts in this chapter have allowed us to better understand the effects of decellularization on liver biomechanical properties in order to design experiments optimizing the cellular mechanical environment. The first manuscript found that the parenchymal fluid pressure (PFP) is significantly lowered from the decellularization process. However, perfusing the decellularized tissue at 6-12 ml/min results in PFP values that are similar to physiological PFP, measured *in vivo* to be 2.86 ± 1.04 mmHg.

The second manuscript details the experimental and modeling approaches used to generate a three-dimensional finite element model of perfused liver tissue. The successful development of this model is critical in fully characterizing the liver biomechanical environment because it integrates solid matrix mechanics and fluidic forces, including PFP, in a single computational model. This model successfully extracted the stiffness of the solid matrix and the complex interplay between solid and fluid components under scaffold perfusion, such as the tissue permeability, velocity of fluid flow and PFP. The solid matrix was found to have shear and bulk moduli of 200 and 600 Pa, respectively, which is lower than most literature values. However, these values of are of the solid matrix alone and many literature values of tissue stiffness do not differentiate the solid and fluid components. It was found that the fluidic component of liver tissue greatly contributes to the overall compressive force which many references include in calculations of tissue stiffness. Importantly, this model found that native liver tissue permeability was 4mm/s, which is much higher than experimentally measured values in other tissues commonly used

in soft tissue mechanics, such as articular cartilage and intervertebral discs (52), but is within the range of experimentally measured liver permeability (49).

The PHVE model was simplified to a 2D axisymmetric model in the third manuscript to evaluate the effects of decellularization on tissue mechanics. Decellularization was found to greatly influence the biomechanical properties of the tissue on both a macro- and nano-scale. On the macroscale, decellularized tissue was found to have a Young's Modulus roughly 10 times lower than native and 5 times lower on a nano-scale. These findings are incredibly important due to the impact of stiffness on a wide variety of cell types, include stem cell differentiation, hepatocyte function, liver stromal cell activation and cancer cell migration (18, 19, 91-94). Another important finding was that the decellularized tissue relaxes much faster than native tissue, indicating much higher permeability and ease at which fluid escapes. This finding is supported by measurements of PFP in the first paper. PFP was lower in decellularized tissue than native at the same flow rates, indicating that fluid is escaping more easily and less is retained within the tissue, leading to lowered fluidic pressures. Fully understanding the interactions between solid and fluid components within native and decellularized liver tissue can help us better understand how cells are interacting with the mechanical microenvironment *in vivo* and in bioengineered liver tissues.

The experimental and modeling work outlined in this chapter has provided valuable information that can be applied to optimization of liver bioengineering experiments. The interplay between flow rate and PFP and differences between native and decellularized liver is vital towards development of perfusion bioreactor conditions that optimize cell behavior and tissue growth. These studies provide a foundation for future computational

modelling efforts focused on optimization of liver bioengineering approaches. First, models can be developed to optimize perfusion bioreactor conditions for cell seeding and tissue maturation by focusing on the interplay between applied flow and internal fluid behavior. Additionally, these models could link experimental organ-scale inputs to downstream cell-scale mechanical forces, such as PFP and shear stress. Finally, future models could provide a computational approach to scaling up technologies from ferrets to larger animals without the need for experimental optimization.

References

1. Hsu WM, Carraro A, Kulig KM, Miller ML, Kaazempur-Mofrad M, Weinberg E, et al. Liver-assist device with a microfluidics-based vascular bed in an animal model. Ann Surg. 2010 Aug;252(2):351-7. PubMed PMID: 20647924. eng.
2. (2011) O. Organ Procurement and Transplantation Network: National Data [November 1 2011]. Available from: http://optn.transplant.hrsa.gov/.
3. Baptista PM, Siddiqui MM, Lozier G, Rodriguez SR, Atala A, Soker S. The use of whole organ decellularization for the generation of a vascularized liver organoid. Hepatology. 2011 Feb;53(2):604-17. PubMed PMID: 21274881. eng.
4. Ozerdem U, Hargens A. A simple method for measuring interstitial fluid pressure in cancer tissues. Microvascular Research. 2005 JUL 2005;70(1-2):116-20. PubMed PMID: WOS:000233386800015. English.
5. Guyton A, Hall J. Human Physiology and Mechanisms of Disease. 6th ed. Philadelphia, Pa: Saunders; 1997.
6. Guyton A, Hall J. Textbook of Medical Physiology.
7. Burczynski FJ, Luxon BA, Weisiger RA. Intrahepatic blood flow distribution in the perfused rat liver: Effect of hepatic artery perfusion. American Journal of Physiology-Gastrointestinal and Liver Physiology. 1996 Oct;271(4):G561-G7. PubMed PMID: WOS:A1996VN42000004.
8. Kogure K, Ishizaki M, Nemoto M, Kuwano H, Makuuchi M. A comparative study of the anatomy of rat and human livers. J Hepatobiliary Pancreat Surg. 1999;6(2):171-5. PubMed PMID: 10398905. eng.
9. Raghunathan S, Evans D, Sparks J. Poroviscoelastic Modeling of Liver Biomechanical Response in Unconfined Compression. Annals of Biomedical Engineering. 2010 MAY 2010;38(5):1789-800. PubMed PMID: ISI:000276204600008. English.
10. Evans DW. A Nanoindentation Device and the Scale-Dependent Mechanical Properties of Native and Decellularized Liver Tissue. Winston Salem, NC: Virginia Tech- Wake Forest School of Biomedical Engineering and Sciences; 2011.
11. Kim R, Brown R, Terrault N, El-Serag H. Burden of liver disease in the United States: Summary of a workshop Atlanta, GA2001.

12. Uygun B, Soto-Gutierrez A, Yagi H, Izamis M, Guzzardi M, Shulman C, et al. Organ reengineering through development of a transplantable recellularized liver graft using decellularized liver matrix. Nat Med. 2010 Jul;16(7):814-20. PubMed PMID: 20543851. PMCID: PMC2930603. eng.
13. Shupe T, Williams M, Brown A, Willenberg B, Petersen BE. Method for the decellularization of intact rat liver. Organogenesis. 2010 Apr-Jun;6(2):134-6. PubMed PMID: WOS:000290262200009.
14. Yagi H, Fukumitsu K, Kadota Y, Kitago M, Shinoda M, Obara H, et al. LARGE-SCALE WHOLE-ORGAN DECELLULARIZATION OF SWINE LIVER FOR TRANSPLANTATION. Hepatology. 2011 Oct;54:763A-A. PubMed PMID: WOS:000295578003082.
15. Soto-Gutierrez A, Zhang L, Medberry C, Fukumitsu K, Faulk D, Jiang H, et al. A Whole-Organ Regenerative Medicine Approach for Liver Replacement. Tissue Engineering Part C-Methods. 2011 Jun;17(6):677-86. PubMed PMID: WOS:000291202200007.
16. Porter B, Zauel R, Stockman H, Guldberg R, Fyhrie D. 3-D computational modeling of media flow through scaffolds in a perfusion bioreactor. Journal of Biomechanics. 2005 Mar;38(3):543-9. PubMed PMID: WOS:000226884200018.
17. Boschetti F, Raimondi MT, Migliavacca F, Dubini G. Prediction of the micro-fluid dynamic environment imposed to three-dimensional engineered cell systems in bioreactors. Journal of Biomechanics. 2006 2006;39(3):418-25. PubMed PMID: WOS:000234869600003.
18. Lozoya O, Wauthier E, Turner R, Barbier C, Prestwich G, Guilak F, et al. Regulation of hepatic stem/progenitor phenotype by microenvironment stiffness in hydrogel models of the human liver stem cell niche. Biomaterials. 2011 OCT 2011;32(30):7389-402. PubMed PMID: ISI:000294829300012. English.
19. Wells R. The role of matrix stiffness in regulating cell behavior. Hepatology. 2008 APR 2008;47(4):1394-400. PubMed PMID: ISI:000254637100031. English.
20. Simon BR. Multiphase Poroelastic Finite Element Models for Soft Tissue Structures. Applied Mechanics Reviews. 1992;45(6):191-218.
21. MOW V, KUEI S, LAI W, ARMSTRONG C. BIPHASIC CREEP AND STRESS-RELAXATION OF ARTICULAR-CARTILAGE IN COMPRESSION - THEORY AND EXPERIMENTS. Journal of Biomechanical Engineering-Transactions of the Asme. 1980 1980;102(1):73-84. PubMed PMID: ISI:A1980JE19600011. English.
22. Mak AF. THE APPARENT VISCOELASTIC BEHAVIOR OF ARTICULAR-CARTILAGE - THE CONTRIBUTIONS FROM THE INTRINSIC MATRIX VISCOELASTICITY AND INTERSTITIAL FLUID-FLOWS. Journal of Biomechanical Engineering-Transactions of the Asme. 1986 May;108(2):123-30. PubMed PMID: WOS:A1986C337000006.
23. DiSilvestro M, Zhu Q, Suh J. Biphasic poroviscoelastic simulation of the unconfined compression of articular cartilage: II - Effect of variable strain rates. Journal of Biomechanical Engineering-Transactions of the Asme. 2001 APR 2001;123(2):198-200. PubMed PMID: ISI:000168310500010. English.
24. Huang CY, Mow VC, Ateshian GA. The role of flow-independent viscoelasticity in the biphasic tensile and compressive responses of articular cartilage. Journal of Biomechanical Engineering-Transactions of the Asme. 2001 Oct;123(5):410-7. PubMed PMID: ISI:000171356500005. English.
25. Suh J, Bai S. Finite element formulation of biphasic poroviscoelastic model for articular cartilage. Journal of Biomechanical Engineering-Transactions of the Asme. 1998 APR 1998;120(2):195-201. PubMed PMID: ISI:000073505100004. English.
26. Yang Z, Smolinski P. Dynamic finite element modeling of poroviscoelastic soft tissue. Comput Methods Biomech Biomed Engin. 2006 Feb;9(1):7-16. PubMed PMID: 16880152. eng.

27. Pitt Ford TR, Sachs JR, Grotberg JB, Glucksberg MR. Perialveolar interstitial resistance and compliance in isolated rat lung. J Appl Physiol. 1991 Jun;70(6):2750-6. PubMed PMID: 1885472. eng.
28. Ng EY, Ghista DN, Jegathese RC. Perfusion studies of steady flow in poroelastic myocardium tissue. Comput Methods Biomech Biomed Engin. 2005 Dec;8(6):349-57. PubMed PMID: 16393872. eng.
29. Cheng S, Bilston LE. Unconfined compression of white matter. J Biomech. 2007;40(1):117-24. PubMed PMID: 16376349. eng.
30. Peña A, Bolton MD, Whitehouse H, Pickard JD. Effects of brain ventricular shape on periventricular biomechanics: a finite-element analysis. Neurosurgery. 1999 Jul;45(1):107-16; discussion 16-8. PubMed PMID: 10414573. eng.
31. Ayyalasomayajula A, Vande Geest JP, Simon BR. Porohyperelastic finite element modeling of abdominal aortic aneurysms. J Biomech Eng. 2010 Oct;132(10):104502. PubMed PMID: 20887020. eng.
32. Marchesseau S, Heimann T, Chatelin S, Willinger R, Delingette H. Fast porous visco-hyperelastic soft tissue model for surgery simulation: Application to liver surgery. Progress in Biophysics & Molecular Biology. 2010 DEC 2010;103(2-3):185-96. PubMed PMID: ISI:000286359900004. English.
33. Bonfiglio A, Leungchavaphongse K, Repetto R, Siggers J. Mathematical Modeling of the Circulation in the Liver Lobule. Journal of Biomechanical Engineering-Transactions of the Asme. 2010 NOV 2010;132(11):-. PubMed PMID: ISI:000283740800011. English.
34. Ricken T, Dahmen U, Dirsch O. A biphasic model for sinusoidal liver perfusion remodeling after outflow obstruction. Biomechanics and Modeling in Mechanobiology. 2010 AUG 2010;9(4):435-50. PubMed PMID: ISI:000279830700005. English.
35. Wu J, Xu S, Long Q, Collins M, Koenig C, Zhao G, et al. Coupled modeling of blood perfusion in intravascular, interstitial spaces in tumor microvasculature. Journal of Biomechanics. 2008 2008;41(5):996-1004. PubMed PMID: ISI:000254943800009. English.
36. Wu J, Herzog W, Epstein M. Evaluation of the finite element software ABAQUS for biomechanical modelling of biphasic tissues. Journal of Biomechanics. 1998 FEB 1998;31(2):165-9. PubMed PMID: ISI:000073974800009. English.
37. Spilker RL, Suh JK, Mow VC. EFFECTS OF FRICTION ON THE UNCONFINED COMPRESSIVE RESPONSE OF ARTICULAR-CARTILAGE - A FINITE-ELEMENT ANALYSIS. Journal of Biomechanical Engineering-Transactions of the Asme. 1990 May;112(2):138-46. PubMed PMID: WOS:A1990EE52700005.
38. ABAQUS. ABAQUS Theory Manual (Version 6.9). Providence, RI: Dassault Systemes Simulia Corp; 2009.
39. Yeoh OH. SOME FORMS OF THE STRAIN-ENERGY FUNCTION FOR RUBBER. Rubber Chemistry and Technology. 1993 Nov-Dec;66(5):754-71. PubMed PMID: WOS:A1993MP58900006.
40. Schwefel HP. Evolutionsstrategie und Numerische Optimierung: Verfahrenstechnik TUBerlin; 1975.
41. Isight 5.0 Component Guide2011.
42. Nelder JA, Mead R. Downhill Simplex Method in Multidimensions. Computer Journal. 1965;7:308-13.
43. Schittkowski K. NLPQL: A Fortran Subroutine for Solving Constrained Nonlinear Programming Problems. Annals of Operations Research. 1985;5:485-500.
44. Anderson AE, Ellis BJ, Weiss JA. Verification, validation and sensitivity studies in computational biomechanics. Computer Methods in Biomechanics and Biomedical Engineering. 2007 Jun;10(3):171-84. PubMed PMID: BIOABS:BACD200700325373.
45. Stokes I, Chegini S, Ferguson S, Gardner-Morse M, Iatridis J, Laible J. Limitation of Finite Element Analysis of Poroelastic Behavior of Biological Tissues Undergoing Rapid

Loading. Annals of Biomedical Engineering. 2010 MAY 2010;38(5):1780-8. PubMed PMID: WOS:000276204600007. English.
46. Vande Geest JP, Simon BR, Rigby PH, Newberg TP. Coupled Porohyperelastic Mass Transport (PHEXPT) Finite Element Models for Soft Tissues Using ABAQUS. Journal of Biomechanical Engineering-Transactions of the Asme. 2011 Apr;133(4). PubMed PMID: WOS:000288706600013.
47. Stops AJF, Heraty KB, Browne M, O'Brien FJ, McHugh PE. A prediction of cell differentiation and proliferation within a collagen-glycosaminoglycan scaffold subjected to mechanical strain and perfusive fluid flow. Journal of Biomechanics. 2010 Mar 3;43(4):618-26. PubMed PMID: WOS:000276008500004.
48. Chung CA, Chen CW, Chen CP, Tseng CS. Enhancement of cell growth in tissue-engineering constructs under direct perfusion: Modeling and simulation. Biotechnology and Bioengineering. 2007 Aug 15;97(6):1603-16. PubMed PMID: WOS:000248158800026.
49. Kerdok A, Ottensmeyer M, Howe R. Effects of perfusion on the viscoelastic characteristics of liver. Journal of Biomechanics. 2006 2006;39(12):2221-31. PubMed PMID: ISI:000240531300008. English.
50. Kyriacou SK, Mohamed A, Miller K, Neff S. Brain mechanics For neurosurgery: modeling issues. Biomech Model Mechanobiol. 2002 Oct;1(2):151-64. PubMed PMID: 14595547. eng.
51. Kerdok A. Characterizing the Nonlinear Mechanical Response of Liver to Surgical Manipulation Cambridge, MA: Harvard University; 2006.
52. Gu WY, Mao XG, Foster RJ, Weidenbaum M, Mow VC, Rawlins BA. The anisotropic hydraulic permeability of human lumbar anulus fibrosus - Influence of age, degeneration, direction, and water content. Spine. 1999 Dec;24(23):2449-55. PubMed PMID: ISI:000084169700004.
53. Chui C, Kobayashi E, Chen X, Hisada T, Sakuma I. Combined compression and elongation experiments and non-linear modelling of liver tissue for surgical simulation. Medical & Biological Engineering & Computing. 2004 Nov;42(6):787-98. PubMed PMID: ISI:000225543500008. English.
54. Lister K, Gao Z, Desai JP. Development of In Vivo Constitutive Models for Liver: Application to Surgical Simulation. Annals of Biomedical Engineering. 2011 Mar;39(3):1060-73. PubMed PMID: WOS:000287199300013.
55. Hostettler A, George D, Remond Y, Nicolau SA, Soler L, Marescaux J. Bulk modulus and volume variation measurement of the liver and the kidneys in vivo using abdominal kinetics during free breathing. Computer Methods and Programs in Biomedicine. 2010 Nov;100(2):149-57. PubMed PMID: WOS:000283040000006.
56. Liu ZZ, Bilston LE. Large deformation shear properties of liver tissue. Biorheology. 2002 2002;39(6):735-42. PubMed PMID: WOS:000179439400003.
57. Uygun BE, Soto-Gutierrez A, Yagi H, Izamis ML, Guzzardi MA, Shulman C, et al. Organ reengineering through development of a transplantable recellularized liver graft using decellularized liver matrix. Nature medicine. 2010;16(7):814-20.
58. OPTN. Organ Procurement and Transplantation Network: National Data 2011 [cited 2011 November 1]. Available from: http://optn.transplant.hrsa.gov/.
59. Scarborough JE, Tuttle-Newhall JE, Pietrobon R, Marroquin CE, Collins BH, Desai DM, et al. Supply and demand for liver transplant surgery: Are we training enough surgeons? HPB. 2008;10(1):25-9.
60. Orlando G, Wood KJ, Stratta RJ, Yoo JJ, Atala A, Soker S. Regenerative Medicine and Organ Transplantation: Past, Present, and Future. Transplantation. 2011;91(12):1310-7 10.097/TP.0b013e318219ebb5.

61. Orlando G, Baptista P, Birchall M, De Coppi P, Farney A, Guimaraes-Souza NK, et al. Regenerative medicine as applied to solid organ transplantation: current status and future challenges. Transplant International. 2011;24(3):223-32.
62. Baptista PM, Siddiqui MM, Lozier G, Rodriguez SR, Atala A, Soker S. The use of whole organ decellularization for the generation of a vascularized liver organoid. Hepatology. 2011;53(2):604-17.
63. Martin I, Wendt D, Heberer M. The role of bioreactors in tissue engineering. Trends in Biotechnology. 2004;22(2):80-6.
64. Guyton AC, Hall JE. Textbook of medical physiology. Philadelphia, Penns.: Elsevier Saunders; 2006.
65. Hsu W-M, Carraro A, Kulig KM, Miller ML, Kaazempur-Mofrad M, Weinberg E, et al. Liver-Assist Device With a Microfluidics-Based Vascular Bed in an Animal Model. Annals of Surgery. 2010;252(2):351-7 10.1097/SLA.0b013e3181e982ba.
66. Hansen LK, Wilhelm J, Fassett JT. Regulation of Hepatocyte Cell Cycle Progression and Differentiation by Type I Collagen Structure. In: Gerald PS, editor. Current Topics in Developmental Biology. Volume 72: Academic Press; 2005. p. 205-36.
67. Wells RG. The role of matrix stiffness in regulating cell behavior. Hepatology. 2008;47(4):1394-400.
68. Lozoya OA, Wauthier E, Turner RA, Barbier C, Prestwich GD, Guilak F, et al. Regulation of hepatic stem/progenitor phenotype by microenvironment stiffness in hydrogel models of the human liver stem cell niche. Biomaterials. 2011;32(30):7389-402.
69. Kerdok AE, Ottensmeyer MP, Howe RD. Effects of perfusion on the viscoelastic characteristics of liver. Journal of Biomechanics. 2006;39(12):2221-31.
70. Markus J B. Multiscale aspects of mechanical properties of biological materials. Journal of the Mechanical Behavior of Biomedical Materials. 2011;4(2):125-7.
71. Cheng S, Bilston LE. Unconfined compression of white matter. Journal of Biomechanics. 2007;40(1):117-24.
72. Ng EYK, Ghista DN, Jegathese RC. Perfusion studies of steady flow in poroelastic myocardium tissue. Computer Methods in Biomechanics and Biomedical Engineering. 2005 2005/12/01;8(6):349-57.
73. Pitt Ford TR, Sachs JR, Grotberg JB, Glucksberg MR. Perialveolar interstitial resistance and compliance in isolated rat lung. Journal of Applied Physiology. 1991 June 1, 1991;70(6):2750-6.
74. DiSilvestro MR, Zhu Q, Suh J-KF. Biphasic Poroviscoelastic Simulation of the Unconfined Compression of Articular Cartilage: II---Effect of Variable Strain Rates. Journal of Biomechanical Engineering. 2001;123(2):198-200.
75. Ayyalasomayajula A, Geest JPV, Simon BR. Porohyperelastic Finite Element Modeling of Abdominal Aortic Aneurysms. Journal of Biomechanical Engineering. 2010;132(10):104502.
76. Yang Z, Smolinski P. Dynamic finite element modeling of poroviscoelastic soft tissue. Computer Methods in Biomechanics and Biomedical Engineering. 2006;9(1):7-16.
77. Evans DW, Rajagopalan P, Devita R, Sparks JL. Compression instrument for tissue experiments (cite) at the meso-scale: device validation - biomed 2011. Biomed Sci Instrum. 2011;47:264-9. PubMed PMID: 21525631. Epub 2011/04/29. eng.
78. Mak AF. The Apparent Viscoelastic Behavior of Articular Cartilage---The Contributions From the Intrinsic Matrix Viscoelasticity and Interstitial Fluid Flows. Journal of Biomechanical Engineering. 1986;108(2):123-30.
79. Mow VC, Kuei SC, Lai WM, Armstrong CG. Biphasic Creep and Stress Relaxation of Articular Cartilage in Compression: Theory and Experiments. Journal of Biomechanical Engineering. 1980;102(1):73-84.
80. Wu JZ, Herzog W, Epstein M. Evaluation of the finite element software ABAQUS for biomechanical modelling of biphasic tissues. Journal of Biomechanics. 1997;31(2):165-9.

81. DiSilvestro MR, Zhu Q, Wong M, Jurvelin JS, Suh J-KF. Biphasic Poroviscoelastic Simulation of the Unconfined Compression of Articular Cartilage: I---Simultaneous Prediction of Reaction Force and Lateral Displacement. Journal of Biomechanical Engineering. 2001;123(2):191-7.
82. Suh J-K, Bai S. Finite Element Formulation of Biphasic Poroviscoelastic Model for Articular Cartilage. Journal of Biomechanical Engineering. 1998;120(2):195-201.
83. Abaqus. ABAQUS User's Manual (Version 6.10). Providence RI: Dassault Systems Simulia Corp; 2010.
84. Johnson KL, Kendall K, Roberts AD. Surface Energy and the Contact of Elastic Solids. Proceedings of the Royal Society of London A Mathematical and Physical Sciences. 1971 September 8, 1971;324(1558):301-13.
85. Gu WY, Mao XG, Foster RJ, Weidenbaum M, Mow VC, Rawlins BA. The Anisotropic Hydraulic Permeability of Human Lumbar Anulus Fibrosus: Influence of Age, Degeneration, Direction, and Water Content. Spine. 1999;24(23):2449.
86. Mansour JM, Mow, Van C. The Permeability of Articular Cartilage Under Compressive Strain and at High Pressures. The journal of Bone and Joint Surgery. 1976;58(4):509-16.
87. Kerdok AE. Characterizing the nonlinear mechanical response of liver to surgical manipulation 2006.
88. Aycock RS, Seyer JM. Collagens of normal and cirrhotic human liver. Connect Tissue Res. 1989;23(1):19-31. PubMed PMID: 2517247. Epub 1989/01/01. eng.
89. Cross SE, Jin Y-S, Rao J, Gimzewski JK. Nanomechanical analysis of cells from cancer patients. Nat Nano. 2007;2(12):780-3.
90. Hay ED. Cell biology of extracellular matrix: Plenum Press; 1991.
91. Engler AJ, Sen S, Sweeney HL, Discher DE. Matrix elasticity directs stem cell lineage specification. Cell. 2006 Aug 25;126(4). PubMed PMID: WOS:000240276700017.
92. Olsen AL, Bloomer SA, Chan EP, Gaca MDA, Georges PC, Sackey B, et al. Hepatic stellate cells require a stiff environment for myofibroblastic differentiation. American Journal of Physiology-Gastrointestinal and Liver Physiology. 2011 Jul;301(1):G110-G8. PubMed PMID: WOS:000292135000012.
93. Schrader J, Gordon-Walker TT, Aucott RL, van Deemter M, Quaas A, Walsh S, et al. Matrix stiffness modulates proliferation, chemotherapeutic response, and dormancy in hepatocellular carcinoma cells. Hepatology. 2011 Apr;53(4):1192-205. PubMed PMID: 21442631. PMCID: PMC3076070. eng.
94. Wirtz D, Konstantopoulos K, Searson PC. The physics of cancer: the role of physical interactions and mechanical forces in metastasis. Nature Reviews Cancer. 2011 Jul;11(7):512-22. PubMed PMID: WOS:000292028300016.

CHAPTER IV

A Bioengineered Liver Platform to Study Fluid Flow Regulation of Liver Tissue Organization

Emma C. Moran*, Pedro M. Baptista*, Dipen Vyas, Maria H. Ribeiro, Anthony Atala, Jessica L. Sparks, Shay Soker

* These authors contributed equally to the work

Experimental work and manuscript writing was performed by Emma C. Moran and Pedro M. Baptista. Jessica L. Sparks and Shay Soker served in an advisory capacity, Dipen Vyas aided in experiments and all other co-authors served in an editing capacity. Text and figure formatting variations are due to journal guidelines. The work has been submitted to *Biomaterials.*

Abstract

Modeling of human liver organogenesis, including vascularization, is fundamental for understanding embryonic development and disease, yet there are no reliable models that fully mimic these processes *ex vivo*. Using an organ engineering approach, we designed a perfusion system that delivers discrete mechanical forces inside an acellular liver extracellular matrix scaffold in order to study hepatic tissue organization, including the effects of mechanical stimulation. We observed a fluid flow rate dependent response in cell deposition, neovascularization and liver tissue organization within the liver scaffold. Since nitric oxide is a major mediator of fluid flow effects on endothelial cells, we validated these results by selective inhibition of endothelial nitric oxide synthase (eNOS) and observed impairment of both neovascularization and liver tissue organization. Similar results were observed in bioengineered livers grown under static conditions. Overall, we created a novel whole organ bioengineering platform, suitable for modeling human organ growth and organization. This study can contribute significantly to the identification of physiological mechanisms of liver organogenesis and regeneration, and support bioengineering of vascularized and functional organs for transplantation in humans.

Introduction

Liver organogenesis and regeneration are both highly complex processes that involve the coordination of numerous cells types and signals resulting in cellular organization and the formation of liver tissue. Better modeling of this process is key in understanding liver development and regeneration. Due to the limitations of animal models

including cost and ethical considerations, the current approach to study these complex phenomena is by modeling these processes in *ex vivo* systems. Since vasculogenesis and angiogenesis are critical for normal organ development and vascular perfusion plays an important role in tissue regeneration, these *ex vivo* models should also include a vascular component (1-6). *In vitro* models have been developed in the past decades to mimic organ development and regeneration, but most employ cells cultured in 2-dimensional (2D) plastic dishes and do not recapitulate the native 3D organ structure. Some more physiological models are based on 3D extracellular matrix (ECM) gels, but they are invariably static in nature and don't incorporate the effect of mechanical stimulation of fluid flow. On the other hand, microfluidic devices have been developed to deliver fluid flow inside cellular constructs but they consist of very small tissue constructs that lack true physiological organ perfusion properties (7).

The emergence of novel decellularization/re-cellularization techniques has recently been employed by us and others in order to create whole organ scaffolds, including livers, for organ bioengineering (8-13). Owing to the preservation of the vascular tree architecture within these acellular organ scaffolds, they support whole organ perfusion, which can be used for cell seeding and maintenance. Additionally, the vascular perfusion network can be used to simulate the effect of fluid flow-derived mechanical forces on specific cell populations. Finally, the acellular scaffolds contain the native tissue microenvironment, including the composition and arrangement of the liver ECM.

In the current study we used an *in vitro* bioengineered whole liver model (8, 11) to study the effects of fluid-flow mechanical stimulation on hepatic tissue organization. The precise control of flow rate/pressure in a perfusion bioreactor allowed us to determine the

role of shear stress in regulating liver vascularization and cellular organization. Furthermore, we identified the NO signaling pathway as a major mediator of shear stress induced liver tissue organization. Collectively, our data suggest that these bioengineered livers, inside a customized perfusion bioreactor, present a unique model to study the complexities of liver organogenesis, regeneration and revascularization *ex vivo*. Subsequently, by using human liver cells, as we have shown previously (8), this model can provide an invaluable platform to develop new therapeutic strategies.

Materials and Methods

Liver ECM Scaffolds Preparation: Briefly, ferret livers were decellularized as described by Baptista *et al.* (8). After decellularization, liver ECM scaffolds were prepared for each experiment by ligating and subsequently removing the left, caudate and quadratic lobes, all ligated with 4-0 silk black-braided suture (Ethicon, Summerville, NJ, USA). The remaining right lobe, cannulated via the portal vein with all the vascular structures intact, weighed between 3 and 4 grams in all experiments. The scaffold was sterilized prior to use with a dose of 1.5Mrad of gamma-radiation by a cobalt 60 gamma-irradiator (J. L. Shepherd and Associates, San Fernando, CA, USA).

Bioreactor Assembly: Bioreactor parts were sterilized with steam at 121ºC and assembled in a sterile hood according to the diagram in Figure 1. Details of bioreactor parts and assembly can be found in the Supplemental Methods. Once connected, the bioreactor was placed in an incubator with 5% CO_2 at 37ºC. Medium perfusion was started at 3ml/min and

pre-conditioning was performed overnight. System pressure was measured and recorded as described in the Supplemental Methods.

Cell Seeding: To model hepatocytes we used HepG2 cells, a well-differentiated human hepatocellular carcinoma line that retains many hepatocyte functions including albumin secretion and liver metabolic enzymes. MS1 cells, a mouse endothelial line that exhibits many endothelial functions including expression of endothelial nitric oxide synthase (eNOS) and nitric oxide (NO) production, to model endothelial cells (EC). A total of 60 million cells ($30x10^6$ HepG2 and $30x10^6$ MS1 mouse endothelial cells) were seeded per scaffold at different flow rates (Supplemental Table 1). The flow rates ranging from 3-12 ml/min were selected based on the physiological hepatic blood flow of an adult rat during rest (85ml/min/Kg) (14, 15). On average, the 5-6 weeks old ferret livers used to generate liver scaffolds have a similar size and weight of an adult rat liver (~10g for a 300g Sprague-Dawley rat) and only the right lobe is used in these experiments, which is roughly one-third the weight of the whole liver. Taking this into consideration, the estimated physiologic portal flow rate for the liver scaffolds was 6 ml/min, which corresponds experimentally to a parenchymal fluid pressure of ~3mmHg, the physiologic value in most species (16). The 40 ml/min flow rate was chosen as a high shear stress control (17). In order to maintain cell delivery constant and equivalent between conditions, the volume of culture medium and the total number of cells in the bioreactor vessel were adjusted (Supplemental Table 1) to allow a maximum cell delivery rate into the scaffold of approximately 400,000 cells/min. The 40 ml/min flow rate was the exception to this condition due to medium volume constraints. Details of the cell seeding process can be found in the Supplemental Methods.

NO/PG Inhibition and No Flow Experiments: All scaffolds were seeded at 9 ml/min using the same protocol described above, with n=3 for each condition. 24 hours after seeding, media was changed in all bioreactors and one of three conditions was implemented. In the first conditions, termed "no flow bioreactor", perfusion of EGM-2 media was stopped and the scaffold remained in the bioreactor for 7 days in static conditions. In the L-NAME/Indomethacin experiments, the second condition, 1mM of L-NAME and 50μM of Indomethacin were added to the normal media to inhibit synthesis of nitric oxide and prostacyclin. This drug-supplemented media was changed every 24 hours, to ensure constant activity of the drugs. The final condition consisted of 9 ml/min control experiments, maintained with the standard conditions as described above. Glucose and pH were monitored throughout the 7 day period and media was collected on days 3 and 7. Details of the static culture control experiments can be found in the Supplemental Methods.

Immunohistochemistry: Following fixation and tissue processing (details in Supplemental Methods), 5μm histological sections were cut using a Leica microtome (Leica Biosystems, Buffalo Grove, IL, USA) and hematoxylin and eosin (H&E) stain was performed on sections of all bioreactors using an Autostainer XL (Leica Biosystems, Buffalo Grove, IL, USA). Nuclear staining was performed with a solution of propidium iodide at 5ug/ml in PBS on sections of all experiments. Cell proliferation quantification was performed for all bioreactors by using immunofluorescence staining for Ki-67 (Cat#. ab15580, Abcam, Cambridge, MA, USA), followed by goat anti-rabbit Texas Red secondary antibody (Vector Labs, Burlingame, CA, USA). Cellular apoptosis detection was performed using the TdT In Situ Apoptosis Detection Kit – Alexa Fluor 594 (R&D Systems, Minneapolis, MN, USA) in all bioreactors. To identify each cell population in the bioscaffold, double

immunofluorescence staining was performed for endothelial nitric oxide synthase (eNOS) using mouse anti-eNOS (Cat#. 610297, BD Biosciences, San Jose, CA, USA) and albumin (ALB) with goat anti-human albumin (Cat#. A80-229A, Bethyl Labs, Montgomery, TX, USA) followed by donkey anti-mouse alexafluor 594 and donkey anti-goat alexafluor 488 (Invitrogen, Grand Island, NY, USA). All sections were mounted in ProLong Gold Antifade Reagent with DAPI (Invitrogen, Grand Island, NY, USA). Details of image analysis methodology can be found in the Supplemental Methods.

Conditioned Media Assays: Media samples from 1-day experiments across all flow rates were taken and assayed for lactase dehydrogenase (LDH) (Pierce LDH Cytotoxicity Assay Kit, Thermo Scientific, Waltham, MA). Cytotoxicity was then calculated by subtracting the LDH activity of the spontaneous LDH release control from the chemical-treated sample LDH activity, dividing by the total LDH activity, and multiplying by 100. Media samples collected from the control, NO/PG inhibition, and no flow conditions along with tissue culture controls on day 3 and day 7 were analyzed using a Nitric Oxide (total) detection kit (EnzoLife Sciences, Farmingdale, NY) and Prostacyclin ELISA kit (Abnova, Walnut, CA).

RNA Extraction and Real Time PCR: Total RNA was extracted from a small sample of re-seeded liver scaffolds using Allprep DNA/RNA Mini Kit (Qiagen, Maryland, USA) with DNAse treatment. cDNA was synthesized from 500ng of total RNA using Superscript III First Strand Synthesis (Life Technologies, Carlsbad, CA, USA). RT-PCR was performed using Taqman Master Mix (Life Technologies, Carlsbad, CA, USA) with mouse KLF2, integrin β1, integrin β3, and eNOS taqman probes with GAPDH housekeeping gene (Life Technologies). Expression of genes within a sample was normalized to GAPDH expression using the $2^{-\Delta Ct}$ method.

Statistics: Results are shown as mean ± standard deviation and statistical analysis was performed using Graphpad Prism v5 (Graphpad Software Inc, La Jolla, CA, USA). A series of one-way ANOVA's with post-hoc Bonferoni analysis were performed to determine differences between groups (i.e. across flow rates). Pearson's correlation coefficient was used to calculate statistically significant correlations between pressure measurements and quantitative outcomes.

Results

Influence of fluid flow-derived mechanical forces on cell seeding, proliferation and viability: To study the mechanical effects of fluid flow on liver tissue organization we used our previously published technique of whole liver bioengineering, using acellular ferret livers seeded with hepatocytic and endothelial cells (8, 18). This model provides two important features: 1) cells are situated inside a 3D extracellular matrix (ECM) scaffolding system that mimics the native liver micro-architecture, biochemical and biomechanical environment and 2) it allows delivery of distinct fluid flow rates through the native liver vascular network. To control fluid flow parameters, the acellular liver scaffold is placed in a perfusion bioreactor equipped with a controllable pump and system pressure measurements with recording capabilities (Fig. 1, Supplemental Methods). To demonstrate cellular response to fluid flow-induced shear stress and pressures, we employed 2 commonly used hepatic and endothelial cell lines, HepG2 and MS1, respectively. Importantly, HepG2 cells express albumin and the metabolic enzymes of the cytochrome P450 family and are used extensively as a robust model in hepatocyte research; MS1 cells

have typical endothelial cell phenotype and function and have helped in the past to characterize the regulation of the endothelial nitric oxide synthase (eNOS) system (19-22). For most studies described below, the acellular scaffolds were seeded with 60 million cells via perfusion at varying flow rates ranging from 3-12 ml/min, as described in Supplemental Table 1. These flow rates were chosen based on a "physiological" flow rate of approximately 6 ml/min for a liver with the volume and weight of the liver scaffold (14). To simulate the effects of high shear stress conditions, representing situations such as partial hepatectomy where hepatic blood flow to the remaining liver can reach nearly 10 times normal levels, additional scaffolds were seeded at 40 ml/min. Twelve hours post-seeding, medium in the bioreactor was changed and continuous media perfusion was performed for an additional 1 or 7 days at the same flow rate used for cell seeding. Bioengineered liver constructs were harvested and analyzed at these time points.

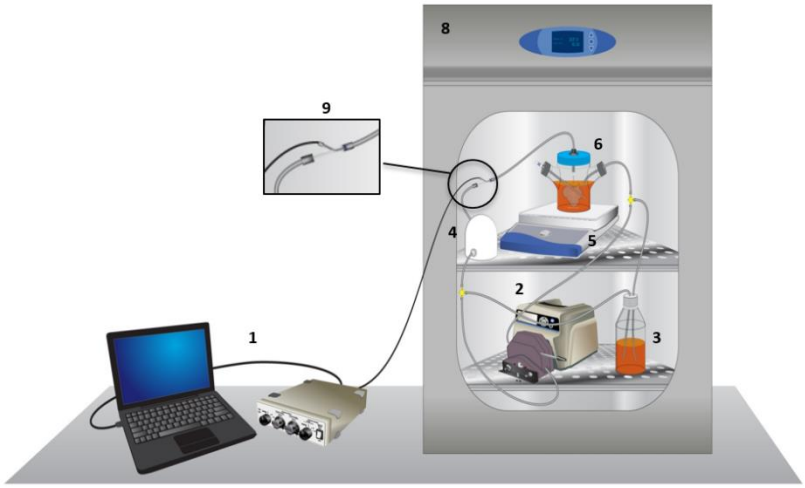

Figure 1: A perfusion bioreactor system. Schematic diagram of a perfusion bioreactor system design; (1) pressure data measurement and recording, (2) peristaltic pump, (3) media reservoir, (4) pulse dampener, (5) magnetic stir-plate, (6) whole organ bioreactor in media, (7) cell injection port (8) cell culture incubator, (9) system pressure probe. A total of $6x10^7$ cells are injected into the culture media and perfused into the portal vein inlet of the acellular liver ECM scaffold.

Initial studies were focused on characterization of the physical aspects of the perfusion system. Details of image analysis procedures can be found in Supplemental Methods. It was first demonstrated that there is a linear correlation between system pressure and flow rate for values of 3-12 ml/min (Fig. 2A). Cell penetration, determined by image analysis quantifying the distance between cell clusters and the nearest vascular channel, is linearly correlated with system pressure (Fig. 2B). Cell occupancy 1 day after cell seeding, quantified through image analysis as the percent area of the scaffold's section surface occupied with cells, is positively correlated with flow rate (Fig. 2C). Cell occupancy 7 days post-seeding peaked at 9 ml/min and decreased at 12 ml/min (Fig. 2D-F). These results suggest that the mechanical forces exerted by the system's flow act in two phases: 1) during cell seeding (measurements taken at day 1), flow primarily affects cell deposition inside the scaffold, with higher flow rates and system pressures driving cells more effectively from the vascular channels into the parenchymal spaces and 2) during the subsequent 6 days (measurements made at day 7), lower, but "physiological", flow rates support the maintenance of the cells, as indicated by cell occupancy (Fig. 2D, Supplementary Fig. 1), as well as proliferation, apoptosis and cytotoxicity (Fig. 2G,H). Specifically, we did not observe significant differences in cell proliferation, apoptosis and cytotoxicity one day post-seeding between flow rates ranging from 3-12 ml/min (Fig. 2G,H). However, at a flow rate of 40 ml/min there was significantly lower cell proliferation and higher apoptosis and cytotoxicity (Fig. 2G,H). The findings at 40 ml/min may be due to elevated shear stress effects, which suppressed cell proliferation and significantly increased apoptosis and cytotoxicity, demonstrating the influence of high fluid flow rates on cell survival. Accordingly, we did not include the 40 ml/min flow rate in the subsequent

studies on liver tissue organization. At flow rates between 3-12 ml/min, cell proliferation increased between 1 and 7 days post-seeding, with peaks at 6 and 9 ml/min (Fig. 2G). There were no significant changes in cell apoptosis and toxicity between 1 and 7 days post-seeding for these flow rates (Fig. 2H). Collectively, these results demonstrate that the perfusion system model can deliver discrete flow rates and pressures into the liver ECM scaffold that specifically affect cellular distribution and viability inside the scaffold, in a correlative manner.

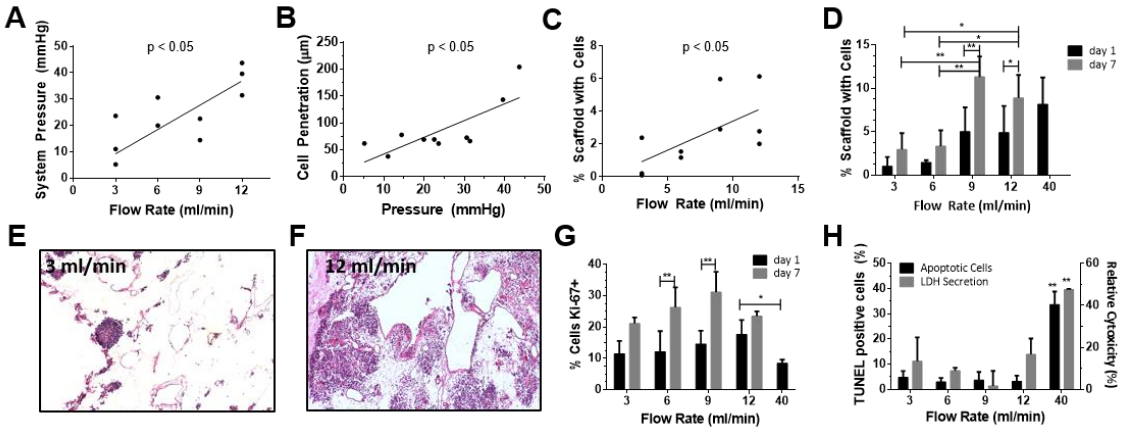

Figure 2: Effect of flow rate and system pressures on cell deposition inside the liver ECM scaffold. (A) System (portal) pressure as a function of flow rate. (B) Image-based quantification of cell penetration into the scaffold as a function of system pressure. (C) Cell occupancy inside the scaffold as a function of flow rate, 1 day after cell seeding. (D) Cell occupancy as a function of flow rate after 1 or 7 days in the perfusion bioreactor. (E, F) Representative H&E images of liver scaffolds after 1 day in the perfusion bioreactor post-seeding at 3 ml/min (E) and 12 ml/min (F). (G) Cell proliferation, as quantified as the percentage of Ki-67-positive cells as a function of flow rate at 1 and 7 days. (H) Cell viability, the percentage of apoptotic cells, as determined by TUNEL staining and by LDH concentrations in the media as function of flow rate after 1 day. Due to massive cell death experienced at 40 ml/min, experiments at this flow rate did not proceed to day 7. Results presented as mean ± SD, N=3. * $p < 0.05$, ** $p < 0.01$.

Fluid flow-derived mechanical forces control liver tissue organization **:** We next analyzed the effects of increasing fluid flow rates on liver tissue organization inside the ECM scaffolds. Analysis of the bioengineered liver tissue 1 day post seeding revealed a mixed population of HepG2 and MS1 in both the scaffold parenchyma and vascular channels, at all flow rates tested (Fig. 3A, top). In contrast, after 7 days of perfusion, EC were mostly localized at the vascular channels of the liver ECM scaffold, while HepG2 cells formed large cell clusters in the parenchyma (Fig. 3A, bottom). Specific staining for each cell type and for cell proliferation marker, Ki-67, confirmed that both hepatocytic cells and EC were proliferating after 7 days (Fig. 3B).

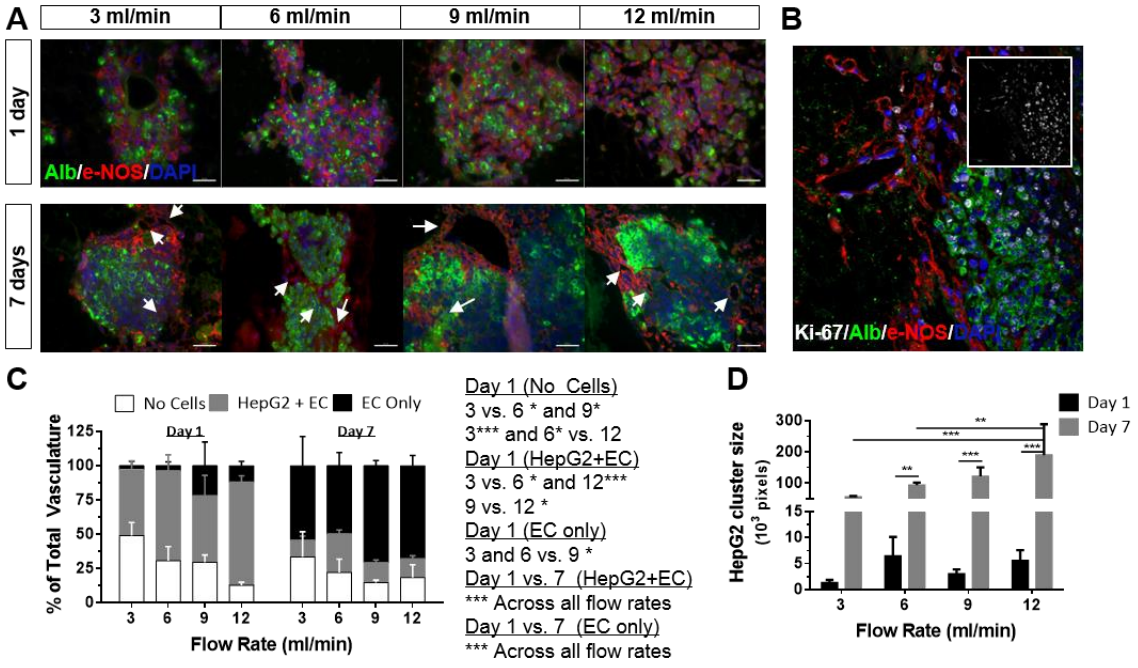

Figure 3: Effects of fluid flow rate on liver tissue organization. (A) Representative images of albumin staining of HepG2 cells (green) and eNOS staining of MS1 cells (red) from days 1 (top) and 7 (bottom), at the indicated flow rates (white arrows point to vascular structures). (B) Co-immunostaining of cells expressing albumin, eNOS and Ki-67 (inset). (C) Analysis of cell types (MS1+HepG2, MS1 only and no cells) covering the vascular structures at 3, 6, 9 and 12 ml/min, 1 and 7 days post cell seeding. (D) HepG2 cluster size at 1 and 7 days post cell seeding. Results presented as mean ± SD, N=3. * $p < 0.05$, ** $p < 0.01$, *** $p < 0.001$. Scale bars: 100 μm (A), 50 μm (B).

Subsequently, we quantified cellular distribution within the vascular structures and the parenchyma using image analysis. At all flow rates tested, there were significantly more vascular structures lined with only endothelial cells at the day 7 compared to day 1, suggesting that the EC migrated to the vascular channels and proliferated between days 1 and 7 (Fig. 3C). Accordingly, the number of vascular structures lined by a mixture of hepatic cells and EC significantly decreased between days 1 and 7. Similarly, there was a significant increase in the size of hepatocytic cell clusters from days 1 to 7 (Fig. 3D). When comparing different flow rates, we found a significant correlation with the localization of cells in the vascular channels and the parenchyma (Fig. 3C, D). We observed an increase in vascular channel coverage at higher flow rates at day 1. Additionally, there was a linear correlation between flow rate and the size of hepatocytic cell clusters, at day 7. Collectively, these results clearly show that the perfusion flow rate has a significant effect on the organization of vascular and hepatocytic structures inside the liver ECM scaffolds. Moreover, we were able to demonstrate progressive cellular niche selection and liver tissue reorganization in response to specific flow rate values.

The role of the nitric oxide pathway in bioengineered liver tissue organization: The effects of shear stress on EC are largely mediated by the nitric oxide (NO) pathway during liver regeneration post injury (23, 24). Since the perfusion system creates a dynamic mechanical environment within the liver scaffold, it enabled us to determine if the effects of fluid flow and shear stress on the bioengineered liver tissue organogenesis involved this particular pathway. We first analyzed the expression of genes involved in EC response to flow-induced shear stress in media supplemented with a NO inhibitor (1mM L-NAME) 1 day post seeding. In this experiment, it was also vital to inhibit the prostaglandin (PG)

synthesis pathway with a PG inhibitor (50μM indomethacin) to prevent a reported compensatory effect on angiogenesis and EC migration of one pathway over the other when one is pharmacologically inhibited (25).

Quantitative RT-PCR using primers specific to the murine MS1 endothelial cells revealed a significant decrease in integrin β1 (m-ITGB1), β3 (m-ITGB3) and KLF2 (m-KLF2) expression under NO/PG inhibition compared to controls (Fig. 4A). To confirm that this effect was due to fluid flow inside the liver scaffold, media perfusion was stopped 1 day post seeding and the bioengineered liver constructs were maintained under "no flow" conditions for additional 6 days. Further decrease in the expression of these genes was observed under no flow conditions (Fig. 4A). In parallel, NO/PG synthesis inhibition affected the reorganization of the bioengineered liver tissue and revealed a mixture of EC and HepG2 cells inside the liver ECM scaffolds, with a visible reduction in organized vascular and hepatic cellular structures (Fig. 4B). Similar results of an unorganized liver tissue, containing very few EC and HepG2 cells, were observed under no flow conditions (Fig. 4B).

Quantification of the histological data showed a significant decrease in the proportion of EC-coated vascular structures under NO/PG synthesis inhibition (31%), compared to controls (63%) (Fig. 4C). Under no flow conditions there were very few vascular structures lined by EC (7.1%), a significant decrease compared to control and NO/PG inhibition (Fig. 4C). In addition, there was a significant decrease in the size of HepG2 clusters in the no flow condition ($7.8x10^3$ pixels), compared to the control ($129x10^3$ pixels) (Fig. 4D). On the other hand, there was no change in cell proliferation under NO/PG synthesis inhibition and no flow conditions, suggesting that the decreased cellular

organization is not a result of reduced cell growth under these conditions (Fig. 4E). Measurements of NO concentrations in the bioreactor media 3 and 7 days post seeding revealed a significant decrease under NO/PG synthesis inhibition compared to controls at day 7 (Fig. 5A). There was only a modest decrease in NO concentrations under no flow conditions 3 days post seeding, which was further decreased by day 7 post seeding, suggesting a progressive adjustment of the cells to the static conditions (Fig. 5A). Additionally, a significant decrease in eNOS expression was observed under NO synthesis inhibition and no flow conditions compared to controls (Fig. 5B). Similarly, there was also a significant decrease of COX2 expression in EC with PG inhibitors (Fig. 5C). Interestingly, in the no flow condition, there was an up-regulation of this enzyme, possibly due to hypoxia in these experimental conditions (26-28). To confirm that the EC cells were the main target for the NO/PG synthesis inhibition, we incubated each cell type separately in culture dishes with the inhibitors, or together in transwell dishes that allow exchange of paracrine factors without direct cell-cell interactions (Fig. 6). There were no significant changes in NO levels for either EC or HepG2 cells, or their combination in transwell plates, with the addition of the inhibitors. Bradykinin, an inducer of NO secretion, induced a significant increase in NO synthesis, only in dishes with EC and NO/PG synthesis inhibition significantly reduced NO concentration down to its baseline, un-induced levels. As expected, HepG2 cells showed only marginal NO secretion, which was not affected by bradykinin and/or NO/PG synthesis inhibition.

These results can serve to validate the role of specific pathways in mediating the effects fluid flow induced shear stress and underscore the novelty of the current model to simulate these effects *in vitro* in bioengineered liver tissues.

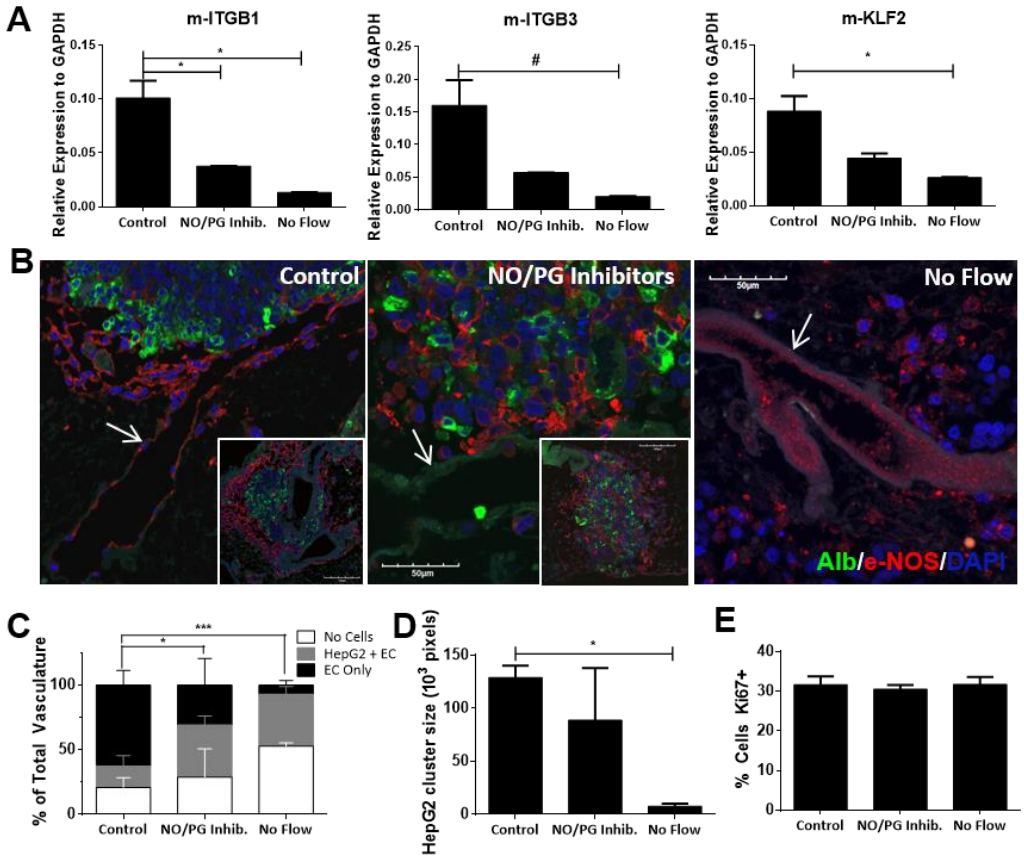

Figure 4: NO inhibition reduces liver tissue organization. (A) Quantitative-PCR of RNA isolated from seeded scaffolds using standard 9 ml/min perfusion conditions (control), addition of NO and PG synthesis inhibitors (NO/PG inhibitors), and no flow conditions. Mouse-specific primers were used to analyze endothelial cell expression of integrin β1 (m-ITGB1), integrin β3 (m-ITGB3) and KLF2 (m-KLF2). (B) Representative images of albumin staining of HepG2 cells (green) and eNOS staining of MS1 cells (red) under the three conditions described in A (white arrows point to vascular structures covered with EC). (C) Analysis of cell types covering the vascular structures at 7 days post cell seeding, quantified as described in Fig. 3C. (D) HepG2 cluster size at 7 days post cell seeding (E) Proliferation; quantified as the percentage of Ki-67-positive cells. Results presented as mean ± SD, N=3. # $p<0.1$, * $p<0.05$, ** $p<0.01$, *** $p<0.001$.

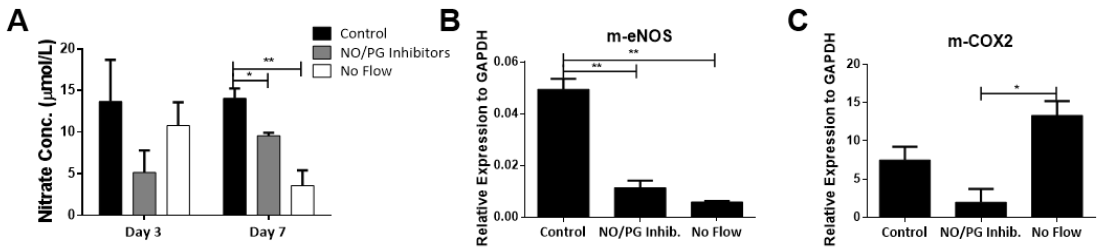

Figure 5: Shear stress-induced NO regulates liver tissue organization. (A) Nitrate (NO) concentration in the conditioned media of liver ECM scaffolds at 3 and 7 days post cell seeding in standard perfusion conditions (control), with the addition of NO and PG synthesis inhibitors (NO/PG inhibitors), and under no flow conditions. **(B)** Quantitative-PCR of mouse specific endothelial nitric oxide synthase (m-eNOS) expression under the three conditions described in **A**. **(C)** Quantitative-PCR of mouse-specific COX2 (m-COX2) expression under the three conditions described in **A**. Results presented as mean ± SD, N=3. * $p<0.05$, ** $p<0.01$.

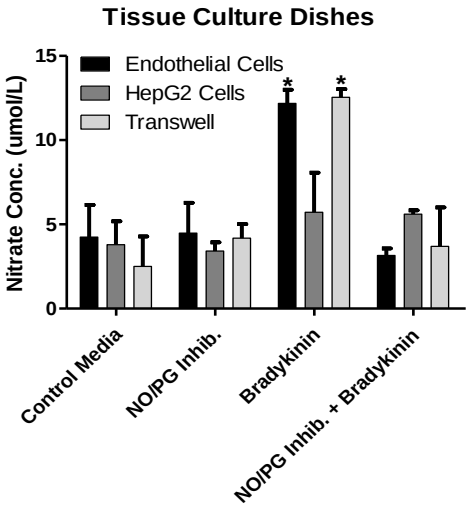

Figure 6: Nitrate (NO) static culture control. Nitrate (NO) concentrations in the media of HepG2 and MS1 cells grown separately in tissue culture dishes or together in "transwell" plates. Some cells were cultured in the presence of bradykinin and a combination of bradykinin and NO and PG synthesis inhibitors. *$p<0.05$.

Discussion

To date, there is a lack of comprehensive *ex vivo* systems for studying the dynamics of human liver development and regeneration. Such models can provide essential information on human embryonic development, congenital and post-natal defects, diseases and tissue regeneration after injury. Although human embryonic and induced pluripotent stem cell systems can model specific hepatic tissue development (29, 30), they often lack the macro-organ elements such as the ECM skeleton, a native vascular tree and organ compartmentalization. In the current study, we have developed a whole liver perfusion system that better mimics tissue organization for applications such as studying liver organogenesis and regeneration. In particular, this system can evaluate the impact of defined mechanical forces on these processes. We validated this system by demonstrating the effects of specific fluid flow rates and pressures on liver tissue organization and maturation. Furthermore, using this model we were able to implicate one specific agent, NO, and its signaling pathway, as an important element mediating the effects of fluid flow induced shear stress on liver tissue organization.

Since the acellular whole liver ECM scaffold preserves both the large and small vascular channels of the native organ, it is a unique system for modeling the effects of fluid flow on tissue organization (8). For example, this system can be applied to embryonic development, where different regions are exposed to differential shear stresses and pressures (31). As "proof of principle" we tested different flow rates and found that near-physiological flow rates of 9-12 ml/min resulted in increased cell proliferation and tissue organization, while non-physiologic hyper-perfusion conditions of 40 ml/min led to cell death and 3-6 ml/min led to sub-optimal tissue organization. These results are in agreement

with the observations that "small-for-size" liver transplantations causing extreme hyper-perfusion, indicative of elevated portal vein pressure and high shear stress, led to significant cell death and ultimately, graft dysfunction (32, 33). In contrast, mild elevations in flow rate resulted in successful liver regeneration following small-for-size transplantation (34), which we believe are represented by the 9-12 ml/min flow rates used in this study. Taken together, these results demonstrate that this bioengineered liver perfusion system has the potential to reliably model the effects of portal flow increases in cases such as small-for-size liver transplantations, partial hepatectomy, or surgical procedures that may alter liver hemodynamics. The outcomes of experiments using this model have the potential to identify optimal conditions to improve cell viability and regeneration following these procedures.

Neovascularization, a fundamental process in every tissue, organ development and regeneration, combines vasculogenesis, the formation of blood vessels from unorganized endothelial cells, and angiogenesis, the branching of new vessels from preexisting blood vessels. The first process is mostly based on EC migration whereas the latter requires both migration and proliferation (35, 36). The bioengineered human liver tissue inside a perfusion bioreactor successfully recapitulated EC migration, proliferation and organization within the vascular channels *ex vivo.* The EC migrated over a 7 day period to cover the vascular structures of the liver ECM scaffold and were also dividing during this period. Furthermore, both processes were specifically affected by changes in the flow rate of culture media perfused inside the liver scaffold. Other *ex vivo* systems that have attempted to model neovascularization are mostly performed by co-culture of EC with other cells types in 2-D or in 3-D systems, which may include a fibrous scaffolding system,

and are perfused with culture media only from the surface (35, 36). Our model has a unique advantage over these other systems in that it allows for physiological perfusion through vascular channels within the liver scaffold.

Furthermore, we have shown that our model is useful in investigating the role of EC in tissue development and organization, in addition to their role in neovascularization and tissue perfusion (37). EC have been reported to have an essential role during embryonic development of the liver prior to vascular function, where EC signals are necessary for normal hepatic organogenesis (1, 3). We were also able to validate a potential mechanism that mediates the effects of fluid flow on the organization of EC inside of the liver scaffold vasculature. Pharmacological suppression of NO production significantly impaired tissue organization within the scaffold confirming the differential response in liver tissue organization to different flow rates or mechanical stimuli, as previously described. Such effects of EC-released NO are also seen during liver development and regeneration (5, 23, 24, 38-41). In addition, NO is capable of sensitizing rat adult hepatocytes for proliferation by switching them into a growth factor-responsive state through the down-regulation of S-adenosylmethionine levels (42), while on the other hand, increased oxygen and nutrient transport alone is able to increase HepG2 function and growth (i.e. cluster size) (43, 44). In our model, similar to the observations of other authors (44), lowered oxygen and nutrient transport under static or low flow rate conditions limit HepG2 growth. Additionally, lack of EC migration due to either reduced mechanical stimulation or NO inhibition, contributed to the small size of HepG2 clusters. In addition, there was a significant decrease in the expression of genes that have an important role in mechanotransduction, angiogenesis and vasculogenesis, such as KLF2, eNOS, COX2, ITGB1 and ITGB3. However, there is the

possibility that some of these effects may be due to cell stress due to lack of perfusion of oxygen and nutrients under static conditions. On the other hand, there were no differences in cellular growth and organization between the surface and the center of the tissue. For example, the potential upregulation of COX2 and eNOS expression under low oxygen tensions may be unrelated to mechanical stimulation (45). Thus, we propose that eNOS may serve as a better mechanotransducer than COX2 in our system because its expression was not affected by hypoxia.

In conclusion, we described here a unique model employing an acellular whole liver ECM scaffold inside a perfusion bioreactor to test the effects of fluid flow mechanical stimulation on liver neovascularization and tissue organization. Unlike previously published *in vitro* models, our approach creates a whole organ system, including a branched vascular network capable of delivering a range of flow rates that provide a unique model of that can be applied towards studies of human liver development and regeneration. This methodology confirmed the vital role of mechanical stimulation in vascularization and tissue organization, mediated in part by NO secretion and its direct impact on EC migration and function. This system can be further extended to test the effects of other mechanical forces and cellular cues that may additionally impact organogenesis and regeneration after liver injury. Ultimately, this novel liver model can significantly contribute to the bioengineering of vascularized and functional organs for transplantation in human patients.

References

1. Matsumoto K, Yoshitomi H, Rossant J, Zaret KS. Liver organogenesis promoted by endothelial cells prior to vascular function. Science. 2001 Oct 19;294(5542):559-63. PubMed PMID: WOS:000171695600037.
2. Lammert E, Cleaver O, Melton D. Induction of pancreatic differentiation by signals from blood vessels. Science. 2001 Oct 19;294(5542):564-7. PubMed PMID: WOS:000171695600038.
3. Lammert E, Cleaver O, Melton D. Role of endothelial cells in early pancreas and liver development. Mechanisms of Development. 2003 Jan;120(1):59-64. PubMed PMID: WOS:000180421400006.
4. Abshagen K, Eipel C, Vollmar B. A critical appraisal of the hemodynamic signal driving liver regeneration. Langenbecks Archives of Surgery. 2012 Apr;397(4):579-90. PubMed PMID: WOS:000302261000010.
5. Sato Y, Koyama S, Tsukada K, Hatakeyama K. Acute portal hypertension reflecting shear stress as a trigger of liver regeneration following partial hepatectomy. Surgery Today-the Japanese Journal of Surgery. 1997;27(6):518-26. PubMed PMID: WOS:A1997XB00900007.
6. Sato Y, Tsukada K, Hatakeyama K. Role of shear stress and immune responses in liver regeneration after a partial hepatectomy. Surg Today. 1999;29(1):1-9. PubMed PMID: 9934824.
7. Huh D, Torisawa Y-s, Hamilton GA, Kim HJ, Ingber DE. Microengineered physiological biomimicry: Organs-on-Chips. Lab on a Chip. 2012 2012;12(12):2156-64. PubMed PMID: WOS:000304448700008.
8. Baptista PM, Siddiqui MM, Lozier G, Rodriguez SR, Atala A, Soker S. The use of whole organ decellularization for the generation of a vascularized liver organoid. Hepatology. 2011 Feb;53(2):604-17. PubMed PMID: 21274881. eng.
9. Soto-Gutierrez A, Zhang L, Medberry C, Fukumitsu K, Faulk D, Jiang H, et al. A Whole-Organ Regenerative Medicine Approach for Liver Replacement. Tissue Engineering Part C-Methods. 2011 Jun;17(6):677-86. PubMed PMID: WOS:000291202200007.
10. Bao J, Shi Y, Sun H, Yin X, Yang R, Li L, et al. Construction of a Portal Implantable Functional Tissue-Engineered Liver Using Perfusion-Decellularized Matrix and Hepatocytes in Rats. Cell Transplantation. 2011 2011;20(5):753-66. PubMed PMID: WOS:000292532000013.
11. Uygun B, Soto-Gutierrez A, Yagi H, Izamis M, Guzzardi M, Shulman C, et al. Organ reengineering through development of a transplantable recellularized liver graft using decellularized liver matrix. Nat Med. 2010 Jul;16(7):814-20. PubMed PMID: 20543851. PMCID: PMC2930603. eng.
12. Barakat O, Abbasi S, Rodriguez G, Rios J, Wood RP, Ozaki C, et al. Use of Decellularized Porcine Liver for Engineering Humanized Liver Organ. Journal of Surgical Research. 2012 Mar;173(1):E11-E25. PubMed PMID: WOS:000300612500002.
13. Yagi H, Fukumitsu K, Fukuda K, Kitago M, Shinoda M, Obara H, et al. Human-Scale Whole-Organ Bioengineering for Liver Transplantation: A Regenerative Medicine Approach. Cell Transplantation. 2013 2013;22(2):231-42. PubMed PMID: WOS:000316158100003.
14. Pollack GM, Brouwer KL, Demby KB, Jones JA. Determination of hepatic blood flow in the rat using sequential infusions of indocyanine green or galactose. Drug metabolism and disposition: the biological fate of chemicals. 1990 Mar-Apr;18(2):197-202. PubMed PMID: 1971573. Epub 1990/03/01.
15. Davies B, Morris T. Physiological parameters in laboratory animals and humans. Pharmaceutical research. 1993 Jul;10(7):1093-5. PubMed PMID: 8378254.
16. Moran EC, Baptista PM, Evans DW, Soker S, Sparks JL. Evaluation of parenchymal fluid pressure in native and decellularized liver tissue. Biomed Sci Instrum. 2012;48:303-9. PubMed PMID: 22846298. Epub 2012/08/01. eng.

17. Fukuchi T, Hirose H, Onitsuka A, Hayashi M, Senga S, Imai N, et al. Effects of portal-systemic shunt following 90% partial hepatectomy in rats. Journal of Surgical Research. 2000 Apr;89(2):126-31. PubMed PMID: WOS:000086342900002. English.
18. Baptista PM, Vyas D, Moran E, Wang Z, Soker S. Human liver bioengineering using a whole liver decellularized bioscaffold. Methods in molecular biology (Clifton, NJ). 2013 2013;1001:289-98. PubMed PMID: MEDLINE:23494438.
19. Yang YZ, Yang YS, Xu Y, Lick SD, Awasthi YC, Boor PJ. Endothelial glutathione-S-transferase A4-4 protects against oxidative stress and modulates NOS expression through NF-kappa B translocation. Toxicology and Applied Pharmacology. 2008 Jul;230(2):187-96. PubMed PMID: WOS:000257577500007. English.
20. Wang L, Yang Y, Dwivedi S, Xu Y, Chu ET, Li J, et al. Manipulating glutathione-S-transferases may prevent the development of tolerance to nitroglycerin. Cardiovascular Toxicology. 2006 Jun;6(2):131-44. PubMed PMID: WOS:000203009900005.
21. Huch M, Gehart H, van Boxtel R, Hamer K, Blokzijl F, Verstegen MMA, et al. Long-Term Culture of Genome-Stable Bipotent Stem Cells from Adult Human Liver. Cell. 2015 Jan;160(1-2):299-312. PubMed PMID: WOS:000347923200026.
22. Knowles BB, Howe CC, Aden DP. HUMAN HEPATOCELLULAR-CARCINOMA CELL-LINES SECRETE THE MAJOR PLASMA-PROTEINS AND HEPATITIS-B SURFACE-ANTIGEN. Science. 1980;209(4455):497-9. PubMed PMID: WOS:A1980JZ57000021. English.
23. Schoen JM, Wang HH, Minuk GY, Lautt WW. Shear stress-induced nitric oxide release triggers the liver regeneration cascade. Nitric Oxide-Biology and Chemistry. 2001 Oct;5(5):453-64. PubMed PMID: WOS:000171571700004.
24. Smith JMS, Lautt WW. The role of prostaglandins in triggering the liver regeneration cascade. Nitric Oxide-Biology and Chemistry. 2005 Sep;13(2):111-7. PubMed PMID: WOS:000231491300003.
25. Schoen Smith JM, Lautt WW. The role of prostaglandins in triggering the liver regeneration cascade. Nitric oxide : biology and chemistry / official journal of the Nitric Oxide Society. 2005 Sep;13(2):111-7. PubMed PMID: 16006158. PMCID: 2925888. Epub 2005/07/12. eng.
26. Colgan SP, Taylor CT, Narravula S, Synnestvedt K, Blume ED. Endothelial COX-2 induction by hypoxia liberates 6-keto-PGF1 alpha, a potent epithelial secretagogue. Advances in experimental medicine and biology. 2002;507:107-12. PubMed PMID: 12664572.
27. Inoue H, Taba Y, Miwa Y, Yokota C, Miyagi M, Sasaguri T. Induction of cyclooxygenase-2 expression by fluid smear stress in vascular endothelial cells. Advances in experimental medicine and biology. 2003;525:141-4. PubMed PMID: 12751754.
28. Wu G, Luo J, Rana JS, Laham R, Sellke FW, Li J. Involvement of COX-2 in VEGF-induced angiogenesis via P38 and JNK pathways in vascular endothelial cells. Cardiovascular research. 2006 Feb 1;69(2):512-9. PubMed PMID: 16336951.
29. Zhu Z, Huangfu D. Human pluripotent stem cells: an emerging model in developmental biology. Development. 2013 Feb 15;140(4):705-17. PubMed PMID: WOS:000314405000002.
30. Takebe T, Sekine K, Enomura M, Koike H, Kimura M, Ogaeri T, et al. Vascularized and functional human liver from an iPSC-derived organ bud transplant. Nature. 2013 Jul 25;499(7459):481-+. PubMed PMID: WOS:000322157900041.
31. Collardeau-Frachon S, Scoazec J-Y. Vascular development and differentiation during human liver organogenesis. Anatomical Record-Advances in Integrative Anatomy and Evolutionary Biology. 2008 Jun;291(6):614-27. PubMed PMID: WOS:000256718800002.
32. Dahm F, Georgiev P, Clavien PA. Small-for-size syndrome after partial liver transplantation: Definition, mechanisms of disease and clinical implications. American Journal of Transplantation. 2005 Nov;5(11):2605-10. PubMed PMID: WOS:000232393000004.

33. Yagi S, Uemoto S. Small-for-size syndrome in living donor liver transplantation. Hepatobiliary & Pancreatic Diseases International. 2012 Dec 15;11(6):570-6. PubMed PMID: WOS:000312170400001.
34. Hessheimer AJ, Fondevila C, Taura P, Munoz J, Sanchez O, Fuster J, et al. Decompression of the Portal Bed and Twice-Baseline Portal Inflow Are Necessary for the Functional Recovery of a "Small-for-Size" Graft. Annals of Surgery. 2011 Jun;253(6):1201-10. PubMed PMID: WOS:000290664100023.
35. Ucuzian AA, Greisler HP. In vitro models of angiogenesis. World journal of surgery. 2007 Apr;31(4):654-63. PubMed PMID: 17372665.
36. Morin KT, Tranquillo RT. In vitro models of angiogenesis and vasculogenesis in fibrin gel. Exp Cell Res. 2013 Oct 1;319(16):2409-17. PubMed PMID: 23800466. PMCID: 3919069.
37. Greene AK, Wiener S, Puder M, Yoshida A, Shi B, Perez-Atayde AR, et al. Endothelial-directed hepatic regeneration after partial hepatectomy. Annals of Surgery. 2003 Apr;237(4):530-5. PubMed PMID: WOS:000185834400015.
38. Cantre D, Schuett H, Hildebrandt A, Dold S, Menger MD, Vollmar B, et al. Nitric oxide reduces organ injury and enhances regeneration of reduced-size livers by increasing hepatic arterial flow. British Journal of Surgery. 2008 Jun;95(6):785-92. PubMed PMID: WOS:000258391500020.
39. Mei Y, Thevananther S. Endothelial nitric oxide synthase is a key mediator of hepatocyte proliferation in response to partial hepatectomy in mice. Hepatology. 2011 Nov;54(5):1777-89. PubMed PMID: 21748771. PMCID: 3579770. Epub 2011/07/13. eng.
40. Diaz-Juarez J, Hernandez-Munoz R. The Role of Calcium and Nitric Oxide During Liver Enzyme Release Induced by Increased Physical Forces as Evidenced in Partially Hepatectomized Rats. Liver Transplantation. 2011 Mar;17(3):334-43. PubMed PMID: WOS:000288178100015.
41. Yoshida D, Akahoshi T, Kawanaka H, Yamaguchi S, Kinjo N, Taketomi A, et al. Roles of Vascular Endothelial Growth Factor and Endothelial Nitric Oxide Synthase During Revascularization and Regeneration After Partial Hepatectomy in a Rat Model. Surgery Today. 2011 Dec;41(12):1622-9. PubMed PMID: WOS:000297939900007.
42. Garcia-Trevijano ER, Martinez-Chantar ML, Latasa MU, Mato JM, Avila MA. NO sensitizes rat hepatocytes to proliferation by modifying S-adenosylmethionine levels. Gastroenterology. 2002 May;122(5):1355-63. PubMed PMID: WOS:000175305500021.
43. Tanaka Y, Yamato M, Okano T, Kitamori T, Sato K. Evaluation of effects of shear stress on hepatocytes by a microchip-based system. Measurement Science & Technology. 2006 Dec;17(12):3167-70. PubMed PMID: WOS:000242528500011.
44. Anada T, Fukuda J, Sai Y, Suzuki O. An oxygen-permeable spheroid culture system for the prevention of central hypoxia and necrosis of spheroids. Biomaterials. 2012 Nov;33(33):8430-41. PubMed PMID: WOS:000310401000023.
45. Searles CD. Transcriptional and posttranscriptional regulation of endothelial nitric oxide synthase expression. American Journal of Physiology-Cell Physiology. 2006 Nov;291(5):C803-C16. PubMed PMID: WOS:000241193100001.

Chapter V

A Bioengineered Liver Model to Study Cancer Metastasis and Investigation of Biomechanical Factors Governing Tumor Invasion

Emma C. Moran, Matthew Brovold, Leegan Lim, Brandon Gaston, Jessica Sparks, Anthony Atala, Pedro Baptista, Shay Soker

Emma Moran designed and performed experiments and wrote the manuscript. Matthew, Leegan and Brandon assisted in experiments. Jessica Sparks, Anthony Atala, Shay Soker and Pedro Baptista served in an advisory capacity. When complete, the work will be submitted to Plos One.

Abstract

The underlying processes of liver-specific metastasis are not fully understood, partly because of the difficulties studying it in a laboratory setting. Bioengineered human livers can provide the ideal system for studying cancer metastasis due to the retention of the native liver microenvironment, giving this model a distinct advantage over current *in vitro* systems. In this study, whole acellular liver organoids were seeded with HCT116 colon carcinoma cells and incubated in perfusion bioreactors. The 3D liver tumor organoids exhibited nodular formation around vascular structures with a significant increase in the average size of nodules from 1 to 7 days, demonstrating the effectiveness of the perfusion bioreactor in modelling the physiological progression of colon cancer metastasis to the liver. In order to generate a high-throughput model of cancer metastasis to study specific microenvironmental perturbations on tumor behavior, we created acellular liver ECM discs that fit into a 96-well plate format. The acellular liver ECM discs were seeded with HCT116 cells and harvested after 1 or 7 days for tumor growth analysis. Liver ECM discs had slower growth rates than cells grown in tissue culture plastic, but demonstrated well-developed cell-cell and cell-matrix interactions and increased matrix metalloproteinase expression over standard 2D culture. The mechanical properties of liver discs were then modified through chemical crosslinking to study the impact of matrix stiffness on tumor growth. Substrate mechanics were found to impact the pattern of tumor cell growth, with more nodular growth and cellular migration occurring on stiffer substrates. In conclusion, we have developed a novel *in vitro* platform for studying metastatic colon cancer in the liver using acellular liver ECM which allows us to examine the impact of tumor

microenvironment, including microenvironmental perturbations, on tumor growth and behavior.

Introduction

Colorectal cancer (CRC) is the third most common cancer and third leading cause of cancer-related deaths in both men and women in the United States (1). In almost 30% of cases the original cancer metastasizes to the liver and is the major cause of death of patients with CRC (2). CRC frequently metastasize to the liver due to colon and upper rectal drainage directly into the hepatic-portal circulatory system (3, 4). Once in the liver, the cancer spreads easily into the parenchyma through the large fenestrae in between sinusoidal endothelial cells of the hepatic sinusoid. (4, 5). Additionally, tumor cells entering the hepatic parenchyma may trigger a pro-inflammatory response by resident Kupffer cells that allows cancer cells to adhere to liver microvasculature (6).

Metastatic potential and progression are highly dependent on both the primary tumor as well as the microenvironment of the host tissue (7, 8). Animal models are the most common tool to study CRC metastasis to the liver but they possess a number of limitations such as the failure to properly reproduce human metastatic progression and the inability to capture real-time data (9). Many *in vitro* models lack tissue complexity, although recent advancements have included the use of liver microtissues in dynamic fluidic environments to study tumor/host tissue cell-cell interactions (10, 11). However, these advanced systems still fail to fully capture the host tissue microenvironment,

including ECM components, organization and mechanical structures that may play a large role in tumor behavior.

Tissue engineering approaches to study cancer metastasis address many of these limitations by providing an *in vivo* microenvironment with which the cancer cells can interact. We have developed a model of CRC metastasis to the liver using acellular liver ECM derived by decellularizing native liver tissue (12). The acellular liver retains all of the ECM components and microarchitecture of native liver tissue, allowing us to examine the interaction of tumor cells with host tissue microenvironment. CRC metastasis is examined by seeding CRC cells in an acellular liver ECM organoid, which contains intact vasculature that can be perfused in a dynamic bioreactor system. We also created a higher-throughput model by fabricating acellular liver ECM discs within a 96-well plate format that allows us to study the role of microenvironmental perturbations on tumor cells. In this study, we examine the impact of the mechanical environment on tumor cells by modifying the stiffness of the underlying ECM, an important factor in tumor cell behavior (13).

The processes underlying migration and invasion in metastatic organs are largely unknown but most likely involve tumor cell interactions with ECM. The research outlined here demonstrates the successful development of a novel culture system that better mimics these complex interactions between tumor cells and the host tissue microenvironment through the use of acellular liver ECM scaffolds. Future work will further characterize the molecular pathways involved in cell-matrix interactions, including those that occur in matrix stiffening, prior to manuscript submission.

Materials and Methods

Ferret Liver Harvest and Decellularization: Livers from ferrets age 5-6 weeks were harvested and decellularized according to the protocol described in Baptista *et al* (12). Briefly, the native liver tissue was harvested leaving the vascular network intact and the portal vein was cannulated for perfusion. Decellularization was carried out with perfusion of two liters of deionized water, followed by 4 liters of a 1% Triton X-100, 0.1% Ammonium Hydroxide solution and finally washed with 8 liters of deionized water, per liver.

Acellular Whole Organoid Experiments: Whole organoid experiments were performed by seeding HCT116 cells in the right lobe of intact acellular liver. Following decellularization, liver ECM scaffolds were prepared for each experiment by ligating and subsequently removing the left, caudate and quadratic lobes, all ligated with 4-0 silk black-braided suture (Ethicon, Summerville, NJ, USA). The remaining right lobe, cannulated via the portal vein with all the vascular structures intact, weighed between 3 and 4 grams in all experiments. The scaffold was sterilized prior to use with gamma irradiation. The scaffold was placed in a spinner flask in 250 ml of media and portal vein perfusion was carried out with a peristaltic pump and pulse dampener (Cole-Parmer Instrument Company, Vernon Hills, IL, USA). Cell seeding was performed by injecting 25 million HCT116 cells into the spinner flask in 4 batches 4 hours apart, for a total cell number of 100 million cells. The day following cell seeding, media was changed and the organoids were perfused with media for 1 (n=4) or 7 (n=4) days. In experiments lasting 7 days, media was changed every 2-3 days. At experiment termination, the organoids were fixed with 10% NBF via perfusion overnight and prepared for histological analysis as described above.

Image Analysis: Image analysis of nodule growth in whole organoids was performed using ImageJ. H&E images were taken at 5x magnifications, with five images per section and three sections per scaffold. These images were then imported into ImageJ and the size of tumor nodules was quantified and averaged for each organoid. Cell proliferation was quantified in a custom Mathematica program (Wolfram Mathematica 8.0, Wolfram Research, Champaign, IL, USA). Fluorescent images were taken at 10x magnifications in 6 separate areas of the section, with two sections per bioreactor. The images were imported into Mathematica and thresholding was applied to the images to calculate the number of pixels the Ki-67 and DAPI stains occupied. The percentage of proliferating cells was quantified by dividing the Ki-67 by DAPI pixel values.

Acellular Disc Fabrication: Following decellularization, pieces of the acellular scaffolds were frozen in OCT and sectioned using a cryostat to 300 micron thickness. A 6mm biopsy punch was used to create the liver discs. The discs were then placed in a 96-well plate, washed with PBS to remove the excess OCT and sterilized with a dose of 1.5Mrad of gamma-radiation.

HCT116 Cell Culture: HCT116 cells were cultured in DMEM:F12 with 10% fetal bovine serum (FBS) and 1% Pen/Strep (Sigma Aldrich, St.Louis, MO). For disc experiments, 2,000 cells were seeded on dry liver discs in 100µl of media. Tissue culture plate (TCP) controls were performed by seeding the same number of cells in tissue culture treated 96 well plates (Corning Inc., Corning, NY). The day after seeding, media was changed and that time was deemed day 0 of experiments. Media was changed every 2 days after that.

Growth Rate Experiments: To analyze the growth rate of cells, cell viability assays were performed on the discs and TCP controls on days 1, 3, 5 and 7 of culture, with n=4 at each timepoint (Cell CellTiter-Glo® Luminescent Cell Viability Assay, Promega, Madison, WI). Images of TCP controls were taken at each timepoint.

Histological Analysis: At each timepoint, 3 discs were fixed in 10% neutral-buffered formalin, tissue processed and paraffin embedded for histological analysis. 5µm sections were taken and stained with hematoxylin and eosin (H&E). Cell proliferation was analyzed through immunofluorescence staining for Ki-67 (Cat#. ab15580, Abcam, Cambridge, MA, USA), followed by goat anti-rabbit Texas Red secondary antibody (Vector Labs, Burlingame, CA, USA) and the nuclei were counterstained with DAPI. Scaffolds were also stained with β-catenin (Invitrogen 71-2700, 1:100) and E-cadherin (E-cad, SantaCruz sc8426, 1:50) with donkey anti-rabbit 660 and donkey anti-mouse 568 secondaries (Life Technologies).

Real Time PCR: Total RNA was extracted from TCP cells, liver discs and organoids using Allprep DNA/RNA Mini Kit (Qiagen, Maryland, USA) with DNAse treatment. cDNA was synthesized from 500ng of total RNA using Superscript III First Strand Synthesis (Life Technologies, Carlsbad, CA, USA). RT-PCR was performed using Taqman Master Mix (Life Technologies, Carlsbad, CA, USA) with MMP-1, -2, -9, and -10 taqman probes with GAPDH housekeeping gene (Life Technologies). Expression of genes within a sample was normalized to GAPDH expression using the $2^{-\Delta Ct}$ method.

Matrix Stiffness Experiments: Acellular liver discs were crosslinked with 100mM and 400mM of EDS:NHS (1-Ethyl-3-(3-dimethylaminopropyl)carbodiimide, Proteochem) (N-

hydroxysuccinimide, Thermo Scientific) in 0.1M MES buffer (2-(N-Morpholino)ethanesulfonic Acid, M.W. 195.2, Calbiochem) (pH=6.0) overnight at 4℃ at 200RPM. Scaffolds were then washed for 24 hours with DI water followed by 48 hours of PBS and sterilized with gamma irradiation. Growth rate studies and histology were carried out as described above.

Rheological Testing: Mechanical properties of cylindrical pieces of uncrosslinked and crosslinked decellularized livers were characterized with rheological testing (Discovery HR2 Rheometer, TA Instruments). Samples were hydrated until right before testing and sandpaper was placed on the top and bottom surfaces to prevent slippage. A 12mm flat bottom geometry was used in this testing. The geometry was lowered to compress the sample to 10% compressive strain followed by 2 minutes of relaxation prior to testing. Frequency sweep testing, ranging from 0.01 to 20 Hz, was performed at a fixed strain of 0.1%, to ensure that the sample was being tested within the linear viscoelastic region. This technique works by applying a sinusoidal strain on the material, which for linearly viscoelastic materials, results in a sinusoidal stress response that is phase-shifted at an angle δ. The complex viscoelastic modulus, G*, is then defined as the ratio of stress to strain. This value can be broken in to two components, the storage modulus (G') representing the portion of the stress in phase with the strain and the loss modulus (G'') as the portion out of phase. G' represents the elastic modulus of the material, while G'' represents the viscosity. These values experimentally determined from G* and δ as:

$$G' = G^* cos\delta, \quad G'' = G^* sin\delta$$

The phase angle δ is often represented as its tangent (tanδ=G''/G') and represents the viscous damping of the material and is an indicator of the relative viscosity of a material.

Confocal Imaging: After liver ECM discs (of three different stiffnesses) were seeded with HCT116 cells and cultured for 5 days, discs were fixed with 10% NBF for 30 minutes and then stained with Alexa Fluor 594 Phalloidin (A12381, 1:40, Life Technologies) and DAPI (1:500). Intact scaffolds were then imaged using a confocal microscope (Leica Macroconfocal TCS LSI).

Results

Acellular Liver ECM Whole Organoid Perfusion Culture: H&E images of whole organoids cultured in the perfusion bioreactor revealed tumor nodule formation around vascular structures. Nodules were significantly larger after 7 days in the perfusion bioreactor compared to 1 day (Figure 1). Cellular proliferation was observed throughout the tumor nodules within the perfused acellular livers (data not shown). Significant increases in MMP-10 expression were observed after 1 ($p<0.01$) and 7 days ($p<0.05$) in cells cultured in acellular liver ECM within the perfusion bioreactor compared to tissue culture plastic (Figure 1). Increasing trends were observed for MMP-1, -2, and -9 at both timepoints (data not shown).

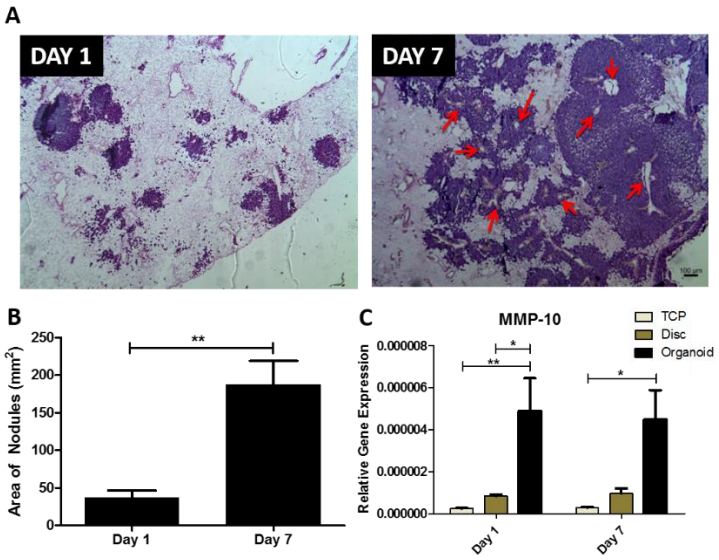

Figure 1: Metastatic growth of colon carcinoma cells in acellular liver organoid perfusion bioreactor. (A) H&E images of organoids after 1 and 7 days in perfusion bioreactors. Red arrows at day 7 indicated vascular structures which tumor nodules are forming around. (B) Image analysis quantification of the size of tumor nodules, which significantly increase from day 1 to 7 ($p<0.01$). (C) RT-PCR of MMP-10 gene expression, demonstrating significant upregulation in liver organoids compared to TCP at days 1 and 7 ($p<0.01$, $p<0.05$) and compared to liver discs at day 1 ($p<0.05$).

Acellular Liver ECM Discs: H&E images demonstrate cellular penetration of HCT116 cells into the acellular liver ECM discs after 7 days in culture with strong cell-cell and cell-matrix interactions (Figure 2). However, the morphology of the cell clusters was atypical of *in vivo* nodule formation. From image analysis, cells grown on liver ECM discs seemed to grow more slowly than cells grown on tissue culture plastic, but this difference was not significant in a cell proliferation analysis at day 5 (Figure 2). Quantification of cell proliferation found that 64% and 57% of cells were proliferating in the acellular discs after 1 and 7 days and no significant change in cell proliferation was observed between timepoints. After 1 day in culture, higher expression levels of MMP-1, -2, -9, and -10 were observed in the liver ECM discs compared to tissue culture plastic. After 7 days in culture,

there was significantly higher expression of MMP-1 and MMP-10 in the acellular discs compared to tissue culture plastic controls ($p<0.01$) and an increasing trend was observed for MMP-2 (Figure 3).

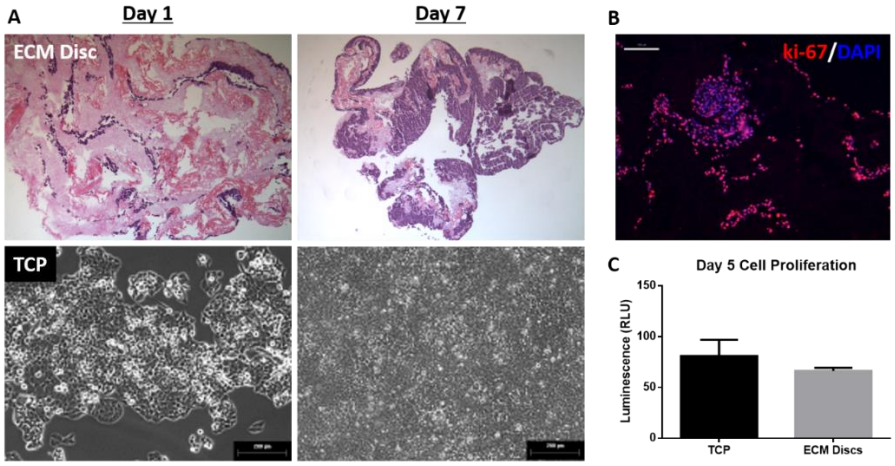

Figure 2: Growth rate evaluation of metastatic colon carcinoma cells in acellular liver discs versus tissue culture plastic (TCP). (A) H&E of ECM discs and brightfield images of cells grown on plastic at days 1 and 7. (B) Immunohistochemistry of ki-67+ cells grown on liver ECM discs for 7 days. (C) Cell proliferation, quantified by Cell Titer Glo Assay on TCP and ECM discs on day 5 of culture.

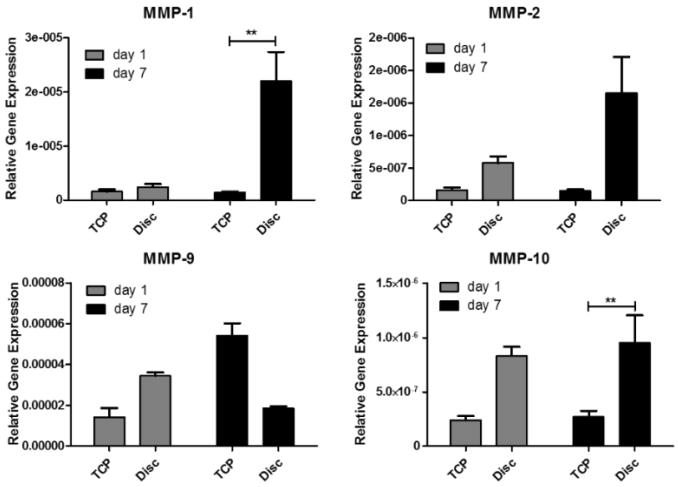

Figure 3: RT-PCR gene expression analysis of matrix metalloproteinase (MMP) markers in colon carcinoma cells seeded on liver ECM discs versus tissue culture plastic (TCP).

Effects of Matrix Stiffness on Colon Carcinoma Cells: Rheological testing of decellularized liver samples uncrosslinked, crosslinked with 100mM EDC:NHS and crosslinked with 400mM EDC:NHS resulted in average storage moduli (G') of 200, 600 and 1800 Pa respectively (Figure 4). We also analyzed the viscous dampening of the substrates and found that these were inversely related to storage moduli, indicating the samples are becoming less viscous with elastic stiffening (Figure 4).

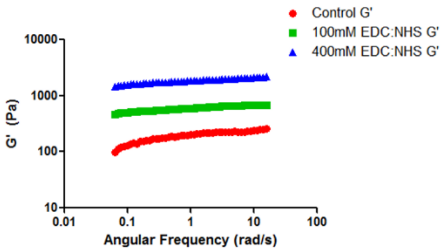

Sample	G' ± SD (Pa)
Uncrosslinked	194 ± 40.4
100mM EDC:NHS	596 ± 63.7
400mM EDC:NHS	1834 ± 189

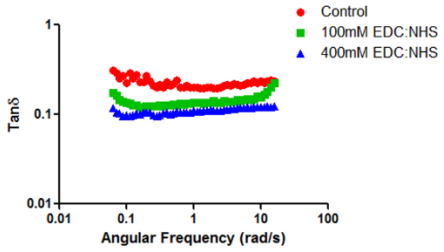

Sample	Tanδ ± SD
Uncrosslinked	.225 ± .028
100mM EDC:NHS	.141 ± .020
400mM EDC:NHS	.109 ± .008

Figure 4: Results of rheological testing of acellular liver ECM uncrosslinked or crosslinked with 100 or 400mM EDC:NHS. The top row shows storage moduli (G') results and the bottom row displays viscous dampening tanδ, which is equal to G''/G'.

Cell growth was not significantly affected by matrix stiffness after one week in culture, as quantified by cell proliferation assays (data not shown). However, the stiffness of the matrix influenced the pattern of cell growth on acellular liver ECM discs. On 200Pa substrates (softest matrix), the cells formed homogenous monolayers on the top of the discs, with little penetration into the ECM. As the scaffold got stiffer, cells began to form distinct nodules, rather than monolayers (Figure 5). Additionally, cell migration from nodules into the scaffold was observed. Immunohistochemistry staining revealed that cells

in stiffer discs were losing expression of E-cadherin (E-cad) and membrane-bound β-catenin (β-cat), indicating epithelial-to-mesenchymal transition (EMT). This transition was not observed in cells on the softest substrate (Figure 6).

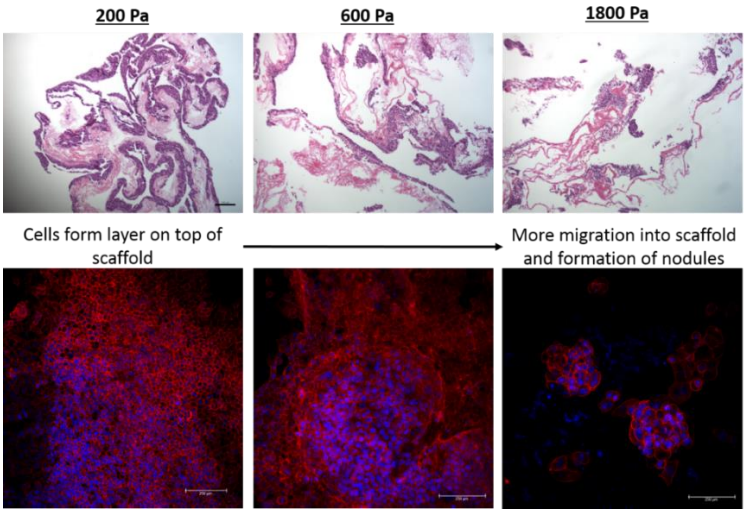

Figure 5: Effects of matrix stiffness on growth pattern of colon carcinoma cells on liver ECM discs. The top row is H&E images of scaffold after 7 days in culture and the bottom row are birds-eye view of liver discs stained with Phalloidin (red) and DAPI (blue) at each stiffness.

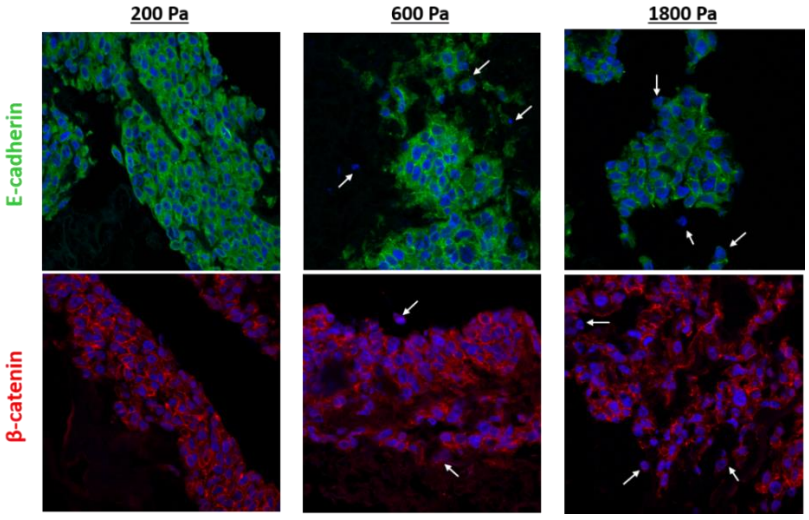

Figure 6: Effects of matrix stiffness on epithelial-to-mesenchymal transition (EMT). At 200Pa, all cells demonstrate membrane expression of E-cad (green) and β-cat (red). At higher G' values, there is evidence of cell migration, with loss of cell membrane expression of these markers (white arrows).

Discussion

Cancer metastasis is one of the most challenging areas in cancer research, partly because it is very difficult to study in a laboratory setting. Current *in vitro* systems used to study cancer metastasis frequently lack the proper tumor microenvironment and animal models often fail to recapitulate human cancer progressions. We have developed an *in vitro* model of colon cancer metastasis to the liver by seeding CRC cells in whole acellular liver organoids. The decellularized scaffolds retain the native liver tissue microenvironment, allowing tumor cell-ECM interactions that occur *in vivo* which are known to influence the fate of metastatic progression (7, 8). This model, in which whole organoids are re-seeded and cultured in a perfusion bioreactor, takes advantage of the retained acellular liver vascular system to enhance the growth of bioengineered livers (12). The liver vascular network is vitally important in colon cancer metastasis to the liver in two ways. First, it provides a route for colon carcinoma cells to travel to and invade the liver parenchyma and second, it perfuses the seeded tumor which may influence cell behavior. In these preliminary experiments, we seeded HCT116 cells through portal vein perfusion in an acellular liver whole organoid. Following cell seeding, the scaffold was continuously perfused at 6 ml/min for up to one week. H&E images of these organoids demonstrated nodular growth of tumor cells, with tumor nodules forming around the vascular structures. Likely, this organization results from the cells entering the parenchyma through the vascular network as well as these vessels being the entry point for media in the perfusion culture system. The size of the nodules, investigated by image analysis, significantly increases from 1 to 7 days, indicated continued tumor growth over that time period.

We have also successfully developed a high-throughput model of cancer metastasis using acellular liver ECM discs in a 96-well plate format seeded with HCT116 colon carcinoma cells. In these studies, we have demonstrated that culturing HCT116 cells on acellular liver discs significantly influences cell morphology and growth rate compared to cells grown on tissue culture plastic. Additionally, there was a significant up-regulation of certain matrix-metalloproteinases (MMPs) when cells are cultured on acellular liver ECM discs compared to tissue culture plastic, demonstrating the importance of ECM microarchitecture in re-capitulating *in vivo* tumor behavior. MMP expression in discs was also compared to whole organoids cultured in perfusion bioreactors. Expression of MMP-10 was significantly higher in whole organoids compared to the two other culture systems, perhaps resulting from increased perfusion. However, expression levels of MMP-1, -2, and -9 had similar levels to the discs which may indicate that ECM composition may play a larger role in MMP secretion compared to the effects of perfusion.

Another distinct advantage of the acellular liver ECM model in studying cancer metastasis is the potential for answering targeted research questions addressing the influence of certain microenvironmental parameters on metastatic progression. One of these biophysical parameters is the stiffness of the underlying ECM, an important *in vivo* influencer of tumor cell behavior (13, 14). We successfully created acellular liver ECM discs with storage moduli (G') ranging from 200-1800 Pa by crosslinking the scaffolds with EDC:NHS. We found that scaffold stiffness significantly affects the patterns in which the cells grow on the scaffold. In softer substrates, the cells form a monolayer on top of the scaffold, with little observations of cell migration. However, on stiffer substrates, the HCT116 cells tend to form nodular cell clusters with increased occurrences of individual

cell migration. This migration was accompanied by decreases in expression of membrane bound E-cad and β-catenin, indicating the cells are going through epithelial-to-mesenchymal transitions (EMT) on the stiffer substrates. Future studies will aim to elucidate the molecular pathways involved in mechanotransduction and matrix migration through PCR analysis. We will also perform control experiments modifying substrate stiffness without changing microarchitecture (such as porosity) to isolate the effects of stiffness alone.

Conclusions

In conclusion, we have developed a model of colon cancer metastasis using acellular liver ECM scaffolds. We demonstrated the ability to model colon cancer metastasis to the liver using an acellular liver ECM whole organoid cultured in a perfusion bioreactor. This system allows us to study the influence of the vascular network in tumor behavior in both cell deposition and perfusion. Processing the decellularized liver into disc shapes allows us to culture tumor cells in a high-throughput 96-well platform that demonstrates significant advantages over standard cell culture models, including better tumor growth and morphology and increased MMP expression levels. The liver ECM disc model also has the distinct advantage of being capable of studying microenvironmental perturbations in a systematic and repeatable manner, a capability lacking in animal models. In the studies outlined in this manuscript, we developed a model investigating the effects of matrix mechanics on tumor cells by crosslinking our acellular scaffolds to an array of stiffnesses. Our model can also be adapted to study other biophysical parameters, such as

ECM composition and arrangement, as well as chemical and biological factors, including the effects of hypoxia, pH, cytokines and ECM peptides. Future studies will engineer organoids with both cancer cells and healthy liver cells to investigate cancer-host cell interactions. This model has the potential to be a valuable tool in not only elucidating mechanisms involved in metastatic tumor progression but also driving the development of new therapies and treatments.

References

1. Siegel R, Jemal A. Colorectal Cancer Facts & Figures 2014-2016. Atlanta: American Cancer Society, 2014.
2. Manfredi S, Lepage C, Hatem C, Coatmeur O, Faivre J, Bouvier AM. Epidemiology and management of liver metastases from colorectal cancer. Annals of Surgery. 2006 Aug;244(2):254-9. PubMed PMID: WOS:000239358700012.
3. Chambers AF, Groom AC, MacDonald IC. Dissemination and growth of cancer cells in metastatic sites. Nature Reviews Cancer. 2002 Aug;2(8):563-72. PubMed PMID: WOS:000180447300010. English.
4. Gupta GP, Massague J. Cancer metastasis: Building a framework. Cell. 2006 Nov;127(4):679-95. PubMed PMID: WOS:000242330600016.
5. Nguyen DX, Bos PD, Massague J. Metastasis: from dissemination to organ-specific colonization. Nature Reviews Cancer. 2009 Apr;9(4):274-U65. PubMed PMID: WOS:000264500800012. English.
6. Auguste P, Fallavollita L, Wang N, Burnier J, Bikfalvi A, Brodt P. The host inflammatory response promotes liver metastasis by increasing tumor cell arrest and extravasation. American Journal of Pathology. 2007 May;170(5):1781-92. PubMed PMID: WOS:000246050400032. English.
7. Fidler IJ, Kim SI, Langley RR. The role of the organ microenvironment in the biology and therapy of cancer metastasis. Journal of Cellular Biochemistry. 2007 Jul;101(4):927-36. PubMed PMID: WOS:000247694600012. English.
8. Langley RR, Fidler IJ. Tumor cell-organ microenvironment interactions in the pathogenesis of cancer metastasis. Endocrine Reviews. 2007 May;28(3):297-321. PubMed PMID: WOS:000246358600003. English.
9. de Jong GM, Aarts F, Hendriks T, Boerman OC, Bleichrodt RP. Animal Models for Liver Metastases of Colorectal Cancer: Research Review of Preclinical Studies in Rodents. Journal of Surgical Research. 2009 Jun;154(1):167-76. PubMed PMID: WOS:000266080000025.
10. Yates C, Shepard CR, Papworth G, Dash A, Stolz DB, Tannenbaum S, et al. Novel three-dimensional organotypic liver bioreactor to directly visualize early events in metastatic progression. In: VandeWoude GF, Klein G, editors. Advances in Cancer Research, Vol 97. Advances in Cancer Research. 97. San Diego: Elsevier Academic Press Inc; 2007. p. 225-+.

11. Kim JY, Fluri DA, Marchan R, Boonen K, Mohanty S, Singh P, et al. 3D spherical microtissues and microfluidic technology for multi-tissue experiments and analysis. J Biotechnol. 2015 Jan. PubMed PMID: 25592049. ENG.
12. Baptista PM, Siddiqui MM, Lozier G, Rodriguez SR, Atala A, Soker S. The use of whole organ decellularization for the generation of a vascularized liver organoid. Hepatology. 2011 Feb;53(2):604-17. PubMed PMID: 21274881. eng.
13. Wirtz D, Konstantopoulos K, Searson PC. The physics of cancer: the role of physical interactions and mechanical forces in metastasis. Nature Reviews Cancer. 2011 Jul;11(7):512-22. PubMed PMID: WOS:000292028300016.
14. Chaudhuri O, Koshy ST, da Cunha CB, Shin JW, Verbeke CS, Allison KH, et al. Extracellular matrix stiffness and composition jointly regulate the induction of malignant phenotypes in mammary epithelium. Nature Materials. 2014 Oct;13(10):970-8. PubMed PMID: WOS:000342743100018.

CHAPTER VI

CONCLUSIONS

Emma C. Moran

The field of liver bioengineering arose due to the shortage of available donor organs for liver transplantation, the only long-term treatment option for many liver diseases (1). However, the applications for bioengineered livers have extended far beyond engineering organs for transplantation. Bioengineered livers can serve as valuable models to study tissue development, various states of disease, cancer growth and metastasis and drug toxicity (2-5). Our lab, as well as others, has engineered whole livers using the technique of decellularization and recellularization, which removes all of the cellular components of the donor liver but retains the vascular network, extracellular matrix proteins and tissue micro-architecture (6-9). The resulting engineered scaffold can be re-populated with both hepatic and non-hepatic cells types which behave more physiologically due to retention of the three dimensional microenvironment than they would in standard *in vitro* culture models (10). A key component of *in vivo* tissue microenvironments are the mechanical forces that cells experience, including the stiffness of the underlying matrix and the stresses exerted by fluid flow.

This thesis examines the influence of mechanical forces in various applications and models of liver tissue engineering. The first component of this thesis, Chapter 3, evaluates the effects of the decellularization process on liver tissue mechanics. Although the extracellular matrix is retained in the acellular scaffolds, there are other factors that may influence the stresses experienced by re-seeded cells, such as the interaction between solid and fluid components of the liver and the loss of cell-cell and cell-matrix interactions impacting overall tissue mechanics. These studies laid the groundwork for the subsequent development of acellular scaffold models and provided insight into the interpretation of findings. Chapter 4 details the development of the first acellular scaffold model

investigating the impact of fluidic forces on aspects of liver tissue development and regeneration in bioengineered livers created using a perfusion bioreactor system. Whole organ perfusion bioreactors are commonly used in liver tissue engineering, but the effects of fluid flow in terms of shear stresses and parenchymal fluid pressure are not well understood. Next, another acellular scaffold model was developed to study cancer metastasis and elucidate the role of biomechanical factors in tumor invasion, which is detailed in Chapter 5. Finally, preliminary work outlined in the appendix researches the impact of matrix mechanics and fluidic shear stress on liver progenitor cells.

The three manuscripts in Chapter 3 concluded that tissue decellularization has a significant effect on the biomechanical properties of liver tissue. One of the main influencers of mechanical property changes following decellularization is the large increase in scaffold permeability, or the ease at which fluid flows through the solid ECM matrix. This finding is not surprising due to the complete removal of cellular components, which in normal tissue act as barriers to flow, decreasing the porosity of the tissue. The increased permeability in acellular tissue effects the parenchymal fluid pressure (PFP), or hydrostatic pressure force, within the scaffold. It was found that PFP was significantly lower in decellularized versus native tissue when perfused at the same flow rate (11). These experiments were able to determine the range of flow rates (~6-9ml/min) when perfusing decellularized liver that corresponds to *in vivo* PFP measurements. These flow rates were used in perfusion bioreactors experiments that engineered liver tissue to evaluate the impacts of fluid flow on tissue organization (Chapter 4) and formation of tumor nodules (Chapter 5). These findings are significant because it is important to deliver the correct mechanical cues to cells when engineering tissue so that the cells behave as they would *in*

vivo. PFP is known to impact hepatocyte viability (12) and may influence the behavior of other liver cell types due to evidence that elevated PFP in small-for-size liver transplantations can have detrimental effects (13, 14). We found that delivery of extremely high PFP (40ml/min perfusion rate) led to significant increases in cell death and sub-optimal perfusion (3ml/min) led to decreases in cell proliferation and organization (Chapter 4), confirming the need for PFP and flow rate optimization.

Cells seeded and perfused in acellular liver scaffolds will also experience different levels of shear stress than they would *in vivo*, due to the increased permeability of the scaffold and the lack of a completely endothelialized vasculature which *in vivo* shields parenchymal cells from large shear stress magnitudes. However, actual shear stress values are very difficult to quantify due to the inherent complexity of the liver vascular network. After decellularization, the vascular structures become much more permeable, leading to complex fluid flow patterns within the scaffold parenchyma. Therefore, cells residing within this space would experience a wide range of shear stress. Results from Chapter 4 demonstrate that changes in scaffold perfusion rate can lead to large differences in cell seeding, tissue growth, proliferation, death and organization due to changing fluid flow forces. Currently, the only way of optimizing this fluidic mechanical environment is through experimental techniques. Future studies integrating the liver vascular network with the poroviscoelastic finite element models developed in Chapters 3.2 and 3.3 would greatly aid our understanding of fluid flow within acellular liver scaffolds and may lead to modelling optimization of bioreactor conditions. An alternative approach would be to use experimental imaging techniques, such as ultrasound or particle image velocimetry (PIV),

to quantitatively determine fluid flow direction and velocity within acellular scaffolds (15, 16).

Perfusion also greatly impacts tumor cell growth in our bioengineered liver model of colon cancer metastasis, described in Chapter 5. Whole acellular organoids seeded with colon carcinoma cells developed parenchymal tumor nodules around the scaffold vasculature, greatly resembling physiological tumor formation. However, when cells were seeded on discs of acellular liver ECM, without perfusion, there was cell growth but no nodule formation. There is an abundance of evidence that perfusion impacts tumor cell behavior, both in metastasizing cells traveling to distant sites and perfusion of tumors once the cells have seeded in the tissue parenchyma (17, 18). Therefore, providing the proper fluidic environment in terms of shear stress and PFP allows us to better mimic *in vivo* tumor growth and may allow us to study the impact of various fluidic forces on tumor cell behavior.

Aside from changes in the permeability and perfusion of acellular liver tissue, the decellularization process was also found to reduce the stiffness of the tissue (results detailed in Chapter 3.3). This finding is significant because it signifies that cells seeded on acellular scaffolds experience different tensile forces than they experience physiologically, which may impact cell behavior (19-21). We have developed an experimental model to study the effects of substrate stiffness by crosslinking acellular liver scaffolds with various concentrations of EDC:NHS to create liver ECM scaffolds with storage moduli of 200 (uncrosslinked), 600 and 1800Pa. Future experiments will test native healthy and fibrotic liver tissue using the same rheological protocol followed above so that we can directly match *in vitro* moduli to *in vivo* conditions. It is expected that native liver will fall in the

~600Pa range, based on our findings from Chapter 3.3 and fibrotic liver can reach up to five times the stiffness of healthy tissue (22). Experiments detailed in Chapter 5 found that colon carcinoma cells organize differently based on the mechanical properties of the substrate. Cells formed a uniform monolayer on the softest substrate and became progressively more nodular as stiffness increased. Additionally, we saw evidence of epithelial-to-mesenchymal transition (EMT), a critical process in metastatic progression, in cells cultured on stiffer substrates. Future studies will aim to determine the mechanisms by which cancer cells sense matrix stiffness and further characterize the effects that these mechanical modifications have on cells. It is hypothesized that crosslinking the ECM to the value of native liver tissue will better reproduce physiological cell behavior and tumor progression than decellularized ECM. We will also be able to assess how further increases in stiffness, a hallmark of many cancers, impacts tumor growth and treatment strategies (23-25).

Although we have discovered that decellularization changes the biomechanical properties of liver tissue, the ramifications of these changes on many cell types are not fully known. One such cell type are human liver progenitor cells, which are used in liver tissue engineering approaches due to their ability to differentiate into both hepatocytes and cholangiocytes. The appendix of this thesis describes preliminary experiments investigating the impact of matrix stiffness and fluid shear stress on the behavior of this cell population. Fully understanding the influence of these biomechanical forces on liver progenitor cell behavior may allow us to tune the mechanical microenvironment within our bioengineering process to optimize cell growth, function and differentiation. Preliminary results indicate that these cells sense and respond to changes in matrix stiffness and fluid

shear stress. Future experiments will focus on determining the specific cellular reactions to these stresses, especially cell differentiation, and elucidating the mechanisms involved in these processes.

Tissue biomechanics are vital to how cells behave in health and disease. Therefore, understanding and characterizing the mechanical environment cells experience in *in vitro* systems, such as bioengineered liver tissue, is crucial in attaining physiological cell behavior and function. The model system used in this thesis uses acellular liver scaffolds, which retain native ECM while removing all cellular components. This process impacts both fluid and solid characteristics of the material, including increasing permeability and lowering matrix stiffness. The impact of biomechanical forces and changes that occur with tissue decellularization was investigated in subsequent chapters which developed bioengineered liver models to study liver tissue growth and organization and cancer metastasis. In summary, understanding and manipulating the mechanical micro-environment can greatly enhance the development of bioengineered liver models to study tissue development, disease, cancer and drug toxicity.

References

1. Zakim D, Boyer T. Hepatology A Textbook of Liver Disease. Fourth Edition ed. Philadelphia, Pennsylvania: Elsevier Science; 2003.
2. Griffith LG, Wells A, Stolz DB. Engineering Liver. Hepatology. 2014 Oct;60(4):1426-34. PubMed PMID: WOS:000342662100034.
3. Bhatia SN, Underhill GH, Zaret KS, Fox IJ. Cell and tissue engineering for liver disease. Science Translational Medicine. 2014 Jul;6(245). PubMed PMID: WOS:000339661200002.
4. Khetani SR, Bhatia SN. Microscale culture of human liver cells for drug development. Nature Biotechnology. 2008 Jan;26(1):120-6. PubMed PMID: WOS:000252222500032. English.

5. Moran EC, Gaston B, Baptista PM, Atala A, Soker S. Acellular Liver Scaffolds as a Model to Study Colon Cancer Metastasis. Tissue Engineering Part A. 2014 Dec;20:S28-S9. PubMed PMID: WOS:000345684300104.
6. Baptista PM, Siddiqui MM, Lozier G, Rodriguez SR, Atala A, Soker S. The use of whole organ decellularization for the generation of a vascularized liver organoid. Hepatology. 2011 Feb;53(2):604-17. PubMed PMID: 21274881. eng.
7. Uygun BE, Soto-Gutierrez A, Yagi H, Izamis ML, Guzzardi MA, Shulman C, et al. Organ reengineering through development of a transplantable recellularized liver graft using decellularized liver matrix. Nature Medicine. 2010 Jul;16(7):814-U120. PubMed PMID: WOS:000279631900033.
8. Soto-Gutierrez A, Zhang L, Medberry C, Fukumitsu K, Faulk D, Jiang H, et al. A Whole-Organ Regenerative Medicine Approach for Liver Replacement. Tissue Engineering Part C-Methods. 2011 Jun;17(6):677-86. PubMed PMID: WOS:000291202200007.
9. Shupe T, Williams M, Brown A, Willenberg B, Petersen BE. Method for the decellularization of intact rat liver. Organogenesis. 2010 Apr-Jun;6(2):134-6. PubMed PMID: WOS:000290262200009.
10. Griffith LG, Swartz MA. Capturing complex 3D tissue physiology in vitro. Nature Reviews Molecular Cell Biology. 2006 Mar;7(3):211-24. PubMed PMID: WOS:000235590500016. English.
11. Moran EC, Baptista PM, Evans DW, Soker S, Sparks JL. Evaluation of parenchymal fluid pressure in native and decellularized liver tissue. Biomed Sci Instrum. 2012;48:303-9. PubMed PMID: 22846298. Epub 2012/08/01. eng.
12. Hsu WM, Carraro A, Kulig KM, Miller ML, Kaazempur-Mofrad M, Weinberg E, et al. Liver-assist device with a microfluidics-based vascular bed in an animal model. Ann Surg. 2010 Aug;252(2):351-7. PubMed PMID: 20647924. eng.
13. Dahm F, Georgiev P, Clavien PA. Small-for-size syndrome after partial liver transplantation: Definition, mechanisms of disease and clinical implications. American Journal of Transplantation. 2005 Nov;5(11):2605-10. PubMed PMID: WOS:000232393000004.
14. Yagi S, Uemoto S. Small-for-size syndrome in living donor liver transplantation. Hepatobiliary & Pancreatic Diseases International. 2012 Dec 15;11(6):570-6. PubMed PMID: WOS:000312170400001.
15. Gessner RC, Hanson AD, Feingold S, Cashion AT, Corcimaru A, Wu BT, et al. Functional ultrasound imaging for assessment of extracellular matrix scaffolds used for liver organoid formation. Biomaterials. 2013 Dec;34(37):9341-51. PubMed PMID: WOS:000326901200011.
16. Antoine E, Buchanan C, Fezzaa K, Lee WK, Rylander MN, Vlachos P. Flow Measurements in a Blood-Perfused Collagen Vessel Using X-Ray Micro-Particle Image Velocimetry. Plos One. 2013 Nov;8(11). PubMed PMID: WOS:000327308500200.
17. Gupta GP, Massague J. Cancer metastasis: Building a framework. Cell. 2006 Nov;127(4):679-95. PubMed PMID: WOS:000242330600016.
18. Yates C, Shepard CR, Papworth G, Dash A, Stolz DB, Tannenbaum S, et al. Novel three-dimensional organotypic liver bioreactor to directly visualize early events in metastatic progression. In: VandeWoude GF, Klein G, editors. Advances in Cancer Research, Vol 97. Advances in Cancer Research. 97. San Diego: Elsevier Academic Press Inc; 2007. p. 225-+.
19. Engler AJ, Sen S, Sweeney HL, Discher DE. Matrix elasticity directs stem cell lineage specification. Cell. 2006 Aug 25;126(4). PubMed PMID: WOS:000240276700017.
20. Discher DE, Janmey P, Wang YL. Tissue cells feel and respond to the stiffness of their substrate. Science. 2005 Nov 18;310(5751). PubMed PMID: WOS:000233437300033.
21. Mammoto A, Mammoto T, Ingber DE. Mechanosensitive mechanisms in transcriptional regulation. Journal of Cell Science. 2012 Jul;125(13):3061-73. PubMed PMID: WOS:000308417300005.

22. Yin M, Woollard J, Wang XF, Torres VE, Harris PC, Ward CJ, et al. Quantitative assessment of hepatic fibrosis in an animal model with magnetic resonance elastography. Magnetic Resonance in Medicine. 2007 Aug;58(2):346-53. PubMed PMID: WOS:000248488300017. English.
23. Lu P, Weaver VM, Werb Z. The extracellular matrix: a dynamic niche in cancer progression. J Cell Biol. 2012 Feb;196(4):395-406. PubMed PMID: 22351925. PMCID: PMC3283993. eng.
24. Butcher DT, Alliston T, Weaver VM. A tense situation: forcing tumour progression. Nat Rev Cancer. 2009 Feb;9(2):108-22. PubMed PMID: 19165226. PMCID: PMC2649117. eng.
25. Wirtz D, Konstantopoulos K, Searson PC. The physics of cancer: the role of physical interactions and mechanical forces in metastasis. Nature Reviews Cancer. 2011 Jul;11(7):512-22. PubMed PMID: WOS:000292028300016.

Appendix A

Investigation of the Influence of Matrix Stiffness and Shear Stress on Liver Cell Behavior and Differentiation

Overview

Cell behavior is highly dependent on the surrounding microenvironment, including factors that exert biomechanical forces on the cell such as the stiffness of the surrounding tissue and the stresses exerted by fluid flow. However, the precise mechanisms by which many cells, especially those within the liver, detect and respond to mechanical cues are still unclear. One such cell type are liver progenitor cells, which are often used in liver bioengineering approaches. If provided the correct environment these cells will differentiate into mature liver cells, hepatocytes and cholangiocytes, in a manner similar to that which occurs during liver organogenesis and regeneration. However, the role of mechanical forces in liver progenitor cell behavior, including growth, migration, apoptosis and differentiation, are less well understood.

The research studies described in this appendix are preliminary experiments investigating liver progenitor cell response to matrix stiffness and external shear stress. The aim of these studies is to elucidate the role of mechanical forces in liver cell behavior in development, homeostasis and diseases such as liver fibrosis and cancer. Fully understanding how cells sense and respond to these forces is also vital in creating engineered tissues that properly mimic their *in vivo* counterpart.

Appendix A1: Effects of Matrix Stiffness on Liver Progenitor Cells

A1. Introduction

It is known that matrix stiffness is a significant factor in the behavior of multiple liver cell types, including hepatocytes (27-29), portal fibroblasts (30) and hepatic stellate cells (31-34). Matrix stiffness also plays a vital role in stem cell differentiation and has recently been found to impact the behavior of hepatic stem cells (9, 10). Due to importance of substrate mechanical properties in liver and stem cell populations, we aimed to investigate the role of matrix stiffness in the growth, differentiation, and overall behavior of human fetal liver cells. This cell population includes liver progenitor cells (hepatoblasts) capable of differentiating into hepatocytes and cholangiocytes as well as stromal support cells, including fibroblasts, stellate cells, endothelial cells and Kupffer cells. Experiments were performed by altering the stiffness of acellular liver extracellular matrix through EDC:NHS crosslinking and seeding various populations of human fetal liver cells. Characterization of these liver organoid constructs was completed using cell growth analysis, immunohistochemistry and PCR analyzing cell differentiation and cell phenotype markers. Preliminary results from these studies indicates that matrix stiffness effects each liver cell population differently and may influence the behavior and differentiation of hepatoblast cells.

A1. Methods

Human fetal liver cell culture: Human fetal liver cells (hflcs) are isolated from fetal liver gestational age 18-21 weeks and cultured according to the protocol in Schmeltzer *et al.*(35).

The isolation protocol contains a density gradient separation in which the lower fraction contains mostly liver stem and progenitor cells (dictated as hflc) and the upper fraction contains stromal support cells, which includes stellate, Kupffer, mesenchymal and endothelial cells and fibroblasts. It is important to note that there are some stromal cells in the lower fraction of cells that are seeded alongside the stem and progenitor cell population in disc experiments. Hflc cells were cultured in Kubota media (Pheonix Biosongs, Chapel Hill, NC) on plates coated with collagen IV (5µg/cm^2) and laminin (1µg/cm^2). Stromal cells are cultured on tissue culture treated plates with DMEM:F12 with 10% fetal bovine serum (FBS) and 1% Pen/Strep (Sigma Aldrich, St. Louis, MO).

Acellular liver discs fabrication: Acellular liver discs were prepared by freezing pieces of decellularized liver matrix in OCT and sectioning to 300µm thickness using a cryostat. An 8mm biopsy punch was used to create discs that fit in 48-well plates. Details of decellularization and disc fabrication can be found in chapters 4 and 5.

Matrix stiffness experiments: Acellular liver discs were crosslinked with 100mM and 400mM of EDS:NHS (1-Ethyl-3-(3-dimethylaminopropyl)carbodiimide, Proteochem) (N-hydroxysuccinimide, Thermo Scientific) in 0.1M MES buffer (2-(N-Morpholino)ethanesulfonic Acid, M.W. 195.2, Calbiochem) (pH=6.0) overnight at 4℃ at 200RPM. This resulted in scaffolds with storage moduli (G') of 200 Pa (uncrosslinked), 600 Pa (100mM EDC:NHS) and 1800 Pa (400mM EDC:NHS), characterized by rheology. Details of crosslinking and rheological tests can be found in Chapter 5. Following crosslinking, scaffolds were washed for 24 hours with DI water followed by 48 hours of PBS and sterilized with gamma irradiation.

Cell seeding: Experiments were carried out by seeding 250,000 lower fraction hflc on liver discs and culturing the cells in differentiation media containing Advanced RPMI 1640, 10mg/ml ascorbic acid, 10^{-7}M dexamethasone, 2.45mg/L cyclic-AMP, 1µg/L human prolactin, 1mg/L human glucagon, 40µg/L human epidermal growth factor (EGF), 5mM niacinamide, 0.67µg/L Tri-iodothyronine, 0.105mg/L alpha-lipoic acid, 0.056µg/L (D-Ala2, D-Leu5)-Enkephalin Acetate, 20µg/L hepatocyte growth factor (HGF), 76µl/L free fatty acid mixture, 3.33µg/L hepatocyte growth hormone (HGH), 10mg/L high-density lipoprotein (HDL) and 10µg/L oncostatin M. Stromal cell control experiments were carried out by seeding 65,000 upper fraction stromal cells on the discs with DMEM:F12 10%FBS. Discs with lower fraction hflc were cultured for three weeks with media change every 3 days. Discs with upper fraction stromal cells were cultured for one week with cell viability assay performed on day 7 to analyze stromal cell growth (Cell CellTiter-Glo® Luminescent Cell Viability Assay, Promega, Madison, WI). N=4 discs were analyzed in each condition.

Real-time PCR: Total RNA was extracted from liver discs using Allprep DNA/RNA Mini Kit (Qiagen, Maryland, USA) with DNAse treatment. cDNA was synthesized from 500ng of total RNA using Superscript III First Strand Synthesis (Life Technologies, Carlsbad, CA, USA). RT-PCR was performed using Power SYBR® Green Master Mix (Life Technologies, Carlsbad, CA, USA) using custom primers for alpha feto-protein (AFP), albumin (ALB), E-cadherin (E-cad), gluco 6-phosphate (G6P), hepatocyte nuclear factor 1β (HNF1β), hepatocyte nuclear factor 4α (HNF4α) and hepatocyte nuclear factor 6 (HNF6). Expression of genes within a sample was normalized to GAPDH expression using the $2^{-\Delta Ct}$ method.

Histological Analysis: After 3 weeks in culture, 3 discs of each stiffness were fixed in 10% neutral-buffered formalin, tissue processed and paraffin embedded for histological analysis. 5µm sections were taken and stained with hematoxylin and eosin (H&E). Immunohistochemistry was performed using primary antibodies α-smooth muscle actin (α-SMA, Abcam ab5684, 1:200), cytokeratin-18 (CK-18, Novocastra NCL-CK18, 1:100), cytokeratin-19 (CK-19, Novocastra, NCL-CK19, 1:100), Epithelial Cell Adhesion Molecule (EpCAM, Abcam ab124825, 1:200), β-catenin (Invitrogen 71-2700, 1:100), E-cadherin (E-cad, SantaCruz sc8426, 1:50) and secondary antibodies donkey anti-rabbit, anti-goat and anti-mouse Alexa Fluor 568 and 660 (Life Technologies). Nuclei were counterstained with DAPI. Confocal imaging was performed on an Olympus Fluoview FV10i microscope.

A1. Results

Cell Growth Kinetics: After 3 weeks in culture, there are significant differences in the amount of human fetal liver cells on discs in the three stiffness conditions. Uncrosslinked discs (200Pa) had the highest number of cells, quantified by DNA, and the 1800Pa discs had the fewest amount of cells (Figure 1). These results can be visualized by analyzing H&E images of discs (Figure 2). Next, we wanted to investigate which of the cell populations was being affected by the modified mechanical properties. Immunohistochemistry indicated that the stiffer discs had fewer stromal cells compared to the softer scaffolds by analyzing alpha-smooth muscle actin (α-SMA, marker for stromal cells) and cytokeratin-18 (CK-18, marker for liver epithelial cells) (Figure 3). In order to confirm this hypothesis that stiffer substrates inhibit the growth of the liver stromal cell

population, only stromal cells were seeded on the discs and cell proliferation assays were performed on day 7. Stromal cell proliferation was found to decrease with increases in scaffold stiffness, with a significant difference in proliferation between 200Pa and 1800Pa discs (Figure 1).

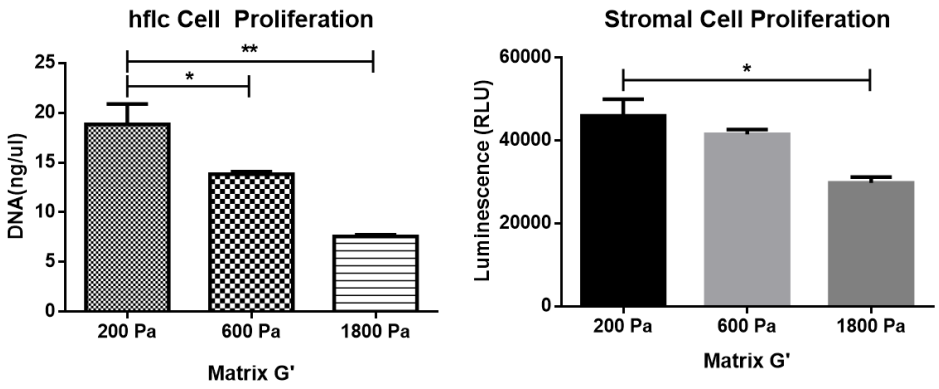

Figure 1: Left: Quantification of DNA in discs with seeded with human fetal liver cells (hflc) after 3 weeks in culture. 200Pa discs had significantly higher amounts of DNA than 600Pa ($p<0.05$) and 1800Pa discs ($p<0.01$). Right: Cell proliferation assay, measured by luminescence, of stromal cells seeded on liver discs after 1 week of culture. 200Pa discs had significantly higher levels of proliferation compared to 1800Pa ($p<0.01$).

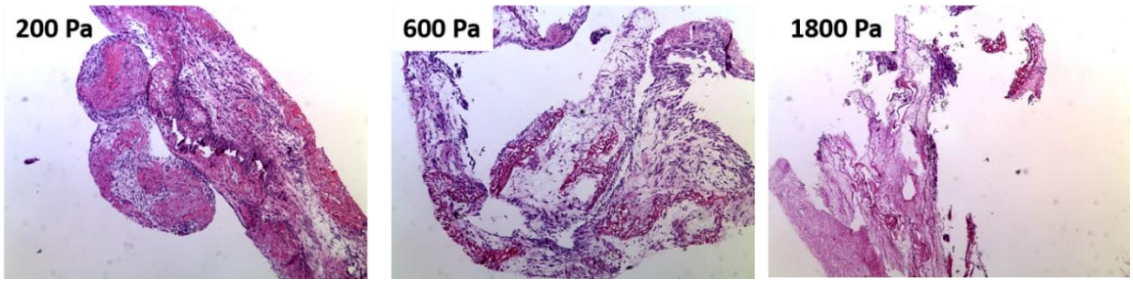

Figure 2: H&E images of hflc seeded on liver ECM discs after 3 weeks of culture, demonstrating that cell number decreases with increasing matrix stiffness.

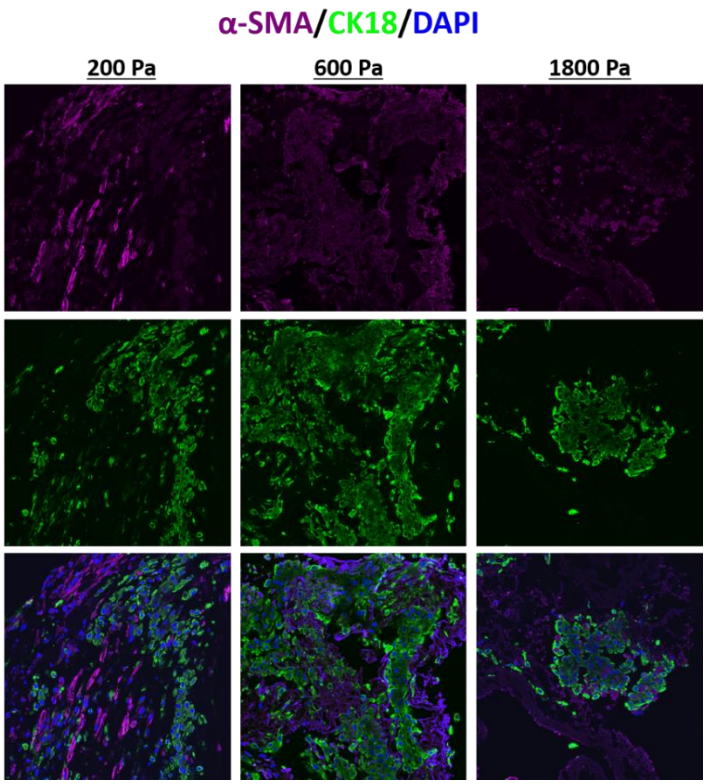

Figure 3: Immunohistochemistry of hflc seeded liver discs after 3 weeks in culture. The largest number of α-SMA+ stromal cells is observed in the 200Pa scaffold. CK18+ epithelial cells are present in all scaffolds. Nuclei were counterstained with DAPI.

Cell Phenotype: As described above, the stiffer discs consisted of mostly liver epithelial cells, while the softer discs had a mix of stromal and epithelial cell populations. We wanted to investigate whether this difference in the softer discs was due to growth of the original stromal cell population, or if the liver epithelial cells (hepatoblasts and mature hepatocytes and cholangiocytes) were de-differentiating into stromal cells. Discs with a stiffness of 600Pa (middle condition) showed a reduction in E-cadherin in epithelial populations, indicative of EMT. Additionally, we observed colonies of cells that co-expressed α-SMA and CK-18 with mesenchymal cell morphology, indicative of epithelial cell de-differentiation (Figure 4). This was not observed in the 200 Pa discs, where there were

epithelial cell colonies surrounded by stromal cells, or in the 1800 Pa discs, which consisted of mostly epithelial cells.

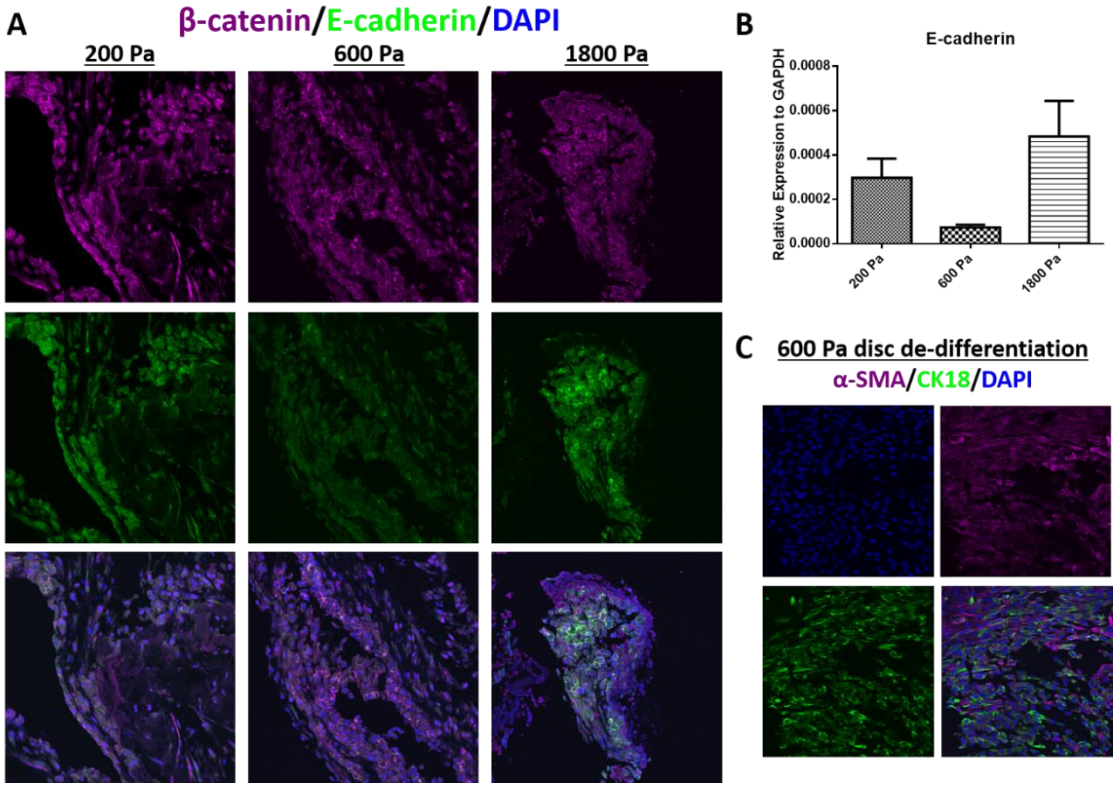

Figure 4: EMT and de-differentiation evidence in 600 Pa disc. (A,B): There were reduced levels of E-cad+ cells in 600Pa discs, analyzed with histology and RT-PCR. (C) Also observed in discs of this condition were areas of cell de-differentiation, with co-localization of CK-18 and α-SMA on cells with mesenchymal phenotypes.

Cell Differentiation: Quantitative PCR analysis was used to analyze hepatoblast differentiation towards hepatocytes and cholangiocytes in discs seeded with hflc after 3 weeks in culture. Hepatocyte markers albumin (ALB), HNF4α, and G6P were significantly higher in the stiffest discs, with storage moduli of 1800Pa, compared to the other two conditions ($p<0.01$). However, these results may be skewed due to decreased levels of stromal cell proliferation in these discs (Figure 1), so further analysis must be completed.

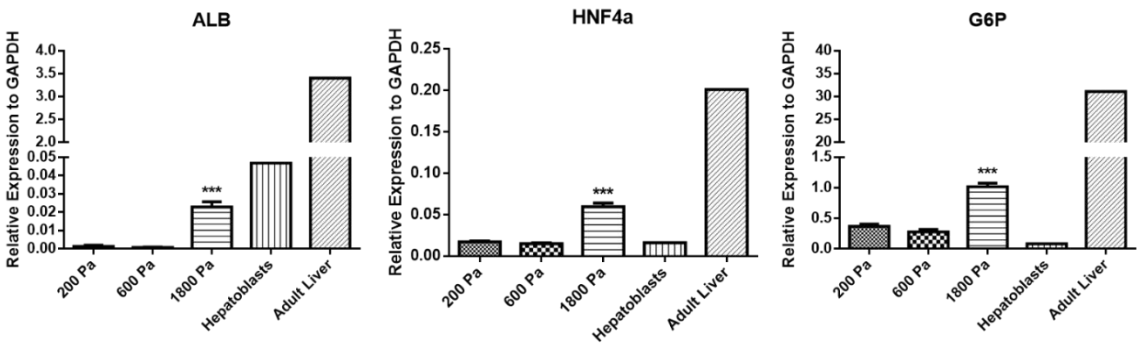

Figure 5: Hepatocyte cell differentiation. RT-PCR of RNA from hflc cells seeded on liver discs for 3 weeks. 1800Pa discs had significantly higher levels of albumin (ALB), HNF4α and G6P than 200 and 600Pa discs, when normalized to total cell population.

Histological analysis revealed bile duct formation, demonstrating differentiation of hepatoblasts towards cholangiocytes in discs of all stiffnesses, however the most bile ducts were observed in the middle stiffness discs (600 Pa). RT-PCR analysis of biliary marker HNF1β after 3 weeks in culture revealed an increasing trend in 600 Pa, although no significant changes were observed (Figure 6).

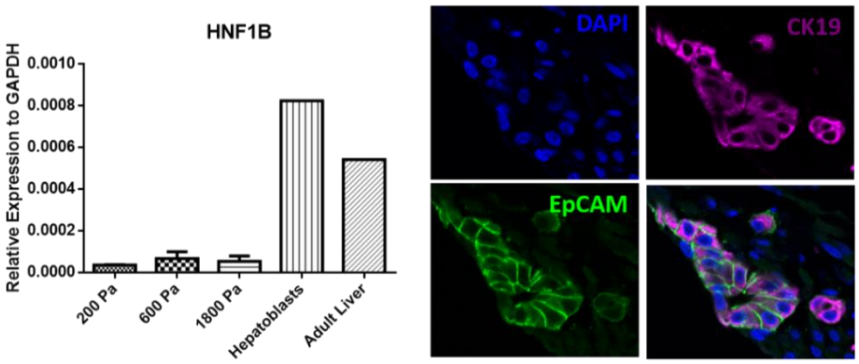

Figure 6: Biliary differentiation and bile duct formation. Left: There were no significant differences in HNF1β expression across stiffnesses. Right: Bile duct formation, observed through histological staining of CK19 and EpCAM, was most prevalent in discs with stiffness of 600Pa.

A1. Discussion

The mechanical properties of the substrate that cells are cultured on can have a significant influence on cell behavior, including growth, morphology and differentiation. It is known that matrix mechanics, such as stiffening that occurs in liver fibrosis, effects many liver cell types including hepatocytes (27-29), portal fibroblasts (30) and hepatic stellate cells (31-34). Matrix stiffness has also been implicated in the behavior of liver stem cells, including the organization of human hepatic stem cells (10), mouse hepatic stem cell growth and differentiation (11) and in maintaining the differentiated state of ES-derived hepatocytes (12). However, there is still much research needed to fully elucidate the role of matrix stiffness in the hepatoblast cell-fate decision as well as growth and function. To this end, we have performed preliminary experiments demonstrating the use of acellular liver ECM scaffolds in evaluating the effects of matrix mechanical properties on liver progenitor cells. Discs of acellular liver ECM were crosslinked to increase stiffness and seeded with human fetal liver cells which contain mostly epithelial liver progenitor cells (hepatoblasts) that are capable of differentiating into hepatocytes and cholangiocytes. However, this population of cells also contains some stromal cells, which help epithelial cell growth and differentiation through secretion of factors and ECM (36-39).

Analysis of DNA content and H&E images of hflc-seeded scaffolds after three weeks in culture revealed that cell number decreased as stiffness increased. It was observed that the number of α-SMA+ cells (stromal cells) decreased with increases in stiffness, while the number of CK-18+ cells (epithelial cells) remained stable across matrix conditions. To confirm this observation, we seeded only the stromal cell population on liver discs and confirmed slow growth rates on stiffer discs. Future experiments will use magnetic sorting

for EpCAM+ cells which isolates the epithelial cell population. These cells will then be seeded on liver discs to determine if this cell population is influenced by the stiffness of the underlying matrix.

In observing scaffolds stained with α-SMA and CK-18, we observed areas of cells on the 600Pa discs that co-expressed these two markers and displayed a mesenchymal phenotype. These characteristics are indicative of epithelial-to-mesenchymal transition (EMT), also known as de-differentiation. To gain further evidence of this process occurring in 600Pa scaffolds, we stained the cells with E-cadherin and β-catenin, both of which will be membrane bound on tight epithelial cell-cell junctions. Although we did not notice changes in β-catenin expression, there was a marked decrease in E-cad+ cells in 600Pa discs. RT-PCR demonstrated this trend as well, although data was not significant. These results indicate that the mechanical properties of the matrix may affect cell phenotype. This phenomena has been observed before, where hepatocytes cultured on stiff substrates de-differentiate and become proliferative (27-29). Due to the fact that CK-18 does not differentiate between hepatoblasts and hepatocytes, further analysis will need to be done to determine if these were progenitor or mature cells undergoing de-differentiation. Furthermore, we will analyze more timepoints to determine at which stage this process occurs and confirm the effects of stiffness on this behavior.

Finally, we performed a preliminary examination of the effects of matrix stiffness on hepatoblast differentiation towards hepatocyte and cholangiocyte lineages. While we observed upregulation of the hepatocyte markers albumin, HNF4α and G6P in the stiffest discs, these results may be skewed by the decrease number of stromal cells on these substrates. Since the RNA is normalized to total cell number, rather than just epithelial

cells, epithelial cells take up a larger percentage of cells analyzed on the 1800Pa discs than they do on the 200 and 600Pa discs. Future experiments will be performed on purified populations of hepatoblasts, through EpCAM+ sorting, which should normalize differentiation data. This limitation also occurs when looking at cholangiocyte differentiation. Although the number of developed bile ducts was observed on the 600Pa discs through histology, RT-PCR quantification is limited by the fact that mature cholangiocytes take up a small percentage of total cell number. Future experiments will seed cells on 6-8 discs, each stiffness, for three weeks, and then use histological analysis to quantify the number of mature bile ducts to determine if this process is affected by substrate stiffness.

The preliminary experiments described here provide evidence that the mechanical properties of the matrix influence sub-populations of liver cells differently. There is evidence that liver stromal cell growth is slowed on stiffer substrates, which may have impacted analysis of the epithelial cell population through indirect and direct cell-cell interactions between these two populations. It was also observed that matrix mechanics can result in epithelial cell de-differentiation. Confirmation of this observation will occur through PCR analysis of genes involved in EMT and proliferating cell cycle, which are upregulated during the de-differentiation process. The effects of matrix stiffness on differentiation of liver progenitor cells will be further analyzed by seeding a purified population of liver epithelial cells on the acellular ECM discs. Lastly, although scaffold crosslinking increased the stiffness of the ECM matrix, this process also impact other material properties, such as the porosity and viscosity of the substrate. Future studies will

use hydrogels with the ability of modifying stiffness without impacting these other important material characteristics.

Appendix A2: Investigation into the ability of liver progenitor cells to sense and respond to shear stress

A2. Introduction

The precise mechanisms involved in mechanosensing/transduction during liver development and regeneration are largely unknown. This appendix outlines preliminary work aiming to identify mechanotransduction signaling pathways that are triggered by the application of fluid shear stress to hflcs. These results may provide valuable insight into the downstream effects of fluid shear stress, including differentiation, proliferation, and migration. One potential mechanosensing mechanism in hflcs is the primary cilia. While primary cilia are integral in normal cholangiocyte function, the functional liver cell, the hepatocyte, does not possess a primary cilium (24). However, in liver development, cholangiocytes and hepatocytes are derived from the same cell, the bipotential hepatoblast. The role of primary cilia in liver development, including the presence of primary cilia on liver stem and progenitor cells, signaling mechanisms, and the involvement of primary cilia in liver differentiation, is largely unknown. To this end, we aimed to determine the presence or absence of primary cilia on liver stem and progenitor cells through the use of

immunofluorescent staining. Next, we aimed to evaluate the effects of short-term shear stress on hflc monolayers. Flow chambers were used to provide a range of shear stresses and cellular response was analyzed through real-time PCR. Finally, we propose methods to further evaluate a large array of potential mechanotransduction pathways upregulated in hflcs exposed to longer-term fluid shear stress.

A2. Materials and Methods

Cell Culture of hFLCs: Human fetal liver cells (hflcs) were isolated from livers at 18-20 weeks of gestation, as previously described (35). Cells were seeded at a density of 10,000 cells/mm^2 and cultured on 25 mm glass coverslips coated with collagen IV (25μg/cm^2) and laminin (5μg/cm^2). For the primary cilia experiments, the media was either HepGro and EsbGro media (Millipore) for hepatocyte expansion and liver stem cell colonization, respectively. For shear stress experiments, hepatoblast cells were cultured and perfused using Kubota media (35).

Immunofluorescent Staining: After 5-9 days (hepatoblasts) or 3 weeks (liver stem cells), cells were fixed with 10% Neutral Buffered Formalin for 10 minutes, then washed with phosphate buffered saline (PBS) three times for five minutes each. Serum-free protein block (Dako Inc., Carpinteria, CA) with a 1:100 dilution of saponin was placed on the cells for 30 minutes at room temperature. The following primary antibodies were added for 1 hour at room temperature: (AcTb, Invitrogen, 32-3700, 1:250), Alpha-1-fetoprotein (AFP, Dako, A0008, 1:400), Albumin (Alb, Bethyl, A80-129A, 1:200), Cytokeratin 19 (CK19, Santa Cruz, sc-33120, 1:100), Neural Cell Adhesion Molecule (NCAM/CD56-PE, BD,

340724, 1:50). Secondary antibodies were added for 45 minutes at room temperature, 1:500: DyLight 488 horse anti-mouse IgG (Vector, DI-2488), Molecular Probes; Alexa Flour 594 donkey anti-rabbit IgG (A-21207), Alexa Flour 488 donkey anti-goat IgG (A-11055), Alexa Flour 594 donkey anti-mouse IgG (A-21203), Alexa Flour 594 donkey anti-goat IgG (A-11058). Nuclei were stained with 4',6-diamidino-2-phenylindole (DAPI). Imaging was performed using an Olympus fv-1000 laser scanning confocal microscope with 20x and 60x objectives.

Short-term Shear Stress Experiments: Perfusion was applied to a ProFlow Shear Flow Chamber PFC-1 (Warner Instruments, Hamden, CT) using a peristaltic pump (Masterflex 7523-70, Cole-Parmer) attached to a custom pulse dampener to apply steady flow, or no pulse dampener for pulsatile experiments. Flow was applied at four different shear stresses ranging from 0.03 to 16 dynes/cm^2 for time periods of 1 or 2 hours. 50 ml of Kubota media (or growth factor/drug supplemented media) was continuously perfused over the cells for the designated amount of time. Immediately following the application of flow, cells were harvested from the coverslips and RNA and DNA were extracted using a DNA/RNA extraction kit (AllPrep DNA/RNA Mini Kit, Qiagen, Valencia, CA). Expression of target genes c-fos, LEF1, SERPINE (PAI-1), CDH1 (E-cadherin), CTNNB1 (β-catenin), and NFKB1 were analyzed by quantitative real-time polymerase chain reaction (qRT-PCR). GAPDH was used as an endogenous control in all samples and results were analyzed using the $2^{-\Delta\Delta CT}$ method(40). Fold changes in gene expression were calculated by normalizing the shear stress stimulated cells to static controls, which received no flow.

A2. Results

Identification of Primary Cilia in hFLCs: After 5-9 days (hepatoblasts) or 3 weeks (stem cells), cells were fixed and stained with acetylated α-tubulin to identify primary cilia, in conjunction with other antibodies to confirm cell type. When hflcs were cultured in hepatoblast expansion media, primary cilia were observed after 3 days in culture (data not shown), and most of the cells within the hepatoblast-like colonies expressed cilia by day 5. A number of cells within these colonies co-expressed α-fetoprotein (AFP), a marker of hepatoblasts, demonstrating the presence of primary cilia on liver progenitors (Figure 7A). Some cells exhibited $ALB^+/AcTb^+$ staining, suggesting that truly bipotential liver progenitors, not yet committed cholangiocytes, express primary cilia (Figure 7B). In addition, some neural cell adhesion molecule (NCAM)-positive hepatic stem cells expressed primary cilia, when cultured in liver stem cell media (Figure 7C). As expected, primary cilia were also present on the apical side of $CK19^+$ biliary cells in the lumen of the developing bile ducts in sections of normal fetal liver tissue (Figure 7D).

Applying Short-Term Shear Stress to hflcs: We found that c-fos is the most activated gene, as it quickly responds to any sort of stress imposed on the cell, and that it is a transient effect, with high expression (4-8 fold change over static controls) within 30 minutes to an hour and then decreasing after that. LEF1, a transcription factor of the Wnt/β-catenin pathway, exhibited significant increase in gene expression in steady flow conditions for 2 hours at shear stress magnitudes of 4 and 16 dynes/cm^2 (Figure 8). There was increasing trends observed at higher shear stress magnitudes in all of the other target genes, but no significant changes.

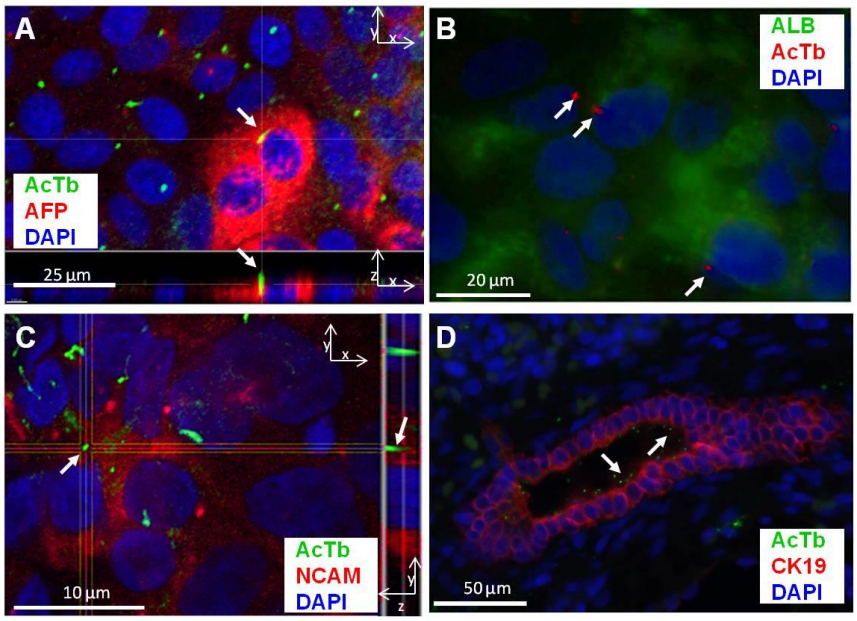

Figure 7: Primary cilia expression in liver stem and progenitor cells. Cultures of hflcs in hepatoblast **(A,B)** and stem cell media **(C)** were immunostained with acetylated α-tubulin (AcTb), α-fetoprotein (AFP), albumin (ALB) and neural cell adhesion molecule (NCAM). Normal human fetal liver paraffin sections **(D)** were immunostained with acetylated α-tubulin (AcTb) and cytokeratin-19 (CK19). Fluorescence imaging was carried out using confocal **(A,C)** and standard microscopes **(B,D)**. Arrows indicate the location of primary cilia.

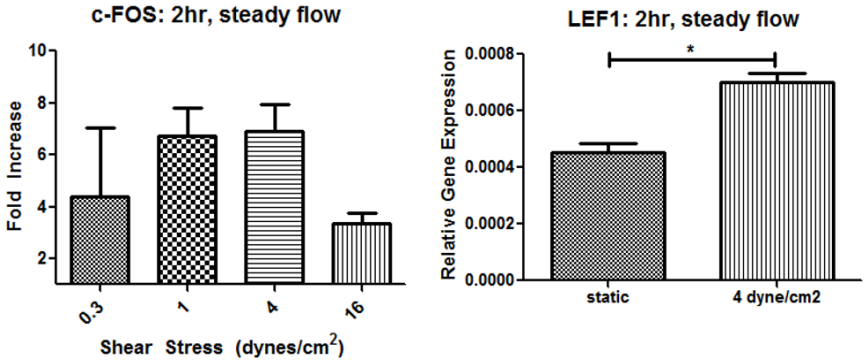

Figure 8: RT-PCR of hflc cultured in flow chamber under shear stress. Genes analyzed were c-fos and LEF1, with fold increases calculated over static culture controls.

A2. Discussion

This preliminary research investigated the potential for liver progenitor cells to respond to shear stress mechanical stimuli. Shear stress has been identified as an important mechanical cue in non-hepatic stem cell differentiation (13-15) and has been found to increase human fetal liver cell hepatocytic differentiation (16). Other studies have demonstrated more functional maturation of hepatic differentiated human embryonic stem cells when cultured under 3D perfusion (17, 18). While the mechanosensitivity of stem and progenitor cells is a promising new area of research, the mechanotransduction pathways involved in these cell fate decisions is yet to be fully realized. Recent research has suggested that the primary cilium may play a role in stem cell differentiation, due to the involvement of primary cilia/ centrosomes in the cell cycle and the association of the primary cilia with the Hedgehog signaling pathway (14, 19-21). Cholangiocytes also contain primary cilia which are used in detecting osmolality and chemical composition of bile and acting as mechanosensors. To this end, this preliminary research aims to investigate the effects of shear stress on hepatoblast differentiation and identify and validate potential mechanotransduction pathways involved in shear stress detection.

Primary cilia, known mechanosensors in adult cholangiocytes and potential mediators of stem cell differentiation, were identified on bipotential hepatoblasts and stem cells isolated from human fetal livers. Short term (1-2 hour) shear stress experiments were performed on these cells and demonstrated that the hepatoblasts respond to shear stress through upregulation of c-fos and LEF1. These findings provide evidence that hflcs have mechanosensing abilities, which may translate to downstream behavior, such as cell differentiation.

Future studies are beginning in which we are using a μ-fluidic system to investigate the role of fluid flow on the behavior of cell aggregates, rather than cell monolayers. Cell monolayers have a large number of advantages when using fluidic systems, including device fabrication, modeling and extrapolation of shear stress values and real-time imaging capabilities. However, cell monolayers are not a good representation of cell organization *in vivo* and therefore may not accurately predict physiological cell behavior. Collaborators have developed a μ-fluidic system that allows us to deliver shear stress to cells arranged in cell aggregates in high-throughput and low-cost experiments. This system will be used to investigate the effects of medium and long-term shear stress on cell behavior and differentiation. Custom PCR arrays (SABiosciences) will then be used to screen for the upregulation of genes involved in cell signaling pathways associated with mechanotransduction in other cell types, including EGR-1, NF-κB, KLF2, among many others. Additionally, we will evaluate cell signaling pathways associated with liver cell differentiation towards both hepatocytic and cholangiocyte lineages, and processes such as cell cycle, apoptosis, and endothelial-to-mesenchymal transition (EMT).

References

1. Janmey PA, Miller RT. Mechanisms of mechanical signaling in development and disease. Journal of Cell Science. 2011 Jan;124(1). PubMed PMID: WOS:000285242200003.
2. Mammoto T, Ingber DE. Mechanical control of tissue and organ development. Development. 2010 May;137(9):1407-20. PubMed PMID: WOS:000276598200002.
3. Wells R. The role of matrix stiffness in regulating cell behavior. Hepatology. 2008 APR 2008;47(4):1394-400. PubMed PMID: ISI:000254637100031. English.
4. Wirtz D, Konstantopoulos K, Searson PC. The physics of cancer: the role of physical interactions and mechanical forces in metastasis. Nature Reviews Cancer. 2011 Jul;11(7):512-22. PubMed PMID: WOS:000292028300016.

5. Diehl AM, Chute J. Underlying potential: cellular and molecular determinants of adult liver repair Introduction. Journal of Clinical Investigation. 2013 May;123(5):1858-60. PubMed PMID: WOS:000319025100003.
6. Boulter L, Lu WY, Forbes SJ. Differentiation of progenitors in the liver: a matter of local choice. Journal of Clinical Investigation. 2013 May;123(5):1867-73. PubMed PMID: WOS:000319025100005.
7. Boulter L, Govaere O, Bird TG, Radulescu S, Ramachandran P, Pellicoro A, et al. Macrophage-derived Wnt opposes Notch signaling to specify hepatic progenitor cell fate in chronic liver disease. Nature Medicine. 2012 Apr;18(4):572-9. PubMed PMID: WOS:000302617800034.
8. Lemaigre FP. Mechanisms of Liver Development: Concepts for Understanding Liver Disorders and Design of Novel Therapies. Gastroenterology. 2009 Jul;137(1):62-79. PubMed PMID: WOS:000267410100016.
9. Engler AJ, Sen S, Sweeney HL, Discher DE. Matrix elasticity directs stem cell lineage specification. Cell. 2006 Aug 25;126(4). PubMed PMID: WOS:000240276700017.
10. Lozoya O, Wauthier E, Turner R, Barbier C, Prestwich G, Guilak F, et al. Regulation of hepatic stem/progenitor phenotype by microenvironment stiffness in hydrogel models of the human liver stem cell niche. Biomaterials. 2011 OCT 2011;32(30):7389-402. PubMed PMID: ISI:000294829300012. English.
11. Tsai HA, Shen CN, Chang YC. Use of Surface Properties to Control the Growth and Differentiation of Mouse Fetal Liver Stem/Progenitor Cell Colonies. Biomacromolecules. 2012 Nov;13(11):3483-93. PubMed PMID: WOS:000310931900008.
12. Li L, Sharma N, Chippada U, Jiang X, Schloss R, Yarmush ML, et al. Functional modulation of ES-derived hepatocyte lineage cells via substrate compliance alteration. Annals of Biomedical Engineering. 2008 May;36(5):865-76. PubMed PMID: WOS:000254755800018.
13. Freund JB, Goetz JG, Hill KL, Vermot J. Fluid flows and forces in development: functions, features and biophysical principles. Development. 2012 Apr;139(7):1229-45. PubMed PMID: WOS:000301301900002.
14. Wolfe RP, Leleux J, Nerem RM, Ahsan T. Effects of shear stress on germ lineage specification of embryonic stem cells. Integrative Biology. 2012;4(10):1263-73. PubMed PMID: WOS:000309127600011.
15. Stolberg S, McCloskey KE. Can Shear Stress Direct Stem Cell Fate? Biotechnology Progress. 2009 Jan-Feb;25(1):10-9. PubMed PMID: WOS:000263776900003.
16. Schmelzer E, Triolo F, Turner ME, Thompson RL, Zeilinger K, Reid LM, et al. Three-Dimensional Perfusion Bioreactor Culture Supports Differentiation of Human Fetal Liver Cells. Tissue Engineering Part A. 2010 Jun;16(6). PubMed PMID: WOS:000278164800019.
17. Miki T, Ring A, Gerlach J. Hepatic Differentiation of Human Embryonic Stem Cells Is Promoted by Three-Dimensional Dynamic Perfusion Culture Conditions. Tissue Engineering Part C-Methods. 2011 May;17(5). PubMed PMID: WOS:000289937100006.
18. Gerlach JC, Hout M, Edsbagge J, Bjorquist P, Lubberstedt M, Miki T, et al. Dynamic 3D Culture Promotes Spontaneous Embryonic Stem Cell Differentiation In Vitro. Tissue Engineering Part C-Methods. 2010 Feb;16(1):115-21. PubMed PMID: WOS:000274125800012.
19. Kiprilov EN, Awan A, Desprat R, Velho M, Clement CA, Byskov AG, et al. Human embryonic stem cells in culture possess primary cilia with hedgehog signaling machinery. Journal of Cell Biology. 2008 Mar 10;180(5). PubMed PMID: WOS:000254081100007.
20. Schatten H, Sun Q-Y. The Significant Role of Centrosomes in Stem Cell Division and Differentiation. Microscopy and Microanalysis. 2011 Aug;17(4). PubMed PMID: WOS:000293527400004.
21. Awan A, Oliveri RS, Jensen PL, Christensen ST, Andersen CY. Immunoflourescence and mRNA analysis of human embryonic stem cells (hESCs) grown under feeder-free conditions. Methods Mol Biol. 2010;584:195-210. PubMed PMID: 19907979. eng.

22. Masyuk AI, Masyuk TV, Splinter PL, Huang BQ, Stroope AJ, LaRusso NF. Cholangiocyte cilia detect changes in luminal fluid flow and transmit them into intracellular Ca2+ and cAMP signaling. Gastroenterology. 2006 Sep;131(3). PubMed PMID: WOS:000240561800028.
23. Woo K, Dutta AK, Patel V, Kresge C, Feranchak AP. Fluid flow induces mechanosensitive ATP release, calcium signalling and Cl(-) transport in biliary epithelial cells through a PKC zeta-dependent pathway. Journal of Physiology-London. 2008 Jun 1;586(11). PubMed PMID: WOS:000256345800015.
24. D'Angelo A, Franco B. The primary cilium in different tissues-lessons from patients and animal models. Pediatric Nephrology. 2011 May;26(5):655-62. PubMed PMID: WOS:000288712800002.
25. Clotman F, Libbrecht L, Killingsworth MC, Loo CCK, Roskams T, Lemaigre FP. Lack of cilia and differentiation defects in the liver of human foetuses with the Meckel syndrome. Liver International. 2008 Mar;28(3). PubMed PMID: WOS:000253258100012.
26. Masyuk AI, Masyuk TV, LaRusso NF. Cholangiocyte primary cilia in liver health and disease. Developmental Dynamics. 2008 Aug;237(8). PubMed PMID: WOS:000258482300007.
27. Hansen LK, Wilhelm J, Fassett JT. Regulation of hepatocyte cell cycle progression and differentiation by type I collagen structure. Current Topics in Developmental Biology, Vol 72. 2006 2006;72. PubMed PMID: WOS:000236800100004.
28. Fassett J, Tobolt D, Hansen LK. Type I collagen structure regulates cell morphology and EGF signaling in primary rat hepatocytes through cAMP-dependent protein kinase A. Molecular Biology of the Cell. 2006 Jan;17(1). PubMed PMID: WOS:000234399300032.
29. Semler EJ, Ranucci CS, Moghe PV. Mechanochemical manipulation of hepatocyte aggregation can selectively induce or repress liver-specific function. Biotechnology and Bioengineering. 2000 Aug 20;69(4). PubMed PMID: WOS:000088421700002.
30. Li Z, Dranoff JA, Chan EP, Uemura M, Sevigny J, Wells RG. Transforming growth factor-beta and substrate stiffness regulate portal fibroblast activation in culture. Hepatology. 2007 Oct;46(4). PubMed PMID: WOS:000249910500035.
31. Wells RG. The role of matrix stiffness in hepatic stellate cell activation and liver fibrosis. Journal of Clinical Gastroenterology. 2005 Apr;39(4). PubMed PMID: WOS:000227989200019.
32. Guvendiren M, Perepelyuk M, Wells RG, Burdick JA. Hydrogels with differential and patterned mechanics to study stiffness-mediated myofibroblastic differentiation of hepatic stellate cells. J Mech Behav Biomed Mater. 2014 Oct;38:198-208. PubMed PMID: 24361340. eng.
33. Iwamoto H, Sakai H, Nawata H. Inhibition of integrin signaling with Arg-Gly-Asp motifs in rat hepatic stellate cells. Journal of Hepatology. 1998 Nov;29(5). PubMed PMID: WOS:000077182400010.
34. Yee HF. Rho directs activation-associated changes in rat hepatic stellate cell morphology via regulation of the actin cytoskeleton. Hepatology. 1998 Sep;28(3). PubMed PMID: WOS:000075606000036.
35. Schmelzer E, Zhang L, Bruce A, Wauthier E, Ludlow J, Yao H-L, et al. Human hepatic stem cells from fetal and postnatal donors. Journal of Experimental Medicine. 2007 Aug 6;204(8). PubMed PMID: WOS:000248727700025.
36. Matsumoto K, Yoshitomi H, Rossant J, Zaret KS. Liver organogenesis promoted by endothelial cells prior to vascular function. Science. 2001 Oct 19;294(5542):559-63. PubMed PMID: WOS:000171695600037.
37. Gouysse G, Couvelard A, Frachon S, Bouvier R, Nejjari M, Dauge MC, et al. Relationship between vascular development and vascular differentiation during liver organogenesis in humans. Journal of Hepatology. 2002 Dec;37(6):730-40. PubMed PMID: WOS:000179584700004.

38. Yin CY, Evason KJ, Asahina K, Stainier DYR. Hepatic stellate cells in liver development, regeneration, and cancer. Journal of Clinical Investigation. 2013 May;123(5):1902-10. PubMed PMID: WOS:000319025100009. English.
39. Si-Tayeb K, Lemaigre FP, Duncan SA. Organogenesis and Development of the Liver. Developmental Cell. 2010 Feb;18(2):175-89. PubMed PMID: WOS:000275100400005.
40. Livak KJ, Schmittgen TD. Analysis of relative gene expression data using real-time quantitative PCR and the 2(T)(-Delta Delta C) method. Methods. 2001 Dec;25(4):402-8. PubMed PMID: WOS:000173949500003.

EMMA C. MORAN

113 Piedmont Ave Apt.D • Winston-Salem, NC 27101
(518) 469-1270 • emoran3@gmail.com • 4/20/2015

EDUCATION

Doctor of Philosophy in Biomedical Engineering, Anticipated May 2015
Virginia Tech-Wake Forest School of Biomedical Engineering and Sciences
Winston Salem, NC
Thesis: The Role of Biomechanics in Liver Tissue Engineering
Advisors: Shay Soker, Ph.D. and Jessica Sparks, Ph.D.

Bachelor of Science in Biomedical Engineering, May 2010
University of Rochester, Rochester, NY

PROFESSIONAL EXPERIENCE

Biorg, Inc., Winston-Salem, NC
Research Scientist, Fall 2014-Present

- Develop portfolio of tissue engineered products for disease studies and drug screening and toxicity testing in collaboration with industry partners through identification of customer needs, innovative product development, experimental design and product testing

Wake Forest Innovations, Winston-Salem, NC
Technology Commercialization Intern, Fall 2013- Present

- Assist in technology transfer in the areas of pharmaceuticals, biotechnology and medical devices
- Evaluate early-stage ideas and technologies to determine patentability, feasibility and commercial potential
- Conduct comprehensive market analysis of pharmaceutical and biotechnology companies to find licensing and partnering opportunities for university inventions
- Experience in FDA regulatory processes for medical devices, drugs/biologics and combination products

Wake Forest Institute for Regenerative Medicine (WFIRM), Winston-Salem, NC
Graduate Research Assistant, August 2010-Present

- Introduced numerous novel testing platforms to investigate the influence of mechanical forces in liver tissue engineering including the development and implementation of bioreactors, microfluidic systems, finite element models and synthetic and natural polymeric biomaterials
- Improved isolation and culture protocol of primary human liver progenitor cells and liver progenitor cell line and designed *in vitro* systems to study effects of cellular mechanics on cell function and differentiation

- Developed tissue engineering model to study and model cancer metastasis in collaboration with multi-site team consisting of biologists, engineers, physicians and mathematicians
- Research Mentor of three undergraduate students involving training and guidance on various research projects

Ordway Research Institute, Albany, NY
Summer Intern in Albany Medical College Undergraduate Research Program, Summer 2008
Summer Intern in National Science Foundation funded REU, Summer 2007

- Conducted research in Dr. Michael Fasullo's laboratory studying liver and breast cancer inducers.

PUBLICATIONS

- **Moran EC***, Baptista PM*, Vyas D, Riberio MH, Atala A, Sparks JL, Soker S. "A Bioengineered Liver Platform to Study Fluid Flow Regulation of Liver Tissue Organization". Submitted to Biomaterials.
- **Moran EC**, Raghunathan S, Evans DW, Vavalle NA, LeRoith T, Smith TL, Sparks JL. "Porohyperviscoelastic Model Simultaneously Predicts Parenchymal Fluid Pressure and Reaction Force in Perfused Liver". J Biomech, 134(9), 2012.
- Evans DW, **Moran EC**, Baptista PM, Soker S, Sparks JL. "Scale-Dependent Mechanical Properties of Native and Decellularized Liver Tissue". Biomech Model Mechanobiol. DOI 10.1007/s10237-012-0426-3, 2012.
- Orlando G, Farney AC, Iskandar SS, Mirmalek-Sani SH, Sullivan DC, **Moran E**, et al. "Production and Implantation of Renal Extracellular Matrix Scaffolds From Porcine Kidneys as a Platform for Renal Bioengineering Investigations". Annals of surgery, 256 (2): 363-370, 2012.
- Orlando G, Wang Z, Booth C, Totonelli G, Ross C, **Moran EC**, Salvatori M, Maghsoudlou P, Turmaine M, Delario G, Al-Shraideh Y, Farooq U, Farney AC, Rogers J, Iskandar S, Burns A, Marini FC, De Coppi P, Stratta RJ, Soker S. "Discarded human kidneys as a source of renal extracellular matrix scaffolds for kidney regeneration technologies". Biomaterials, 34 (24): 5915-25, 2013

BOOK CHAPTERS

- Pedro M. Baptista, Dipen Vyas, **Emma C. Moran**, Zhan Wang, Shay Soker. "Human Liver Bioengineering Using a Whole Liver Decellularized Bioscaffold". Submitted Book Chapter, Methods in Molecular Biology (3/8/12)
- Pedro M Baptista, **Emma Moran**, Dipen Vyas, Thomas Shupe, Shay Soker. "The Liver Extra-Cellular Matrix and Stem/Progenitor Cells for Liver Regeneration". Book Chapter: Regenerative Medicine Technology as Applied to Organ Transplantation: Elsevier. 2014.

REVIEW ARTICLES

- **Moran EC**, Dhal A, Vyas D, Lanas A, Soker S, Baptista PM. "Whole-Organ Bioengineering: Current Tales of Modern Alchemy". Transl Res. 2014 Apr; 163(4):259-67. doi: 10.1016/j.trsl.2014.01.004
- Pedro Baptista, Dipen Vyas, **Emma Moran**, Zhan Wang, Shay Soker. "Human Liver Bioengineering Using a Whole Liver Decellularized Bioscaffold". Methods Mol Biol. 2013; 1001:289-98. doi: 10.1007/978-1-62703-363-3_24.

PEER-REVIEWED CONFERENCE PAPERS

- **Moran EC**, Baptista PM, Evans DW, Soker S, Sparks JL. Evaluation of Parenchymal Fluid Pressure in Native and Decellularized Liver Tissue. Biomedical Sciences Instrumentation, 48:303-309, 2012.

PODIUM PRESENTATIONS

- **Moran EC**, Baptista PM, Sparks JL, Soker S. Perfusion Driven Shear Stress Leads to Self-Organization of Bioengineered Livers. *TERMIS-AM, Washington D.C., Dec. 13-16th, 2014*
- **Moran EC**, Baptista PM, Sparks JL, Soker S. Acellular Liver Scaffolds as a Model to Study Cancer Metastasis. *TERMIS-AM, Washington D.C., Dec. 13-16th, 2014*
- **Moran EC,** Gaston B., Baptista PM, Sparks JL, Ruderman D, Mumenthaler S, Macklin P, Soker S. Bioengineered Livers as a Model to Study Cancer Metastasis. *BMES 2014 Annual Meeting, San Antonio, TX. Oct 22-25nd, 2014*
- **Moran EC**, Baptista PM, Sparks JL, Soker S. A Bioengineered Liver Platform to Study the Effects of Mechanical Forces on Tissue Organization. *SBES Symposium, Winston-Salem, NC. May 15th 2014*
- **Moran EC**, Baptista PM, Sparks JL, Soker S. Shear Stress-Induced Nitric Oxide Release Mediates Cellular Organization of Bioengineered Livers. *NCTERMS Annual Conference, Winston-Salem, NC. Oct. 28th, 2013.*
- **Moran EC**, Baptista PM, Sparks JL, Soker S. Tissue Growth and Cellular Organization are Influenced by Flow Rate and Pressure in Decellularized Liver Perfusion Bioreactors. *BMES 2013 Annual Meeting, Seattle, WA. Sept. 25-28, 2013.*
- **Moran EC**, Baptista PM, Evans DW, Soker S, Sparks JL. Evaluation of Parenchymal Fluid Pressure in Native and Decellularized Liver Tissue. *Rocky Mountain Bioengineering Symposium, Blacksburg, VA, Mar 22-24nd*

SELECT POSTER PRESENTATIONS

- **Moran EC**, Baptista PM, Nishii K, Wasnick D, Soker S, Sparks JL. Expression of Primary Cilia on Liver Stem and Progenitor Cells; Potential Role for Mechanosensing in Liver Development. *ASME Summer Bioengineering Conference, Sunriver, OR. June 26-29, 2013.*

- **Moran EC**, Raghunathan S, Evans DW, Vavalle NA, LeRoith T, Smith TL, Sparks JL. Three-Dimensional Porohyperviscoelastic Model of Perfused Bovine Liver. *VT-WFU School of Biomedical Engineering and Sciences Symposium, Winston-Salem, NC. May 10, 2012.*
- **Moran EC**, Vavalle N, Raghunathan S, Sparks JL, Poroviscoelastic Finite Element Model of Perfused Liver Tissue: Effect of Fluid Input Geometry on Interstitial Fluid Pressure. *BMES 2011 Annual Meeting, Hartford, CT. October 12-15, 2011.*

AWARDS

- Wake Forest University Three-Minute Thesis (3MT) Competition Award Winner (March, 2014)
- SBES Symposium Best PhD Podium Presentation Award (May, 2014)
- Wake Forest University Graduate Research Day Best Poster Award (March, 2013)
- Wake Forest Institute for Regenerative Medicine Best Poster Award (February, 2013)
- Rocky Mountain Bioengineering Symposium Written Publication Award (March, 2012)

PROFESSIONAL SOCIETIES

- Biomedical Engineering Society, 2010-2015
- Tissue Engineering and Regenerative Medicine Society, 2014-2015
- American Society of Mechanical Engineering, 2013-2014

LEADERSHIP AND TEACHING EXPERIENCE

Wake Forest University, Winston Salem, NC

- Vice President and Secretary of Biomedical Engineering Society Student Chapter, 2011-present
- Invited Speaker at Atkins Academic & Technology High School, October 25, 2012
- Guest Lecturer in Soft Tissue Mechanics course, April 26, 2012
    - Lecture title: *Biomechanics and Tissue Engineering*

University of Rochester

- Teaching Assistant: Introduction to Biomedical Engineering, Fall 2009-2010
- Captain Varsity Women's Soccer Team, 2006-2010

BUSINESS EXPERIENCE

- Nominated as finalist to participate on the Wake Forest University team in National Biotechnology and Business Case Competition sponsored by Boston Scientific
- Continued education through:

- *Commercializing Innovation:* Wake Forest business school course analyzing innovative ideas and strategies of bringing those ideas through to successful commercialization
- Over 20 hours of intensive training in technology transfer
- 12 hours of training in regulatory, process development, manufacturing and commercialization of regenerative medicine technology

LABORATORY AND COMPUTER SKILLS

- **Experimentation:** bioreactor design, construction and implementation, rodent surgery and organ harvesting, tissue decellularization, microfluidic systems, natural and synthetic polymeric biomaterial modification
- **Characterization techniques:** Compression, tensile and rheological mechanical testing, scanning electron microscopy, calcium imaging, real-time pressure measurements, lyophilization.
- **Cell culture:** isolation, culture and expansion of primary cells (human fetal liver) and mammalian cell lines (liver, colon, endothelial), culture media preparation and optimization, cell passaging, aseptic technique**,** banking and freezing, labeling and sorting.
- **Histology:** immunohistochemistry, fluorescent/brightfield and confocal microscopy, paraffin and frozen tissue processing and sectioning
- **Dynamics/ Simulation Software:** Abaqus
- **Programming Languages:** MATLAB, Mathematica, Labview, Powerlab
- **Applications:** Microsoft Office, SPSS, Adobe Photoshop, Image J, Latex, Isight